

WBS: 1.2.2

QA: L

**Civilian Radioactive Waste Management System
Management & Operating Contractor**

**DEGRADED WASTE PACKAGE CRITICALITY:
SUMMARY REPORT OF EVALUATIONS THROUGH 1996**

Document Identifier: BBA000000-01717-5705-00012 REV 00

August 28, 1997

Prepared for:

U.S. Department of Energy
Yucca Mountain Site Characterization Project Office
P.O. Box 30307
Las Vegas, NV 89036-0307


Prepared By:

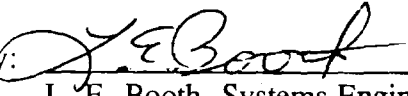
Civilian Radioactive Waste Management System
Management & Operating Contractor
1180 Town Center Drive
Las Vegas, NV 89134

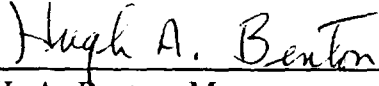
Under Contract Number
DE-AC01-91RW00134

Civilian Radioactive Waste Management System
Management & Operating Contractor

DEGRADED WASTE PACKAGE CRITICALITY:
SUMMARY REPORT OF EVALUATIONS THROUGH 1996

Prepared By:  Date: 8/28/1997
P. Gottlieb, Manager
Degraded Mode and Risk Analysis

Checked By:  Date: 8/29/97
L. E. Booth, Systems Engineering
MGDS Safety Assurance

Approved By:  Date: 9/2/97
H. A. Benton, Manager
Waste Package Development

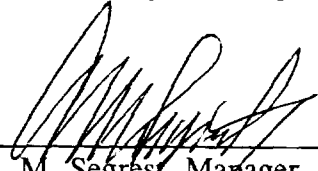
Approved By:  Date: 9/3/97
A. M. Segrest, Manager
Mined Geologic Disposal System

Table of Contents

1. Introduction	1
1.1 Background	1
1.2 Objective	1
1.3 Methodology	1
1.4 Scope	3
1.5 Quality Assurance	3
1.6 Computer Software	5
2. Repository Environment	6
2.1 Environmental Parameters	6
2.1.1 WP Surface Temperature and Humidity	6
2.1.2 Flow Rate of Water onto a WP Below a Dripping Fracture	8
2.1.3 Infiltration Rate	8
2.1.4 WP Drip Rate as a Function of Infiltration Rate	8
2.2 Scenarios: General Characteristics	9
2.3 Scenarios: Repository Environment Events and Processes	11
2.3.1 Internal Criticality: Corrosion Events Common to All Scenarios	11
2.3.2 External Criticality Scenario Development Guidance from Natural Analogs	12
2.3.2.1 Relevant Mineralizations in Geologic Provinces Which are Somewhat Related to the Yucca Mountain Geology	12
2.3.2.2 Potential for Uranium Concentration in the Tuff at Yucca Mountain	13
2.3.3 Accumulation of a Far-Field Critical Mass: Possibility and Probability	14
2.3.3.1 Types of Uranium Deposit	14
2.3.3.2 Maximum Uranium Concentrations from Non-Organic Reducing Zones, Hydrothermal and Zeolite Deposition Process	15
2.3.3.3 Maximum Uranium Concentrations Resulting from Reduction Zones of Organic Origin	16
2.3.3.4 Methodology for Estimating Probabilities	17
2.3.3.5 Probability of Sufficient Reducing Material to Make Accumulation of a Critical Mass Possible, Pr{cluster/log}	17
2.3.3.6 Probability of Encountering a Log, Pr{log}	19
3.0 Chemistry/Geochemistry/Mechanical Processes	21
3.1 WP Barrier Degradation (pre-TSPA95)	21
3.2 Waste Package Basket Degradation: Borated Stainless Steel	22
3.2.1 Minimum Time to Corrosion of a Critical Fraction of the Basket	22
3.2.2 Corrosion Under Continuous Wetting Conditions	23
3.2.3 Corrosion Under Intermittent Wetting Conditions	23
3.3 Mechanical Deformation/Failure Following Partial Basket Degradation	24
3.3.1 Neutron Absorber Plates	24
3.3.2 Fuel Cell Tubes	25
3.4 Rockfall Hazard to a Partially Degraded Waste Package	25
4.0 Configuration Generator Code	28

4.1 Model Description: Commercial SNF Example	28
4.2 Range of Input Parameters Values for Commercial SNF	30
5.0 Waste Package Criticality Analyses for Commercial SNF	34
5.1 MCNP Calculations For Degraded Configurations: Commercial SNF	34
5.2 Regression Analysis of the Data: Commercial SNF	35
6.0 Evaluation of Criticality: Sample Results	36
6.1 Criticality Expectation as a Function of Time	37
6.1.1 Probability Density Function for Infiltration Rate	37
6.1.1.1 PDF for Surface Water Infiltration of Repository Horizon at a Low Rate ..	37
6.1.1.2 PDF for Surface Water Infiltration of Repository Horizon at a High Rate ..	38
6.1.1.3 PDF for Changing to a Very Wet Climate Which Raises the Water Table to Repository Horizon (flooding the repository)	38
6.1.2 Probability Density Function for Time to Breach Waste Package Barriers	41
6.1.3 Probability Density Function for Time to Degrade Borated Stainless Steel Basket	43
6.1.4 Probability of Sufficient Fissile Material in a Waste Package	45
6.1.5 Probability of Sufficient Moderator	47
6.1.6 Expectation of Criticality	47
6.2 Earliest Times To Internal WP Criticality: Commercial SNF Example	49
6.2.1 Nominal Range of Trapped Boron Fraction	49
6.2.2 Sensitivity Analysis: Extending the Range of the Trapped Boron Fraction	53
6.3 Far-Field Criticality Analysis: Commercial SNF	56
6.3.1 Critical Mass of Commercial SNF Uranium	56
6.3.2 Probability That Randomly Selected Cluster Will Have Sufficient Reducing Material	59
6.3.3 Calculation of Expected Number of Criticalities	59
6.3.4 Adjustment for Critical Masses Greater Than a Single Waste Package	61
7.0 Criticality Consequences	63
7.1 Estimated Power and Duration of an Internal Criticality	63
7.2 Effects of an Internal Criticality on the Radionuclide Inventory of the WP	67
7.2.1 ORIGEN-S Calculations	67
7.2.2 Neutron Activation Estimates	67
8.0 Conclusions	75
9.0 References	77

List of Tables

Table 2-1. TSPA-95 Peak Dripping Flow Rates Onto A WP	9
Table 2-2. Alternative Estimations of Probability of Encountering a Log	20
Table 3-1. WP Time To Breach Predicted by Temperature Distribution Model	22
Table 3-2. Summary of Neutron Absorber Degradation Times (years)	24
Table 3-3. Times to Neutron Absorber Plate Collapse	25
Table 3-4. Critical Rock Mass With Respect to Time	27
Table 4-1. Summary of Input Parameters	33
Table 5-1. Progressive Degradation of Borated Stainless Steel Control Panels	34
Table 5-2. MCNP Calculation Data Points for Fully Degraded Basket	35
Table 6-1. Times to Earliest Possible Criticality with One Parameter High	51
Table 6-2. Times to Earliest Possible Criticality with Two Parameters High	52
Table 6-3. Sensitivity to Trapped Boron Fraction with One Parameter High	54
Table 6-4. Sensitivity to Trapped Boron Fraction with Two Parameters High	55
Table 6-5. Representative SNF/Environment Configurations and Resulting Spherical Critical Masses	58
Table 6-6. Upper Bound of Probabilities of Log Clusters Which Could Be Capable Of Precipitating a Uranium Concentration Sufficient For Criticality	59
Table 6-7. Percentile of SNF Having Less Fissile % Than Stated Value	60
Table 6-8. Summary of Upper Bound for Probability of Criticality as a Function of Fissile Content	61
Table 7-1. Effects of 1,000 Year Criticality on the Radionuclide Inventory of a PWR Fuel Assembly	70
Table 7-2. Effects of 5,000 Year Criticality on the Radionuclide Inventory of a PWR Fuel Assembly	71
Table 7-3. Effects of 10,000 Year Criticality on the Radionuclide Inventory of a PWR Fuel Assembly	72
Table 7-4. Percentage Increase in Total Curies of the 36 TSPA-95 Isotopes	73

List of Figures

Figure 2-1.	Waste Package surface temperature as a function of time for a mass loading of 6.0 kg U/m ² (approximately 24 MTU/acre)	6
Figure 2-2.	Illustration of Scenario Generation	10
Figure 3-1.	Mean WP Outer Barrier Thickness as a Function of Time	26
Figure 6-1.	Distribution of time-to-occurrence of the low infiltration initiating event	39
Figure 6-2.	Distribution of time-to-occurrence of the high infiltration initiating event	39
Figure 6-3.	Distribution of WP breach failures from temperature distribution model given continuous wetting	42
Figure 6-4.	Distribution of WP breach failures from temperature distribution model given intermittent wetting	42
Figure 6-6.	Distribution of time to leach 60% of neutron absorbing material from UCF-WP basket structure exposed to intermittent wetting conditions.	44
Figure 6-5.	Distribution of time to leach 60% of neutron absorbing material from UCF-WP basket structure for continuously wetted conditions.	44
Figure 6-7.	Fraction of design basis fuel (3% initial enrichment, 20 GWd/MTU Burnup) as a function of time capable of achieving $k_{eff} > 0.95$ in an UCF-WP geometry with no neutron absorber in the basket structure	45
Figure 6-9.	k_{eff} of various concentrations of UO ₂ , tuff, and water for UO ₂ from PWR SNF with 3% initial enrichment and 20 GWd/MTU burnup	56
Figure 6-10.	k_{eff} as a function of sphere radius for 18.5 vol% 3%/20 UO ₂ in saturated tuff with 47% porosity	56
Figure 7-1.	Inventory of 36 TSPA-95 Nuclides in 3% 20 GWd/MTU PWR SNF as a Function of Time, with the Increase From a 10,000 year Steady State Internal Criticality Indicated	74
Figure 7-2.	Inventory of 36 TSPA-95 Nuclides in 3% 20 GWd/MTU PWR SNF as a Function of Time from 10,000 to 60,000 Years, with the Increase From a 10,000 year Steady State Internal Criticality Indicated	74

1. Introduction

1.1 Background

The purpose of this document is to summarize the degraded waste package disposal criticality evaluations which were performed in fiscal years 1995 and 1996. These evaluations were described in detail in 4 previous documents (Refs. 1 through 4). The initial version of this summary has been described in the 1996 Disposal Criticality Analysis Methodology Technical Report (Ref. 5). A topical report planned for 1998 will present the methodology in its final form for approval by the US Nuclear Regulatory Commission.

1.2 Objective

The objective of this document is to show how the previous documents fit into an overall criticality evaluation methodology. This report is intended to provide technical support for the next revision of Disposal Criticality Analysis Methodology Technical Report (to be issued in September 1997).

1.3 Methodology

The criticality evaluation methodology consists of the following: (1) identification of processes which can occur and consequently rearrange the neutronically significant components of the waste package (so that the neutron absorbers become separated from the fissile material); a sequence of such processes is called a scenario; (2) evaluation of the criticality state of a system containing fissile species in a potentially critical geometry; such a state is the result of a scenario and is called a configuration; (3) implementation of a computer code to track the locations and concentrations of the neutronically active species to determine where and when criticalities might occur; and (4) estimation of consequences of any criticalities which might occur.

The criticality evaluation methodology begins with the parameters of the repository environment. The values of these parameters are determined by the Scientific Investigations program of the Yucca Mountain Site Characterization Office. The values of the environmental parameters used are summarized in Section 2.1. In some cases the official estimates of these parameter values have changed from those used in the 1995 and 1996 evaluations. The new values are being used in ongoing evaluations of this type and will be reflected in a summary report to be issued in September 1997. Several of the individual evaluations summarized in this document will, to varying degrees, be superseded by ongoing evaluations, which will be summarized in the 1997 summary report, primarily because of more precise specification of degradation scenarios. Nevertheless, it is still useful to publish this 1996 summary report at this time for the following reasons: (1) all of the studies summarized are meaningful illustrations of the overall degraded mode probabilistic criticality evaluation methodology; (2) taken together, the studies summarized here cover most of the aspects of the methodology; (3) most of the environmental parameters are still under investigation, and the values may be expected to change significantly before License Application, some even returning to values closer to the ones which were used in the studies summarized here; and (4) several of these studies will not be superseded in the 1997 summary report. In particular, those analyses which will not be superseded do not rely on the environmental parameter assumptions which have been changed. Therefore, it is not necessary to

publish an assessment of the impact of the changed assumptions at this time.

The scenarios which could possibly lead to post-closure criticality are also summarized in Section 2. All such scenarios must begin with the breach of the waste package, and the most likely mechanism for such a breach is corrosion of the waste package barriers by water. Following such a breach, there are two general types of scenario which can lead to criticality: (1) removal of most of the neutron absorber material from the waste package leading to the possibility of internal criticality, and (2) removal of the fissile material from the waste package and reconcentration by some chemical mechanism in the rock. The possibilities for such scenarios are identified in Section 2; some details of the processes which make up such scenarios are discussed in Section 3.

The next step of the methodology is to analyze the chemistry/geochemistry processes to determine degradation rates and the likely composition of degradation products. These are discussed in Section 3. Degradation rates of the criticality control material and the waste form are primarily determined from experimental data, particularly for metal corrosion rates.

The cumulative effects of chemical/geochemical processes, particularly the dissolution of materials containing neutronically significant elements and the removal of one, or more, of these elements from the waste package, are tracked by the configuration generator code, developed specifically for this purpose. Configurations having the potential for criticality are identified and characterized in terms of concentrations of neutronically active species. For the criticality evaluations summarized in this document, the locations tracked are restricted to the interior of the waste package (internal criticality); the development of the code for this purpose is summarized in Section 4. As mentioned above, this document has some discussion of the possibilities for external criticality; however, these analyses do not yet make up complete scenarios, so the configuration generator code has not been applied to them. The extension of the code to locations outside the waste package (external criticality) will be described in future documents, including the 1997 Disposal Criticality Analysis Methodology Technical Report.

Calculations of k_{eff} are performed for the potentially critical configurations and the range of parameters identified with the configuration generator exercises described in the previous paragraphs. The results of the criticality analyses are used to develop a regression for k_{eff} as a function of the neutronically significant species. For the evaluations summarized in this document, commercial spent nuclear fuel (SNF), only iron and boron are used as independent variables in the regression because waste form (SNF) is assumed to degrade much more slowly than the waste package basket. The criticality calculations and the derivation of the k_{eff} regression are summarized in Section 5.

For those configurations which are confirmed as critical by the criticality analyses, the configuration generator code is re-applied, incorporating the appropriate k_{eff} regression to determine the earliest time of criticality occurrence and sensitivity to various parameters of waste package design, waste package materials and repository environment. The results are summarized in Section 6. The waste package materials and repository environment parameters will generally have some uncertainty. If such uncertainties are modeled as probability

distributions which are used to generate inputs to the configuration generator, the resulting criticality output parameters (time of earliest occurrence, etc.) can be interpreted probabilistically. Such probabilistic package analyses are in progress and will be reported in future documents, including the 1997 Disposal Criticality Analysis Methodology Technical Report.

The last step in the methodology is to estimate the consequences of any credible criticality (having a probability greater than a specified threshold). A simple analysis is illustrated in Section 7. For purposes of this simple analysis it is assumed that the criticality reaches a steady state characterized by a constant power output over some long duration. The principal consequence is then the increased radionuclide inventory produced by the burnup (product of the power output times the duration). It is shown that the increased radionuclide inventory is only a small fraction of the radionuclide inventory already present in the SNF at the time of emplacement in the repository. Studies are presently in progress to demonstrate that the pulsed behavior actually expected of any possible waste package criticality will produce a smaller increase in radionuclide inventory than the simple steady state model used in the analyses summarized in this document.

1.4 Scope

The scope of this document is the most likely of the possible criticality configurations resulting from the degradation of the waste package internals (waste form and basket containing it) for a commercial SNF waste package. The analyses are based on the state-of-the-art through 1996. This document will be supplemented (although portions may be superseded) by the 1997 waste package probabilistic criticality evaluation.

1.5 Quality Assurance

The Quality Assurance (QA) program applies to this document. The work summarized in this document is part of the preliminary WP design analyses that will eventually support the License Application Design phase. This activity, when appropriately confirmed, can impact the proper functioning of the Mined Geologic Disposal System (MGDS) waste package; the waste package has been identified as an MGDS Q-List item important to safety and waste isolation (Ref. 45, pp. 4, 15). The waste package is on the Q-List by direct inclusion by the Department of Energy (DOE), without conducting a QAP-2-3 evaluation. As determined by an evaluation performed in accordance with QAP-2-0, *Conduct of Activities*, the work performed for this analysis is subject to *Quality Assurance Requirements and Description* (QARD; Ref. 47) requirements. The applicable procedural controls for this activity are indicated in the QAP-2-0 work control activity evaluation entitled *Perform Probabilistic Waste Package Design Analyses* (Ref. 46). Guidance for the development and review of this document is provided in the *Technical Document Preparation Plan for the Supporting Analysis Results Summary Reports for the Disposal Criticality Analysis Methodology Reports* (TDPP; Ref. 37).

All inputs and assumptions which are identified in this document are for preliminary design and shall be treated as unqualified data; these inputs and assumptions will require subsequent qualification (or superseding inputs) as the waste package (WP) design proceeds. This document

will not directly support any construction, fabrication or procurement activity and therefore is not required to be procedurally controlled as TBV (to be verified). In addition, the inputs associated with this document are not required to be procedurally controlled as TBV. However, use of any data from this document for input into documents supporting procurement, fabrication, or construction is required to be controlled as TBV in accordance with the appropriate procedures.

The assumptions for this document are those given in the assumptions sections (4.3) of the supporting QAP-3-9 analyses (Refs. 1 through 4). In some of the topic areas the assumptions may differ between individual supporting QAP-3-9 documents; in those cases the controlling document is clearly identified.

The correspondence between the QAP-3-5 Section 5.2.C Items and the sections of this document is as follows:

<u>Item</u>	<u>Description</u>	<u>Location</u>
1.	Title page requirements (a - h)	On the cover sheets of the report.
2.	History of Change page	After title page(s), if required (revised).
3.	Table of Contents, Lists etc.	After title page(s) and History of Change page.
4.	Objective and scope	In Sections 1.2 and 1.4.
5.	Discussion of QA Controls	In Section 1.5.
6.	Identification of inputs	In Section 2.1.
7.	Identification of assumptions	Section 1.5 references associated QAP-3-9 documents which have the assumptions listed
8.	Location of unqualified inputs	In Section 2.1.
9.	References	In Section 9.
10.	Technical approach	In Sections 1.3, 2.2, 2.3, 3, 4.
11.	Identification of interfaces	N/A
12.	Presentation of information	In Sections 2 through 7.
13.	Computer software controls	In Section 1.6.
14.	Conclusions	In Section 8.

The correspondence between the items in the TDPP (Ref. 37) annotated outline and the sections of this document is as follows:

<u>Item</u>	<u>Description</u>	<u>Section</u>
1.0	Introduction	Same
1.1	Background	Same
1.2	Objective	Same
1.3	Scope	1.4
1.4	Quality Assurance	1.5
2.0	Analysis Model	1.3, 2.2, 2.3, 3, 4
3.0	Systems Analyzed	2.1
4.0	Analysis Results	6, 7
5.0	References	9

1.6 Computer Software

No computer software, other than a word processor, was used in the preparation of this document. Information on the various software packages and computer codes discussed in the text can be found in the supporting QAP-3-9 analyses in which they were used (Refs. 1 through 4).

2. Repository Environment

Knowledge of the expected range of WP environments is essential for any analysis of post-closure criticality performance. This section details those aspects of the environment which were considered in the analyses to date.

2.1 Environmental Parameters

2.1.1 WP Surface Temperature and Humidity

Two of the most important parameters for determining the rate of corrosion of the waste package barriers are the temperature and relative humidity. The former generally decreases with time, while the latter increases. The specific values are dependent on the hydrothermal model used. For the 1996 analyses, the temperature and relative humidity curves for the 83 MTU/acre low infiltration cases from TSPA-95 (Ref. 6, Figures 4.2-5 and 4.2-6, respectively) have been utilized. For the 1995 analyses, WP surface temperatures for a 24 MTU/acre low thermal loading were used (see Figure 2-1).

The drift wall temperatures of Reference 6 were used to develop waste package surface temperatures as a function of location within the repository according to the following methodology, which is explained in further detail in Reference 1. For early years, the waste package surface temperature depends primarily on its own internal heat and is best determined by a drift-scale calculation; for later years it depends on the average heat from all the packages and is best determined by a repository scale calculation. The calculation in Reference 1 began with the average temperature at the repository horizon as a function of distance from the repository center (approximating the repository by a disk), and used the average waste package heat generation rate (as a function of time) and a phenomenological formula for the waste package to drift wall heat transfer coefficient (incorporating the effects of convective and radiative heat transfer). The resulting blended temperature history is shown in Figure 2-1. The various curves represent time-temperature profiles at different locations in the repository; percentages give the fraction of waste packages that are closer to the center of the repository than the package in question (0% is at the center, 25% is halfway from center to edge, and 100% is the edge).

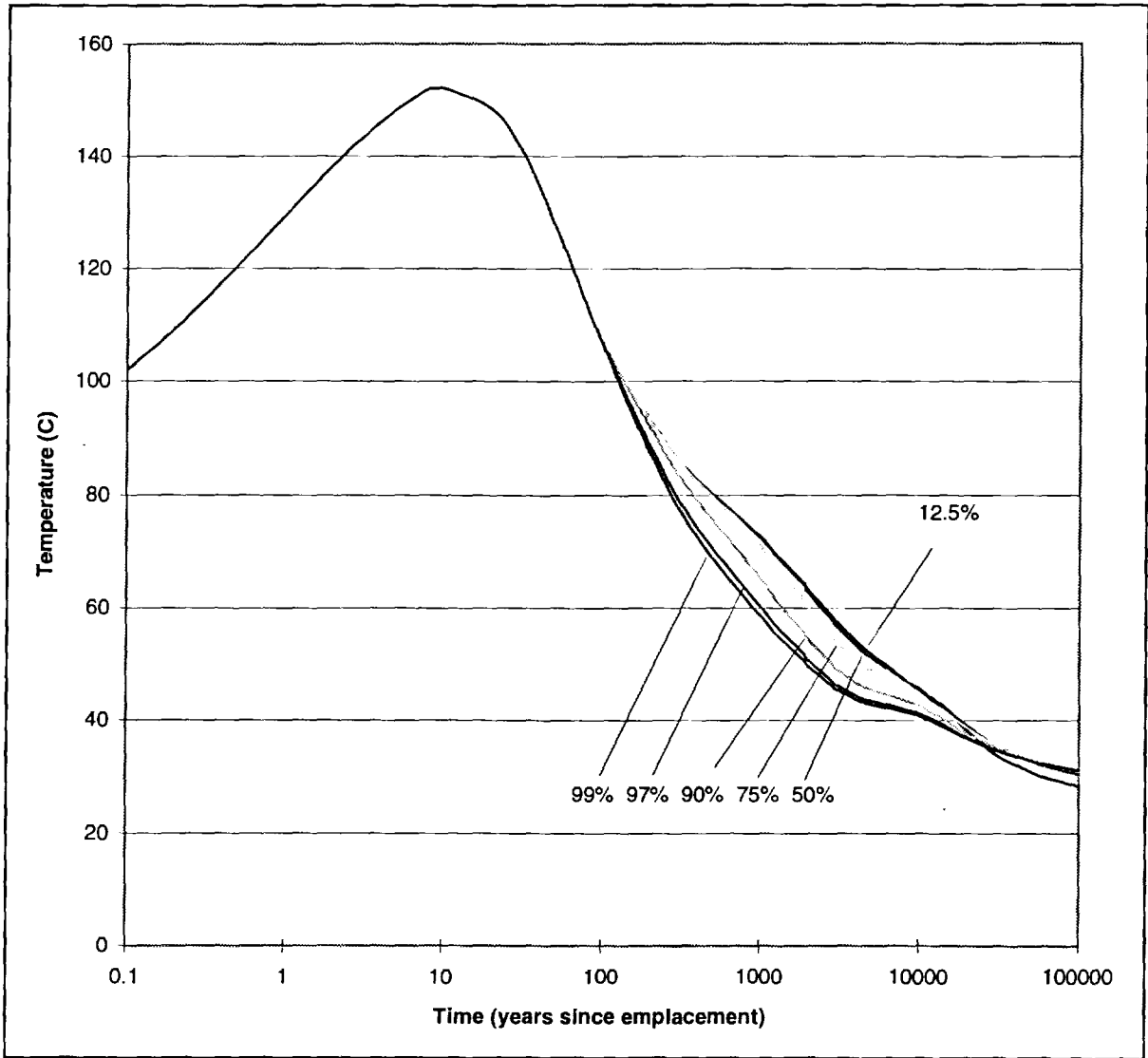


Figure 2-1. Waste Package surface temperature as a function of time for a mass loading of 6.0 kg U/m² (approximately 24 MTU/acre), distances from repository center (0% - center, 25% - mid-way from center to edge, 100% - edge)

2.1.2 Flow Rate of Water onto a WP Below a Dripping Fracture

Estimates of the level of ponding in a breached WP located below a dripping fracture require information about the rate at which water is dripping into the package. Along a similar line, the drip rate will also have an affect on the maximum steady state power level which could be achieved by a critical WP, as well as the duration of the criticality. Power and duration are the determinants of the radionuclide increment resulting from a steady state criticality, as shown in Section 7, below. The analyses summarized in this document use the dripping model which was used for the radionuclide transport calculations in TSPA-95 (Ref. 6). This section provides a summary of that model.

2.1.3 Infiltration Rate

The primary influence on the rate at which water drips on a WP located below a dripping fracture is the rate of water infiltration into Yucca Mountain. For some of the analyses this infiltration rate was assumed constant, usually 1 mm/yr, but also 0.1 mm/yr and 10 mm/yr for sensitivity evaluation. For other analyses, the changes in infiltration rate as a function of time were taken from the climate cycles postulated in TSPA-95 (Ref. 6, Section 7.7). For the TSPA-95 model, there are three parameters which must be defined: the cycle period, the minimum infiltration rate (I_{\min}) for the cycle (rate at time zero), and the maximum infiltration rate for the cycle which is a multiple of I_{\min} . For TSPA-95, this multiplier was uniformly distributed between 1 and 5. These distribution parameters were selected because of information indicating that during the last glacial maximum the annual precipitation rate was 2.5 times that of the present. The cycle period for TSPA-95 was fixed at 100,000 years (peak infiltration occurs at 50,000 years).

For determining the minimum infiltration rate, the two scenarios given in TSPA-95 were used: a low infiltration scenario where I_{\min} was uniformly distributed between 0.01 and 0.05 mm/yr, and a high infiltration scenario where I_{\min} was uniformly distributed between 0.5 and 2 mm/yr. It should be noted that the current hydrologic models of Yucca Mountain have a much higher minimum infiltration rate, 5 mm/yr. Nevertheless, the analyses summarized in this document, which used the then accepted lower infiltration range, are still valid for the following reasons: (1) The current minimum, 5 mm/yr, is within the range of values considered; (2) The extensive hydrothermal testing being done at Yucca Mountain will have to be completed before the final value is determined.

2.1.4 WP Drip Rate as a Function of Infiltration Rate

In transforming from the infiltration rate through the rock above the repository to the actual drip rate of water onto a waste package, TSPA-95 (Ref. 6, Section 7.3) used two multiplication factors. A statistical analysis of fracture density and the fact that matrix flow must be converted to fracture flow before it can drip onto the package (to overcome capillary action) is used to reduce the infiltration rate by a factor ranging from 0.25 at 0.1 mm/yr to 0.5 at 10 mm/yr. This flow must then be focused into a single point over a WP by a concentrating fracture network

covering a specific collection area. This collection area is defined as a multiple of the physical cross-sectional area of the emplaced WP interior as viewed from above (6.634 m² for 21 PWR; Ref. 2). For TSPA-95 the "concentration factor" was taken to be 4, and this value has been used here as well. The flow rate of water onto a WP located below a dripping fracture is then simply 26.54 m² times the drip rate. Table 2-1 below shows the range of peak dripping flow rates for the TSPA-95 low and high infiltration scenarios.

Table 2-1. TSPA-95 Peak Dripping Flow Rates Onto A WP

TSPA-95 Scenario	Peak Dripping Flow Rate (liters/year)		
	Minimum	Mean	Maximum
Low Infiltration	0.011	0.7	2.7
High Infiltration	5.8	68.1	190.8

2.2 Scenarios: General Characteristics

The AUCF PWR waste package design evaluated is summarized in Reference 2. It consists of a 10 cm thick outer barrier of corrosion allowance carbon steel and a 2 cm thick inner barrier of corrosion resistant steel. The specification of these barrier materials is given in Reference 2. The waste package for commercial SNF holds the individual assemblies in a basket with structure support from 0.5 cm thick carbon steel tubes and criticality control from 0.7 cm thick borated stainless steel plates. Before sealing the waste package lid, the interior is dried and filled with an inert gas (helium). This ensures that there will be no corrosion of the fuel rods or the basket materials until the waste package barriers have been breached and water or water vapor has entered the package. Therefore, all scenarios leading to criticality begin with breach of the waste package barriers and entry of water or water vapor.

It is shown in Reference 2 that the borated stainless steel basket provides sufficient neutron absorption that criticality is not possible, even in a waste package filled with water, as long as a significant fraction of this control material remains in proximity with the SNF. Therefore, all scenarios leading to criticality must provide some separation of the neutron absorbing material from the fissile material. The general ways in which this can happen for commercial SNF are shown in Figure 2-2. All scenarios begin with the waste package breached from the top and water entry, followed by dissolution of the basket material. For commercial SNF, the zircaloy cladding is much more corrosion resistant than the basket materials, so the latter will dissolve before the former as shown in Reference 2.

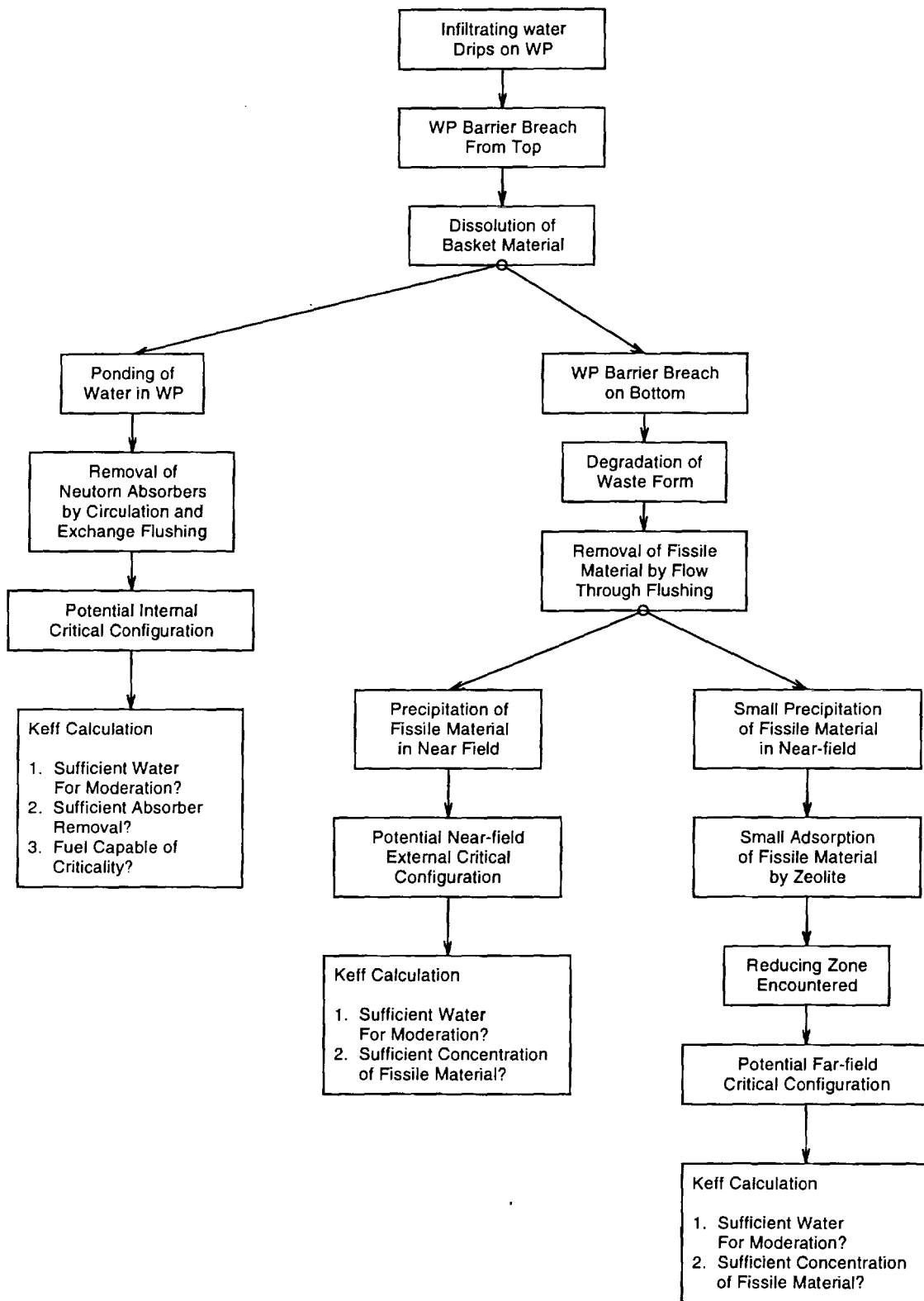


Figure 2-2. Illustration of Scenario Generation

The left branch of Figure 2-2 identifies the processes required to cause an internal criticality. The bottom of the waste package must remain intact while the dripping water circulates through the waste package (generally driven by thermal convection), and flushes the highly soluble boron (released by corrosion of the borated stainless steel basket material) from the package. It is shown in Reference 2 that criticality is possible after nearly all of the boron has been removed from the waste package in this manner. The specific results of this analysis are summarized in Section 6.2.

The other two branches in Figure 2-2 identify the processes which may lead to external criticality. These branches begin with breach of the bottom of the waste package [following the earlier breach of the waste package top] to facilitate the flow through the waste package, thereby permitting faster degradation of the basket and eventually degradation of the SNF itself, with the latter permitting removal of the fissile material (uranium and plutonium). The middle branch of Figure 2-2 indicates the processes for precipitation of the fissile material in the near field (invert of drift liner), while the right branch indicates the processes which could be responsible for accumulating a critical mass in the far-field. One mechanism for such a far-field accumulation is described in Sections 2.3.3 and 6.3, below.

2.3 Scenarios: Repository Environment Events and Processes

This section illustrates some of the more important repository environment processes and how they become essential parts of scenarios which can lead to criticality. These processes are used in partially completed scenarios to estimate criticality parameters in Sections 6 and 7 of this document. By the time of Viability Assessment (1998) these scenarios will be treated comprehensively. By the time of licensing, all possible processes will have been evaluated for significance with respect to enhancing the possibility/probability of criticality.

2.3.1 Internal Criticality: Corrosion Events Common to All Scenarios

The commercial PWR SNF waste package design evaluated in this analysis includes a basket with carbon steel structure for supporting the individual assemblies and stainless steel plates containing the strong neutron absorber boron for criticality control. Of these materials, the carbon steel has the fastest corrosion, but the principal corrosion product, iron oxide, is highly insoluble, so that removal of significant quantities will take upwards of 100,000 years, except at the very highest possible water infiltration rates (which are very unlikely). During this time, the iron oxide performs a significant neutron absorption function. The major neutron absorber, however, is the boron in the stainless steel. It will be shown in Section 3.2 that a major portion of the borated stainless steel is expected to resist corrosion for up to 30,000 years and thereby prevent criticality for at least this time period.

These processes of steel corrosion are quantified in Section 3.3 and applied to two alternative analyses of internal criticality summarized in Sections 6.1 and 6.2, below.

2.3.2 External Criticality Scenario Development Guidance from Natural Analogs

The analysis of naturally occurring uranium deposits provides some indication of geologic formations which could have some possibility of accumulating uranium from a flow out of the waste package. The following paragraphs summarize the efforts to evaluate the possibility of new accumulations and to assess the scenario implications of their occurrence. The objective of these preliminary analyses was to identify key processes in the building of scenarios. Details are provided in Reference 3.

2.3.2.1 Relevant Mineralizations in Geologic Provinces Which are Somewhat Related to the Yucca Mountain Geology

In a study of radioactive mineral occurrences in Nevada, L.J. Garside has suggested (Ref. 7, p. 8) that, "charcoal carbonization of wood at the base of ash-flow tuffs [serves] as a precipitant for uranium." He also suggests that organic matter can serve as a food for anaerobic bacteria producing H_2S which is also an effective uranium reductant. However, there is no direct evidence of any uranium deposits in tuff resulting from this mechanism, and the same reference notes that the uranium deposits at Coaldale Prospect [a low-grade Tertiary occurrence in Miocene sedimentary rock some 200 km northwest of Yucca Mountain] are not replacement deposits.

Although oil occurs in Nevada, it is not likely to be a reductant for dissolved uranium at Yucca Mountain. Oil accumulations in Railroad Valley appear to have migrated up from the Chainman Shale (Ref. 8, p. 10), and are not likely to be duplicated at Yucca Mountain because the recent higher temperature history in that vicinity would have decomposed any oil (Grow et.al., Ref. 9, p. 1298). Therefore, the identified Nevada oil accumulations are not analogous to any known conditions at Yucca Mountain.

With this evidence, it could be assumed that the organic deposits in Nevada are too weak to reduce uranium to concentrations found on the Colorado Plateau, let alone to the much higher concentrations found at Oklo. Nevertheless, since carbonaceous deposits of the log type do exist in Nevada at the base of ash-flow tuffs (Ref. 7, p. 8), and since a recognized geologic study has suggested that they could serve as a precipitant, it will be prudent to include the possibility in this analysis. For calculation purposes it will be assumed that logs could exist at the base of the tuff in Yucca Mountain (which is approximately 1 km below the repository) and in the concentration which appears on the Colorado Plateau. It is also assumed that any distribution of logs which did occur at the base of the tuff would not have a higher concentration than those found on the Colorado Plateau. It is not considered possible to have any significant organic accumulation within the tuff because the hot ash would have oxidized any organic material as it was deposited. The organic accumulations in tuff elsewhere in Nevada are attributable to carbonaceous material that occurs beneath the layers of tuff.

Although a reducing zone in the form of organic logs is conservatively assumed to be possible at the unconformity beneath the tuffs at Yucca Mountain, any significant roll-front deposition in tuff must be considered to be very unlikely, because fractures rather than interstitial porosity are thought to control fluid flow. In contrast, the interconnected porous grain structure of sandstone

provides a more uniform permeability throughout the bulk of the rock.

2.3.2.2 Potential for Uranium Concentration in the Tuff at Yucca Mountain

The maximum concentration of uranium which the zeolite clinoptilolite could accumulate by the ion-exchange mechanism from uranium-bearing outflow from a waste package at Yucca Mountain is most likely constrained by the maximum reported for natural deposits which have formed by this process. These maximum concentration occurrences include 0.9% at the Tono Mine in Japan (Ref. 10, pp. 445, 446, Figure 9 and Table I), or 0.7% at the more closely analogous Northern Reese River Valley (Ref. 11), or just under 1%, the maximum observed in the laboratory using uranium saturated water (Ref. 10, p. 448).

A realistic assessment of the maximum concentration of uranium likely to be adsorbed by zeolite from a flow is summarized in Section 2.3.3.2, below. To make an estimate of the maximum theoretically possible value, it is possible to make a more conservative estimate under the assumption that the uranyl ion could replace all the Ca ion in the clinoptilolite. Using the chemical formula for clinoptilolite, $K_{0.6}Na_{0.2}Ca_3Al_{6.8}Si_{29.2}O_{72} \cdot 1.6H_2O$, and replacing 3 Ca with 3 UO_2 , gives a uranium weight fraction of clinoptilolite of $g_u=0.236$. The following assumptions are used to convert this weight fraction of clinoptilolite to a weight fraction of rock: (1) both tuff and clinoptilolite have a density of approximately 2.52 g/cm³, (2) the rock matrix is 70 vol% clinoptilolite and 30 vol% other mineral phases, and (3) the rock has 30 vol% pore space which is filled with water. These assumptions give the following volume fractions of the rock:

ordinary clinoptilolite	$v_{co} = 0.7*(1-0.3) = 0.49$
tuff	$v_t = 0.3*(1-0.3) = 0.21$
water	$v_w = 0.3$

If R is the ratio of the molecular weight of clinoptilolite with calcium replaced by uranium divided by the molecular weight of ordinary clinoptilolite (R=1.245), the overall density of the rock, with Ca replaced by UO_2 and including water, is:

$$\rho_R = 2.52(Rv_{co}+v_t)+v_w = 2.37$$

The weight and volume fractions of UO_2 can then be computed from:

$$w_{uo2} = g_u R \rho_{co} v_{co} / \rho_R = 0.149$$

$$v_{uo2} = w_{uo2} \rho_R / \rho_{uo2} = 0.032,$$

where ρ_{uo2} is the density of $UO_2 = 10.96 \text{ g/cm}^3$ and ρ_{co} is the density of clinoptilolite = 2.52 g/cm³

Figure 6-9 shows that this volume fraction of UO_2 gives a k_{∞} less than 0.88, so it is impossible to form a critical mass from zeolite in tuff, even if all the Ca is replaced by commercial SNF UO_2 from uranium bearing groundwater.

2.3.3 Accumulation of a Far-Field Critical Mass: Possibility and Probability

This section explores the possible mechanisms for accumulation of uranium beneath a repository in Yucca Mountain by analogy with deposits of uranium found in nature. An organic reducing zone appears to be the mechanism which has the greatest accumulation capability. An upper bound on the probability for such a zone existing in, or beneath, Yucca Mountain is estimated.

This information is used in the following subsections to model an upper bound (on what a more refined model might predict) for the probability of the existence of a reducing zone of sufficient size and concentration to be capable of accumulating a critical mass of uranium from a commercial SNF waste package outflow beneath Yucca Mountain. This upper bound is based on the assumption that the natural environments that accumulated uranium in the past from natural sources will have the greatest probability of accumulating uranium from a future repository stream.

2.3.3.1 Types of Uranium Deposit

The United States (US) has approximately 30% of the world uranium reserves (J.W. Brinck, Ref. 12, p. 22), and most is near the Four Corners area of the Colorado Plateau and in Wyoming. Brinck has also estimated the United States total of 259,000 metric tons consists of individual deposits averaging 2,300 metric tons at an average ore grade is 0.195% (Ref. 12, p. 23). A higher average ore grade has only been reported for one country, South Africa, 0.29% (Ref. 13, p. 463), but that the total amount of uranium in those deposits is only 10% that of the US.

The largest and richest uranium deposits worldwide are associated with organic material in sedimentary rock. This organic material provides a reducing substrate to convert the soluble hexavalent uranium to the insoluble quadrivalent form, particularly the mineral uraninite (pure UO_2). The groundwater solution which flowed through the rock is generally assumed to have been enriched in hexavalent uranium (uranyl) from some upstream source rock of higher uranium concentration. The deposition substrate is either an organic material itself or H_2S (or some form of organic sulfur) generated by bacterial decay of the organic material. These deposits are found only in sedimentary rock, generally sandstone, but sometimes limestone. In one deposit (Oklo), the maximum ore grade of a small portion of the total deposit has been found as high as 60%; otherwise, the local peak ore concentration has never been above 20% (Ref. 14, p. 20). Certain individual uraninite nuggets have uranium concentrations as high as 88%, but these are so small in dimension as to not even be recorded in the general literature.

Another possible mechanism for uranium concentration is by deposition on fracture surfaces from hydrothermal (hypogenic) fluids which could have derived their uranium content directly from volcanic magma or from leaching of some nearby source rock. The precipitation from the hydrothermal fluid could be induced by cooling, by encountering an organic reducing zone, or by increased concentrations of inorganic ions (Ca or silicate) which can displace the uranyl from solution. This is the principal type of uranium concentration observed in tuff. Secondary enrichment can occur as uranium is mobilized in the weathering environment.

These general deposition mechanisms are limited by available surface area for chemical-physical reaction between solution and host rock. For the organic-reduction mechanism the large surface area is provided by either microfractures in the bulk organic material itself (e.g., a log) or the fine interstices of sedimentary rock containing a more refined organic material with little internal surface area. For the hydrothermal mechanism, the surface area is provided by extensive fracturing, which may result from the same hydrothermal process as provides the fluid or may have been pre-existing. For the zeolite exchange process, the effective surface area is provided by the cage structure of the zeolite itself.

2.3.3.2 Maximum Uranium Concentrations from Non-Organic Reducing Zones, Hydrothermal and Zeolite Deposition Process

The Pena Blanca uranium district, located 50 km north of Chihuahua City contains some of the richest uranium ore reported for tuff. The peak concentration of 9% uranium was found in a 13 cm diameter, very highly fractured breccia for a total uranium content of less than 3 kg UO₂. This particularly rich breccia sample is one of several characterized by P.C. Goodell (Ref. 15, Table 3, with the size information from a private communication with the author), as part of the Nopal 1 deposit, which is a pipe-like body 100 meters high with a 20 meter by 40 meter cross section, and an average uranium concentration of 0.11%, as reported by George-Aniel et.al. (Ref. 16, p. 238). The lower grades dominate the rest of the deposit; in fact, the latter reference does not even mention the 3 kg, 9% sample. The source rock for the lower grade deposits is believed to be rhyolites, which range from 10 to 35 ppm U₃O₈.

In the Pena Blanca district, only the peak grade sample (9%) is believed to contain quadrivalent uranium (specifically uraninite, UO₂, Ref. 15, p. 286, uraninite being identified with this peak sample as "in the breccia"). Although even this high a grade is insufficient for criticality of commercial SNF, it is an example of strong organic type reduction from the hexavalent solution which would be necessary to precipitate the higher concentrations required for criticality. The remainder of the district in general, and the Nopal 1 deposit in particular, is the result of a deposition process which does not reduce the hexavalent ions, but only incorporates this hexavalent uranium into carbonate, silicate, and oxide minerals, particularly uranophane [Ca(UO₂)₂(SiO₃)₂(OH)₂] (Ref. 15, p. 286). Similar low grade uranium deposits in tuff are found in Oregon (Ref. 17, p. 55) and in Nevada (Ref. 18, p. 104).

It is, therefore, concluded that there is very little likelihood of finding high organic concentrations in tuff, and those rare exceptions are likely to be small, like the 3 kg sample from Pena Blanca. However, there is a possibility of log-type organic deposits in basal pyroclastic deposits (at the base of the tuff), and this concept is quantified in Sections 2.3.3.5 and 2.3.3.6.

A review of the best known uranium deposit in zeolite, the Tono mine in Japan, has been given by Katayama et.al. (Ref. 10). The maximum uranium concentration reported in this reference is 0.9%. This observed concentration is consistent with the maximum uranium concentration achieved in a laboratory experiment also reported by Reference 10, p. 448. In this experiment the uranium concentration in the zeolite was found to increase linearly with uranium concentration in the contacting water, corresponding to a partition coefficient of 700, and to saturate at just under

1% uranium in the zeolite for uranium concentration in the water above 100 ppm. It should be noted, however, that these concentrations may be misleadingly high for the following reasons: (1) there is no assurance that the peak uranium in the samples from the Tono mine was actually contained entirely in the zeolite; (2) there is no assurance that the peak uranium measured in the laboratory samples was entirely in the solid (versus being partly in the solution which contained uranium); and (3) the peak aqueous concentration of U in the laboratory solution of 100 ppm can only occur under an extreme acidic or an extreme alkaline aqueous environment.

2.3.3.3 Maximum Uranium Concentrations Resulting from Reduction Zones of Organic Origin

The highest recorded grade of uranium ore, 60% was recorded at Oklo, Gabon. The original deposition of the uranium (over 2 billion years ago) is believed to have been due to the reduction of highly concentrated organic material, but the original organic material is no longer distinguishable as such, (Ref. 14, p. 19). On the other hand, the United States deposits with the highest concentrations of uranium ore generally contain organic material (or its fossilized remains) which is still identifiable.

Tabular deposits are of two types, peneconcordant (or true bulk) and roll-front (which is likely to be only a few feet thick). The former occupies a larger volume, but the latter is of higher concentration. This difference reflects the nature of the organic deposit responsible, either directly or indirectly, for the reducing zone which caused the uranium precipitation, the roll-front having been more concentrated than the peneconcordant. Neither of these types of tabular deposits has concentrations as high as the log type deposits, in which the boundaries of the organic material are still recognizable.

The summary of uranium deposits resulting from concentrated organic reducing zones has been given by Breger (Ref. 19); he reports a 64 element sample of mineral concentrations in logs primarily from the Colorado Plateau and Wyoming, with an average of 1.88% uranium (Ref. 19, pp. 102-105). The maximum concentration among these samples is 16.5%. Other reports of maximum concentration near 20% have been given by Hess (Ref. 20, p. 467) and Chenoweth (Ref. 21, p. 168).

The mechanism responsible for the strong deposition capability of organic matter is demonstrated by measurements of the partition coefficient between organic matter (humic material in the form of peat and lignite) and U bearing groundwater, with values as high as 10^4 , as reported in studies cited in Reference 22, p. 44; subsequent experiments, identified in the same reference, also indicate that it is the organic surfaces and not the humic acid in pore spaces which cause the adsorption.

Detailed chemical and X-ray diffraction examination of uranium log samples shows both crystalline and non-crystalline material (the latter of which may be either colloidal material or amorphous solids) (Ref. 19, p. 106). It should be noted that the crystallized mineralization usually only extends over a small fraction of the volume of the log. Furthermore, the uranium concentrations can vary by 2 orders of magnitude from one side of a log to the other, particularly

if the logs were oriented perpendicular to the direction of groundwater flow during mineralization.

The methodology described in this section is for commercial SNF which has low enrichment so the mass of U which can be accumulated by a single log will be insufficient for criticality. Therefore, a methodology must be developed to estimate the probability of occurrence of juxtapositions of randomly located/oriented logs, to form a reducing zone of the required size (or capacity).

2.3.3.4 Methodology for Estimating Probabilities

The upper bound for the probability of the groundwater from a single waste package precipitating into a critical mass is the product of the probability of the flow from a waste package encountering a carbonized log, $Pr\{\log\}$, multiplied by the probability that the log is part of a cluster of sufficient size to precipitate a critical mass, $Pr\{\text{critical_cluster}/\log\}$:

$$Pr\{\text{critical precip per pkg}\} = Pr\{\log\} * Pr\{\text{critical_cluster}/\log\}$$

The fraction of the log volume which is actually replaced by uranium, or on which uranium is actually adsorbed, will be modeled as a uniform distribution over the range of uranium concentrations actually observed in the log uranium deposits. It is found that the required cluster size, or mass, is inversely proportional to the fissile content of the fuel in the waste package which served as the source of the groundwater flow, and is also inversely proportional to the uranium and water concentrations, as indicated in (Ref. 3, Table 7.5-1).

The total probability of criticality is obtained by multiplying $Pr\{\text{critical precip per pkg}\}$ by the number of waste packages having sufficient fissile percentage to produce a criticality with the cluster size associated with the corresponding $Pr\{\text{cluster}/\log\}$.

The next two sections describe the computation of $Pr\{\text{cluster}/\log\}$ and of $Pr\{\log\}$.

2.3.3.5 Probability of Sufficient Reducing Material to Make Accumulation of a Critical Mass Possible, $Pr\{\text{cluster}/\log\}$

This section is a summary of the data analysis and calculations described in Attachment II of Reference 3.

The concentrations of uranium sufficient for a critical mass of low enriched uranium (commercial SNF) can be modeled by the juxtaposition of logs onto a circle through the cross section of the critical mass sphere, to achieve the required critical mass (upwards of 1 metric ton UO_2). The probability of such random juxtapositions is built from the probability distributions of log length and of uranium concentration within the log.

In this model, three parameters of the imputed organic logs are generated from specific distributions: log length, potential concentration of uranium, and log radius. For the distribution

of log lengths, the analysis of Attachment III of Reference 3 shows a negative exponential distribution with a floor of 3.0 meters and a decay length of 4.6 meters.

Based on analysis of 3 data sources in Attachment II of Reference 3, a uniform distribution between 1% and 21.5% is used for potential uranium concentration:

$$f_c(x) = 1/(x_2-x_1) \quad \text{for } x_1 < x < x_2$$

where the variable x is expressed as a fraction (instead of a percent), and the distribution is defined by the constant values $x_1=0.01$, $x_2=0.215$. This distribution gives an average ore grade (U_3O_8 concentration) of 11.25%.

Design analyses have shown that for the highest concentration permitted by this distribution, 21.5 wt% (4.3 vol% assuming 47 vol% water in the remaining rock, or 4.6 vol% assuming 40 vol% water in the remaining rock), $k_{eff} < 0.9$ (Ref. 5, Appendix C, Figure 7-1) so there is no possibility of criticality of any size log of this concentration. It is still necessary, however, to consider the juxtaposition of logs as representing the possibility of higher concentrations, even though no single log could reach such high concentrations. The model assumes, for simplicity, that the organic material is concentrated by the overlapping of multiple logs. This is somewhat conservative, because spreading over a larger volume would generally increase k_{eff} . In other words, the higher concentration of overlap is a surrogate for the larger volume of adjacency, which will be discussed further below.

Although no geological analogs for such an organic reducing zone concentration process exist in the United States, it is thought that some highly concentrated organic reducing zone was responsible for the highest uranium concentrations observed at Oklo (up to 60%, Ref. 14, p. 20). In the absence of a geochemical model of the transformations which would be required for such a concentration process, the probabilistic/analog analysis is offered as a very conservative estimate. The probabilities of occurrence of the actual physical and chemical processes are currently unknown. Because of the lack of direct observations of the actual occurrence of such processes, any associated probabilities are expected to be quite small, but assumed to be unity for this analysis (to be simple and conservative).

For the distribution of log radii, the smallest of 4 diameters cited by Hess (Ref. 20, p. 467) is 16 inches, which translates into a radius of 20 cm, is used as the lower limit. The distribution is taken to be triangular with a peak at this lower limit, based on anecdotal information from those who have seen the logs (Ref. 23) and the assumption that only the few largest logs are of sufficient interest to be reported in the literature. Since the probability density of a triangular distribution decreases to zero at the upper limit, this upper limit is taken to be well above the radius corresponding to the maximum observed diameter, 4 feet (61 cm radius) given by Hess. This distribution is a conservative model because the Hess article is primarily interested in reporting the largest ore concentrations, which would correspond to the largest logs. This conservative designation for the model is also consistent with the Chenoweth (Ref. 21, p. 166) statement cited above that the largest log diameter is 1 meter. The probability density function (pdf) for the resulting triangular distribution is:

$$f_i(r) = 2(r_2-r)/(r_2-r_1)^2 \quad \text{for } r_1 < r < r_2$$

where $r_1=0.20$ meter, $r_2=0.80$ meter.

As a worst case, the potential for criticality of the largest log can be estimated under the further conservative approximation that it contain the maximum possible uranium concentration, 21.5 wt%. It was already shown, above, that $k_{\infty} < 0.9$; however, it is of interest to evaluate k_{eff} for this case. For 4.6 vol% UO_2 , with the remaining rock being 40 vol% water and 60 vol% tuff, $k_{\text{eff}} = 0.79$ (Ref. 24).

The methodology for combining logs can now be summarized by an algorithm stated as follows: (1) determine a critical mass - critical radius pair from the set generated in Reference 30, and apply the adjustment factors 0.325 and 0.686, respectively, as a measure of conservatism to account for the neutron contribution of the portions of the logs falling outside the critical sphere; (2) select the three random parameters for a sample log from the appropriate distributions as described above (log length, log radius, uranium wt%); (3) calculate the contributed mass for this log from the formula:

$$m_j = 2.62\pi r_l^2 r_c u_j (4/\pi),$$

[where 2.62 g/cm^3 is the density of tuff (which is conservative with respect to the logs found in the Uravan Mineral belt which are mostly coal which is half this density); r_l is the radius of the log; the factor $(4/\pi)r_c$ is the average length of a segment falling within a circle of radius r_c for a longer line passing entirely through the circle; and u_j is a random variable representing the weight percent of uranium in the log, with the subscript j to indicate that its Monte Carlo selection process will be distinct from the Monte Carlo selection of log length] and accumulate the sum of the masses of overlapping logs thus far; (4) multiply the accumulated probability by the value for this log as computed from Eq. (1) of Attachment II of Reference 3, using the uncorrected sphere radius; and (5) if the accumulated mass is greater than the required critical mass, end the calculation and report the remaining probability, otherwise repeat steps (2) through (5) for the next log. This algorithm is repeated, starting with step (1), for each critical mass - critical radius pair in the set generated in Reference 24.

2.3.3.6 Probability of Encountering a Log, $\text{Pr}\{\text{log}\}$

The calculations of this section are based on the possible analogy between the planar distribution of logs observed on the Colorado Plateau and logs which could be distributed somewhere at the base of the tuff beneath Yucca Mountain.

Since there are no statistics on logs at the base of the ash-flow tuff of Yucca Mountain, there is no direct way to estimate $\text{Pr}\{\text{log}\}$. A very conservative upper bound can, however, be developed from statistics of the log occurrences on the Colorado Plateau, according to the formula:

$$\text{Pr}\{\text{log}\} = (\text{Area occupied by logs})/(\text{Area of sample space})$$

where the sample space is the area which has been investigated for logs. The analysis starts with the 84 logs counted in the 87,000 m² orebody described by Fischer (Ref. 25). Using the triangular distribution of log radii given above, the average radius can be calculated as 40 cm so that the average diameter is 80 cm. Using the negative exponential distribution of log lengths given above, an average of 7.6 meters is calculated. The total cross-section area of 84 logs lying horizontally is 511 m². The question is what larger area (or sample space) this represents.

Chenoweth (Ref. 48) has estimated that the geologic formation of the Colorado Plateau in which the logs are found occupies 1,100 square miles (2,850 km²). He has also estimated that there are 165 orebodies similar to the one mapped by Fischer in this area. Since these orebodies have not been mapped for log occurrences, the best estimate of the total log area in this 2,850 km² sample space would be to simply multiply the 511 m² of the Fischer orebody by 165, giving a total log area of 84,000 m². This analysis is equivalent to the assumption that the sample space for the distribution of organic deposits (to be found at the base of the tuff under Yucca Mountain) is the entire geologic formation containing log deposits in orebodies on the Colorado Plateau.

An alternative, and more conservative, interpretation would be that the identified orebodies do not represent all the occurrences of logs, only those which would be mineralized. To be mineralized, the organic log must not only exist, it must also be contacted by a uranium-bearing outflow from the repository. Since there is no way to estimate the number of unmineralized logs in the large sample space identified by Chenoweth, the alternative is to use a smaller sample space. This can be defined by examining a map of orebodies in a buried river channel given in Thamm et. al. (Ref. 23, p. 50) which shows the orebodies to be occupying approximately 7% of the riverbed. Since the entire river channel was probably exposed to the same uranium-bearing groundwater, the identified orebodies should represent all the organic matter present. Hence the area of this smaller, more conservative, sample space could be estimated by dividing the area of the orebody by 0.07. This analysis is equivalent to the assumption that the sample space for the distribution of organic deposits (to be found at the base of the tuff under Yucca Mountain) is a typical buried river channel found on the Colorado Plateau and diagrammed in Reference 23, and that such a buried river channel exists at the base of the tuff beneath Yucca Mountain.

The results for the two alternative interpretations are given in Table 2-2.

Table 2-2. Alternative Estimations of Probability of Encountering a Log

Sample Space	Area of sample space (km ²)	Total log area in sample space (m ²)	Pr{log}
Underground river channel	1.24*	511	4.1x10 ⁻⁴
Geologic formation	2850	84,000	2.9x10 ⁻⁵

* Calculated from Reference 23, Figure 16.

3.0 Chemistry/Geochemistry/Mechanical Processes

The purpose of this section is to identify the modes of degradation which may affect the waste package subcomponents (e.g., barriers, fuel assemblies, basket guides, tubes, absorber plates, and fuel rods) and their effect on the configuration/geometry of the waste package. These processes are analyzed to provide guidance for the design of waste package criticality control measures and to illustrate processes which will ultimately become components of definitive scenarios used demonstrate compliance with the licensing regulations for criticality control.

These preliminary findings on degradation processes are also used as inputs to a structural analysis which evaluates the possibility of mechanical failure to partially degraded structures, particularly the degraded waste package barriers and the degraded basket. The forcing/loading functions for this mechanical failure can range from the continuously applied stress of backfill overburden (or the gravitational weight of the remaining package itself) to the impulsive applied rockfall. This analysis is summarized in Sections 3.3 and 3.4, respectively, for these two extremes of mechanical failure forcing/loading function.

3.1 WP Barrier Degradation (pre-TSPA95)

A summary of prior corrosion models was given in Reference 1. It was found that an appropriate equation for integrating the penetration depth (P) in the presence of a time dependent temperature (T) is:

$$\frac{dP}{dt} = cP^{(c-1)/c} A^{1/c} \exp[kh/c - B/(cT)] \quad (3-1)$$

where h is the complement to the relative humidity H , and given by the expression $h = 100 - H$ (in %), and the remaining factors are constants determined from the corrosion test data for the particular steel involved. It should be noted that Eq. 3-1 provides an expression for the corrosion rate that depends only on the amount of corrosion product present and the environmental conditions. For numerical processing of Eq. 3-1 it is convenient to use the integrated form:

$$P_f^{1/c} = P_i^{1/c} + A^{1/c} \int_{t_i}^{t_f} \exp[kh/c - B/(cT)] dt \quad (3-2)$$

where the subscripts i and f indicate initial and final values, respectively. In Reference 1 a C program was used to perform this integration to estimate the times of first penetration for both barriers as a function of the temperature dependence for six WP locations indicated in Figure 2-1, and as a function of the constants which are specified by probability distributions which are derived in Reference 1. The time to penetrate the 120 mm thick dual-barrier waste package was determined by using the parameters for carbon steel until the penetration depth was equal to 100 mm (the thickness of the outer barrier), and then switching to the Alloy 825 parameters for the remaining 20 mm (note that this was the inner barrier material at the time this analysis was performed; current material is Alloy 625). Also, for the Alloy 825 barrier, c was assumed to be 0.75 for the first 5,000 years of inner barrier exposure, and 1.0 thereafter. This is equivalent to

assuming the corrosion product layer becomes unprotective after 5,000 years and adds an extra degree of conservatism to the estimate of inner barrier lifetimes. The results of the evaluation are given in Table 3-1 for both the continuous and intermittent wetting cases. Because this model maps location to temperature distribution and calculates the penetration time as a function of the time history of temperature, it is called the temperature distribution model.

Table 3-1. WP Time To Breach Predicted by Temperature Distribution Model

Repository Location	Intermittent Wetting		Continuous Wetting	
	Outer Barrier Breached (years)	Inner Barrier Breached (years)	Outer Barrier Breached (years)	Inner Barrier Breached (years)
12.5%	3150.1	34807.3	680.9	8188.9
50%	3198.2	33364.5	681.1	8250.1
75%	3496.4	34850	688.4	8594.4
90%	4402.6	38286.2	762.0	9348.2
97%	5279.5	40843.4	876.6	9960.1
99%	5579.7	41665.6	923.9	10174.8

3.2 Waste Package Basket Degradation: Borated Stainless Steel

This section summarizes the development given in Reference 1 for the probability density function for the corrosion of a critical fraction of the basket. This critical fraction of basket corrosion which can be tolerated depends on the actual SNF characteristics. The basket will have sufficient boron that 20% of the basket can be lost before any of the commercial fuel can exceed the 5% sub-critical safety margin with bias and uncertainty. The conservative assumption was made that a loss of 60% of the basket would permit no more than 50% of the expected fuel to exceed the criticality safety margin. A more precise analysis based the expected characteristics of the commercial fuel discharges was given in Section 7.4.4 of Reference 1, and showed this assumption to be very conservative. The following sub-sections summarize the methods used in Reference 1 to develop the parameters for a Weibull distribution for the probability density function for both continuous and intermittent wetting conditions.

3.2.1 Minimum Time to Corrosion of a Critical Fraction of the Basket

The principal criticality control material, boron in borated stainless steel will be released by the congruent dissolution of the steel (which means that the metal borides and the surrounding stainless steel matrix will degrade/corrode at the same rate). In Reference 1 the fastest possible

rate for this process was conservatively taken to be the same as the general corrosion rate of Type 316 stainless steel immersed for 16 years in seawater at the Panama Canal, which was found to have experienced a corrosion rate of 1.25 $\mu\text{m}/\text{yr}$. Since the basket can be attacked on both sides, this rate was doubled to get a minimum time to corrode 10 mm of Type 316 stainless steel of 4,000 years (note that at the time Ref. 1 was performed the WP had 10 mm of borated stainless steel plate, but currently has 7mm of borated stainless plus a 5 mm thick carbon steel tube in each fuel cell). The 60%, or 6 mm thickness of basket material, identified as critical in Section 3.2, above, would be removed in no less than 2,400 years of exposure to seawater. This time has been conservatively taken to be the lower limit for the 60% basket degradation time for three different wetting conditions.

3.2.2 Corrosion Under Continuous Wetting Conditions

For Reference 1 a literature search was performed to locate general corrosion data for Type 316 stainless steel in aqueous environments similar to that which may result on a WP that is continuously wetted by infiltrating water. Information on the corrosion behavior of Type 304 stainless steels was also included because more extensive testing has been performed for Type 304 than 316, and because Types 304 and 316 were found to have relatively similar corrosion rates in tests which included both alloys. The mean-time-to-corrode 6 mm of stainless steel was found to be 19,823 years, with a standard deviation of 8,724 years. Using this mean-time-to-failure (MTTF), standard deviation, and the value of Weibull parameter θ set equal to the minimum to 60% degradation found in Section 3.2.1, above, the remaining parameters of the Weibull distribution were determined using the expressions:

$$MTTF = \theta + \alpha \Gamma(1 + 1/\beta) \quad (3-3)$$

and:

$$\sigma = \alpha \sqrt{\Gamma(1 + 2/\beta) - [\Gamma(1 + 1/\beta)]^2} \quad (3-4)$$

where $\Gamma(n)$ is the gamma function evaluated at n . The parameters, α and β , were found to be 19,671 and 2.098, respectively.

3.2.3 Corrosion Under Intermittent Wetting Conditions

The 60% basket degradation pdf for the intermittent wetting case was developed by modification of the above lower limit, mean-time-to-corrode, and standard deviation developed for continuously wetted stainless steel. As before, this modification was based on the results of general corrosion test data for Types 304 and 316 stainless steel, and a further search of the available literature was performed to locate corrosion tests of intermittently wetted samples. This test condition was assumed to be more applicable to overhead dripping than that of the continuous immersion tests used for flooding, because the level of water in the basket of a breached WP may change with time due to fluctuations in the drip rate, evaporation rate, or the formation of drainage holes. The analysis in Reference 1 indicated that a conservative estimate

of the MTTF under intermittent wetting conditions would be twice that for the continuous wetting case. Doubling of the above mentioned parameters results in a θ of 4,800 years, a MTTF of 39,646 years, and a standard deviation of 17,448. Using the Weibull expressions for MTTF and standard deviation presented in the flooding breach and leach discussion, α and β were determined to have values of 39,343 and 2.098, respectively. A summary of these results is given in Table 3-2, below.

Table 3-2. Summary of Neutron Absorber Degradation Times (years)

Condition	Mean	Std Dev	Min
Intermittent Wetting	39646	17448	4800
Continuous Wetting	19823	8724	2400

3.3 Mechanical Deformation/Failure Following Partial Basket Degradation

This section discusses the three primary basket components responsible for maintaining the initial configuration of the WP, and the anticipated changes in the WP configuration which will occur as a result of their degradation as evaluated in Reference 2. These are the side and corner guides, the neutron absorber plates, and the fuel cell tubes.

3.3.1 Neutron Absorber Plates

The Advanced Unclad Fuel (AUCF) WP neutron absorber plates are fabricated from 7 mm thick borated Type 316L stainless steel plates. Since long-term corrosion testing of this material in repository type environments is just beginning, specific corrosion models are not yet available. However, a preliminary evaluation can be made by using previous data collected for 316 stainless steels (Ref. 26), and scoping corrosion tests which compared borated and unborated stainless steels (Ref. 27). For J-13 well water in the temperature range expected after WP breach for the 83 MTU/acre cases, Reference 26 found that the general corrosion rate of 316L stainless steel ranged from 0.037 $\mu\text{m}/\text{yr}$ at 100°C to 0.154 $\mu\text{m}/\text{yr}$ at 50°C. Scoping corrosion tests (Ref. 27) of borated and unborated Type 304L stainless steels in an extremely aggressive environment (pH = 3.8) found that the borated stainless steel had a corrosion rate that was approximately 4 times higher than that of the unborated stainless steel. Using the above 316L rates, multiplied by an adjustment factor of 4, suggests that it will take 2,000 to 8,500 years following breach of the WP for general corrosion of both sides of the neutron absorber plates to remove the 2.5 mm of material that would be required (Ref. 28) for bending to occur. It will take 4,000 to 17,000 years following breach of the WP for general corrosion of both sides of the neutron absorber plates to remove the 5.05 mm of material that would be required for buckling of the vertical plates to occur if backfill is loading the basket, and 4,300 to 18,000 years to remove the 5.36 mm of material that would be required if backfill is not loading the basket. This information is summarized in Table 3-3 below.

Table 3-3. Times to Neutron Absorber Plate Collapse

Failure Mode	Critical Corrosion Depth	Time After WP Breach To Corrode To Critical Depth
Buckling without Backfill	5.36 mm	4,300-18,000 years
Buckling with Backfill	5.05 mm	4,000-17,000 years
Bending	2.5 mm	2,000-8,500 years

It should be noted that the above failure times assume that the localized corrosion mechanisms, such as pitting or stress corrosion cracking, do not severely affect the structural capability of the absorber plates. This assumption is expected to be valid because the faster localized penetration which can result from pitting typically affects only a small fraction of the overall surface area of stainless steels due to the high aspect ratio of the pits. Stress corrosion cracking in stainless steels typically requires tensile stresses in excess of one-half yield, an aggressive environment, and a sensitized material (chromium carbides precipitated at grain boundaries due to improper heat treatment or welding). The criticality control panel assemblies will be fabricated by interlocking borated stainless steel plates. Structural calculations have shown that stresses in the plates due to the static load of the fuel are below one-half yield. In addition, these plates will not be welded nor exposed to sensitizing temperatures at any time, so sensitization is not expected. However, in some cases (boiling water reactor environments), increased susceptibility to stress corrosion cracking has been associated with exposure to high neutron fluences ($> 10^{20}$ n/cm²). Such fluence levels could not be achieved in the plates under exposure to spent fuel before other mechanisms would cause their failure.

3.3.2 Fuel Cell Tubes

The fuel cell tubes are fabricated from carbon steel and have a wall thickness of 5 mm. The tubes will fully degrade before the failure of the side guides or the criticality control plates. In analyzing the criticality control plates, it was determined that the plates could maintain the basket and SNF assembly configuration without structural support from the tubes. Failure of the tubes will, therefore, not cause collapse of the basket, so no specific analysis was performed for the tubes. However, the remaining corrosion products occupy a greater volume than the original tubes and are fairly insoluble. Thus the presence of the corrosion products may have some impact on WP internal criticality.

3.4 Rockfall Hazard to a Partially Degraded Waste Package

The hazard of rockfall onto a severely degraded waste package illustrates the importance of the interaction between a chemical degradation process and a mechanical impact event. Rockfall onto a severely degraded WP presents a mechanism for collapsing the basket structure and thereby creating an opportunity for rapid reactivity insertion. Although analyses thus far indicate

that a collapsed configuration will be less neutronically active (because of moderator exclusion) it is still of interest to evaluate the potential for such an event. The analysis of WP barrier response to rockfall presented here was performed in Reference 28.

The 100 mm thick outer barrier provides the primary defense against damage from large rockfalls. The TSPA-95 general corrosion models for carbon steel (Eq. 3-5 & 3-6) were used to estimate the outer barrier thickness as a function of time for the purpose of showing how the rockfall mass required to plastically deform the WP outer barrier to the point of crack initiation changes with time. The TSPA-95 model for humid-air general corrosion of carbon steel (Ref. 6, p. 5-25) is given by:

$$D_g(t,RH,T) = \exp[16.984 + 0.6113 \ln(t) - \frac{893.55}{RH} - \frac{833.27}{T}] \quad (3-5)$$

where D_g is the general corrosion depth (μm), t is the exposure time (years), RH is the relative humidity (%), and T is the temperature (K). The TSPA-95 model for aqueous general corrosion (Ref. 6, p.5-26) is given by:

$$D_g(t,T) = \exp[111.5 + 0.5320 \ln(t) - \frac{23300}{T} - 3.193E-4 T^2] \quad (3-6)$$

where the variable definitions are the same as for Eq. 3-5. Humid-air corrosion was initiated when the relative humidity was greater than 70% (middle of the TSPA-95 range of 65-75%,Ref. 2, p. 5-23), and aqueous corrosion was assumed to initiate when the relative humidity was greater than 90% (middle of the TSPA-95 range of 85-95%,Ref. 2, p. 5-23) and the temperature was less than 100°C. Use of the general corrosion rate for this purpose is based on the assumption that localized corrosion mechanisms such as pitting, which may have produced earlier penetrations of the barrier, will not significantly affect the structural capability of the barrier. This study was performed for the 83 MTU/acre, low infiltration, no backfill case only, as rockfall would not be expected to be a concern for the backfill case (most if not all of the space above the waste package would be filled with backfill, thus preventing the rock from contacting the WP). The outer barrier thickness was determined in two-year timesteps. At timestep t_i , the outer barrier thickness remaining is given by:

$$L_i = L_{i-1} - \frac{dD_g(t_i-t_0, RH_i, T_i)}{dt} (t_i - t_{i-1}) \quad (3-7)$$

where i indicates the timestep, L is the outer barrier thickness (μm), t is the time since emplacement (years), t_0 is the time of initial exposure, RH is the average relative humidity for the timestep, T is the average temperature for the timestep, and D_g is either Eq. 3-5 or 3-6 as indicated by the relative humidity and temperature rules discussed above. The results are shown in the Figure 3-1.

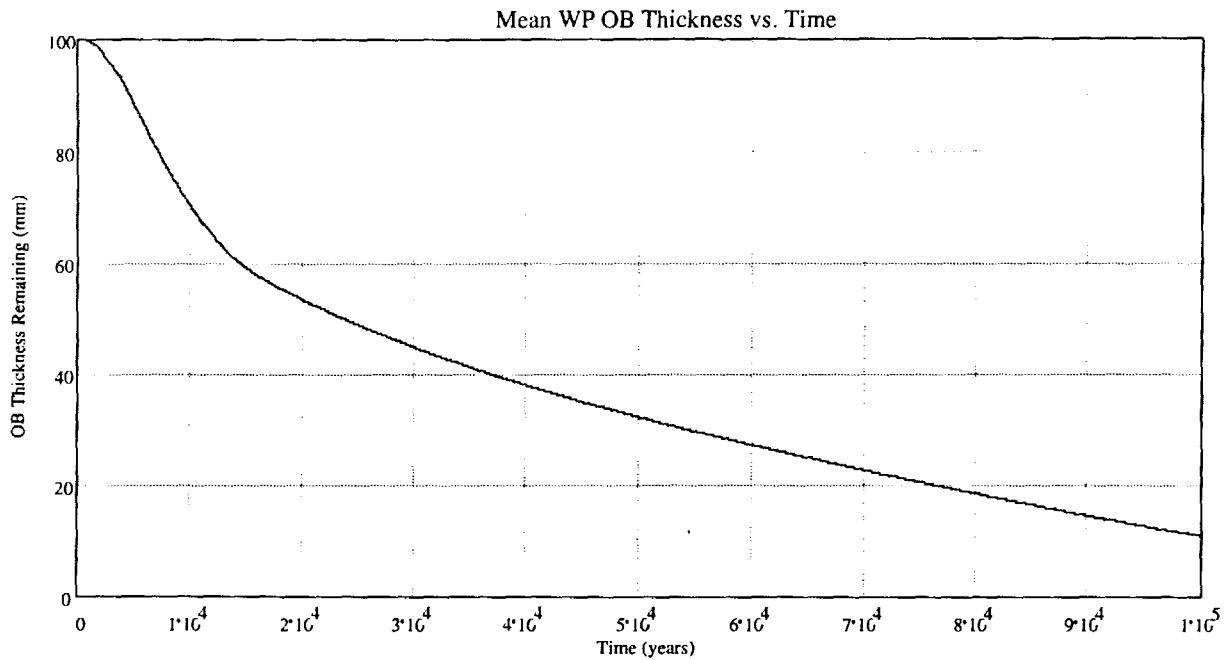


Figure 3-1. Mean WP Outer Barrier Thickness as a Function of Time

Using Figure 3-1 and the preliminary information on critical rockfall mass as a function of outer barrier thickness provided in Reference 44, Table 3-4 has been generated. This table relates critical rock masses with the times that the barriers will have thinned to those dimensions. Based on this information, an initial conclusion can be made that the WP will retain much of its initial robustness against damage from rockfall throughout the time period required for corrosion to cause collapse of the basket. This conclusion, however, is subject to future revision as more information on the distribution of potential rockfall masses becomes available.

Table 3-4. Critical Rock Mass With Respect to Time

Degradation Level	Time (years)	Critical Rock Mass (kg)
0% Outer Barrier Degradation	0.00	38,000
50% Outer Barrier Degradation	23,000	24,000
75% Outer Barrier Degradation	54,000	3,500

4.0 Configuration Generator Code

The configuration generator code (also referred to as the “configuration bookkeeper”) is intended to track the movements of the neutronically significant species from dissolution of their initial forms through local precipitation and through removal from the waste package and accumulation external to the waste package. It is also used to identify the conditions and times at which criticality can occur. This section provides a summary of the algorithms used in the code and an example of its application to evaluate the time required to remove those materials important to criticality control from a WP.

As explained in Section 2.2, the waste package is sealed with an inert interior atmosphere, and the corrosion process cannot start until the waste package barriers have been breached. Therefore, the degradation of the waste package interior begins with corrosive attack from a humid and/or aqueous environment containing oxygen. The time of breach depends on the rate of corrosion of the waste package barriers. This process has been modeled in other studies, with first penetration times ranging from 2,000 years to 10,000 years with very conservative models which have relatively rapid corrosion (Ref. 6). The initial studies summarized in this document did not specifically include the barrier degradation processes or the penetration time, because the neutronics calculations were based on the worst case isotopics of the peak of k_{eff} as a function of time, which occurs between 10,000 and 20,000 years following discharge, irrespective of the actual time since discharge.

4.1 Model Description: Commercial SNF Example

The waste package interior degradation model solves the coupled first order differential equations which connect the concentrations of neutronically significant species and those species which effect the solubility of the neutronically significant species. For the initial analyses, the fissile species in the commercial SNF were assumed to remain intact, so the only species tracked were the neutron absorbers, iron and boron in the three phases: steel, oxide, and in solution. The model follows directly from the standard interpretation of chemical processes in terms of first order, time dependent linear differential equations.

Corrosion of borated stainless steel is assumed to release boron congruently, but a fraction, f , of the boron released thereby is assumed to be trapped in the solid iron oxide as it is being formed. This is a reasonable and conservative assumption since the boron in the stainless steel is in the form of a boride of iron, or other metal component of stainless steel, and such borides are generally found to be very stable and corrosion resistant. In the present illustration the range of values for f will be 0.0 to 0.055.

The model assumes that the water containing dissolved Fe, B, and oxygen is circulated (by convective cooling of the heat generating assembly) so that it passes in the vicinity of waste package holes through which it can overflow or otherwise exchange with the water outside the waste package. The potential for criticality is enhanced by this circulatory exchange in two ways: (1) the removal of the neutron absorbing corrosion products, and (2) the replenishing of the oxygen supply to support further corrosion. The principal processes, and the differential

equations describing their time dependence and coupling, are as follows:

Carbon steel change:

$$dm_{fec}/dt = -c_rate_cs; \quad \text{provided } m_{fec} > 0.$$

Stainless steel change:

$$dm_{fes}/dt = -c_rate_ss*(1-\alpha); \quad \text{provided } m_{fes} > 0.$$

Iron oxide change:

$$dm_{feo}/dt = c_rate_ss + c_rate_cs - ex_rate*fe_sol;$$

in which the first and second terms on the right side are included if the mass of stainless steel and the mass of carbon steel are greater than zero, respectively.

Boron in stainless steel change:

$$dm_{bs}/dt = -c_rate_ss*\alpha; \quad \text{provided } m_{bs} > 0.$$

Boron trapped in the solid iron oxide change:

$$dm_{bor}/dt = f*c_rate_ss*\alpha - ex_rate*fe_sol*m_{bor}/m_{feo};$$

in which the last term on the right side represents the trapped boron released to solution as the iron oxide is permitted to go into solution to replace the amount which was exchanged.

Boron in solution change:

$$dm_{bosol}/dt = (1-f)*c_rate_ss*\alpha + ex_rate*fe_sol*m_{bor}/m_{feo} - ex_rate*m_{bosol};$$

in which the first term on the right side is included only if the mass of stainless steel is greater than 0, and the second term is the same as the second term of the previous equation but with opposite sign.

In these equations, the following symbols have been used:

- m_{fec} Mass of the remaining carbon steel (conservatively assumed to be 100% Fe, although actually only 99% iron, because most of the remainder is manganese which has a higher neutron absorption cross section than iron; the carbon content, from which the steel gets its name is only 0.2%, A516, Ref. 36).
- m_{fes} Mass of the metallic fraction of the remaining borated stainless steel (conservatively assumed to be all Fe, because most of the remainder is chromium, nickel, or manganese, all of which have higher neutron absorption cross section than iron; composition given in Ref. 36).
- m_{feo} Mass of iron as iron oxide not in solution (corrosion product of both the carbon steel and the stainless steel).
- m_{bs} Mass of boron in the remaining stainless steel.

- m_{bosol} Mass of boron oxide in solution.
- m_{bot} Mass of boron trapped in the solid iron oxide.
- $c_{\text{rate_cs}}$ Corrosion rate of carbon steel (kg/yr).
- $c_{\text{rate_ss}}$ Corrosion rate of borated stainless steel (kg/yr).
- ex_{rate} Exchange rate between the water in the waste package and the water in the immediate environment (yr^{-1}).
- f Fraction of the boron being trapped in the oxide corrosion products.
- alph Fraction of boron in stainless steel (used to compute the amount of boron going into solution as the stainless steel is oxidized).
- fe_{sol} The amount of Fe ion in solution at any given time, approximated by a constant equal to the maximum permitted by the solubility limit (kg).

It will be noted that the six differential equations do not include specific accounting for the iron oxide in solution or the boron oxide not in solution. As indicated in the definition of fe_{sol} , above, the amount of Fe in solution is approximated by the maximum permitted by the solubility limit. This assumption (approximation) is justified by the fact that the iron oxide pool is still more than several thousand times the fe_{sol} at the time when the boron reaches very small values and the package reaches the criticality threshold, so that the solution remains saturated with iron, as will be shown in the discussion of calculation results, below.

The initial implementation of the model, described by the equations above, was given by the simple program "deltasd.c", the annotated listing of which is given in Attachment I of Reference 2. The code uses numerical integration of the differential equations. For the cases summarized in this document, the time step for this integration is taken to be 10 years, which is much shorter than the reciprocal of the exchange rate for these cases, so that the concentrations of absorber change little during the time step. The proper implementation of the algorithms is checked by MathCad. The model is intended to serve as a generator of configurations which represent the criticality potential of all the possible internally degraded states of the waste package.

In the exercises with this model the initial basket carbon steel and stainless steel masses are fixed at the current design values, and the corrosion and exchange rates are varied over the range of likely values. For the current analyses, this variation has been performed manually.

4.2 Range of Input Parameters Values for Commercial SNF

This section provides the ranges of parameters input into the configuration generator, as well as a brief basis for each parameter. More detailed information and bases for the values presented is available in Ref. 2).

Carbon steel aqueous general corrosion rate:

- High value in medium oxygen water: 50 microns/yr (Ref. 29)
- Low value in low oxygen water: 5 microns/yr

To convert to kg/yr multiply by:

- 7830 density of carbon steel in kg/m³
- 178 surface area of carbon steel tubes in m² (Ref. 2, Attachment VIII)
- 10⁻⁶ meters/micron

This process gives a high value of 69.7 kg/yr and a low value of 6.97 kg/yr. Since it has been shown in Reference 2 that the maximum oxygen availability for a flooded WP can oxidize no more than 1.65 kg of Fe per year, these estimates must be adjusted downward. As a conservative approximation, this study will use only the limiting value of 1.65 kg/yr.

Stainless steel aqueous general corrosion rate:

- High value measured near 100°C: 0.3 microns/yr (Ref. 30, p. 24)
- Low value measured near 28°C: 0.1 microns/yr (Ref. 26, p. 24)

To convert to kg/yr multiply by:

- 7,770 density of stainless steel in kg/m³
- 70 surface area of stainless steel plate in m² (Ref. 2, Attachment VIII)
- 10⁻⁶ meters/micron

This process gives a high corrosion rate of 0.163 kg/yr and a low value of 0.0544 kg/yr. Both are well below the 1.65 kg/yr upper limit supportable by the oxygen exchange rate, so they will be used for the calculations. This approximation is conservative; the oxygen availability upper limit must be shared between the carbon steel and the stainless steel, so there should be a lowering of the corrosion rate of either carbon steel or stainless steel, or both. The stainless steel corrosion rate used here is consistent with that used in Section 3.2. The carbon steel corrosion rate is lower than that used in Section 3.1, because the basket degradation is not concerned with the faster pitting corrosion which is critical to the barrier breach.

Flush/exchange rate:

The flush/exchange rate is calculated under the assumption that the waste package is nearly filled with water, and the principal physical exchange mechanism is in- and out-flow of water through holes near the top of the package. The thermally driven circulation of water in the package brings all the water near the water surface where it can exchange with the infiltrating water flowing in and out through holes near the top. Although the standing water is not the most likely waste package configuration, it is the only one which can provide sufficient moderation for internal criticality, so this assumption is appropriate.

Multiply the following:

- Drip rate (high 7.19 mm/yr, medium 0.53 mm/yr, low 0.03 mm/yr), based on the TSPA-95 abstraction discussed in Section 2.1
- Efficiency of exchange through holes in the top of the package (high 0.1, medium 0.01, low 0.001); note that the exchange efficiency values are an order of magnitude smaller than the filling efficiency because even in the most favorable hole geometry (water flowing in one hole and out another) there will be some faster path for the entering water to leave than for some general parcel of water already in the package to be exchanged.
- Concentration factor (4)
- Waste package interior area projected on a horizontal plane of 6.634 m²

Divide by:

- Waste package void volume of 4.84 m³ (Ref. 2, Attachment VIII)

The 4 possible combinations of the high and medium values of drip rate and exchange efficiency give the 4 exchange rate values 0.00394, 0.000291, 0.000394, 0.0000291. These are all used in the calculations of Section 6.2, below, but they are tracked according to the individual drip rate and exchange efficiency values, so they will be presented that way in the input summary Table 4-1.

Upper limit of dissolved iron in the waste package filled with water:

- High value 0.00505 mole/liter, more acidic environment than is likely to be produced by radiolysis in the waste package
- Low value 8.0×10^{-5} mole/liter, for neutral water

The calculation of the above solubility limits is given in Attachment IV of Reference 2. To convert to total kg in the waste package solution multiply by:

- 55.8 molecular weight of iron (gm/mole)
- 4.84 cubic meters of water in the waste package.

High result: 1.33 kg; Low result: 0.021 kg

Boron fraction trapped in solid iron oxide:

There has been virtually no quantitative investigation of this phenomenon, neither theoretical nor experimental. It is therefore appropriate to try a range of values to test the sensitivity to this parameter. It will be seen that the range 0.02 to 0.05 shows a large variation in the effect on earliest possible time of criticality, so these two values will represent the low and high values of the parameter f . Since f is the only parameter for which increasing values act to decrease k_{eff} , the value 0.02 will be designated as the high, and 0.05 will be designated low. Of course the actual values could turn out to be outside this rather narrow range after all. It is expected that current

investigations into the solubility and corrosion rates of metal borides, and the corrosion behavior of borated stainless steels, will provide a basis for estimating this parameter, or provide a different model for the removal of boron.

Although the temperature and humidity dependence of the above parameters could have been explicitly modeled, as was done to some degree with the basket stainless steel corrosion in Section 3.2, a constant temperature approximation has been used for this analysis. This is justified because the temperature change is small over the period of interest and the resulting parameter changes would be smaller than the ranges covered above.

These input parameters are summarized in Table 4-1.

Table 4-1. Summary of Input Parameters

Parameter	High	Low
Dissolved Fe upper limit (kg)	1.33	0.021
Stainless steel corrosion rate (kg/yr)	0.163	0.0544
Trapped B fraction, f**	0.02	0.05
Exchange efficiency	0.1	0.01*
Drip rate (mm/yr)	7.19	0.53*

* These values correspond to the medium values given in the analysis above; they are given here because they are the ones which will be used as the basis for the variations used in the calculations of Section 6.2.

** The numerically low value of the trapping fraction, f, is designated high because it goes with the high numerical values of the other parameters causing an increase in k_{eff} .

5.0 Waste Package Criticality Analyses for Commercial SNF

5.1 MCNP Calculations For Degraded Configurations: Commercial SNF

Of the discrete degraded mode configurations discussed in Section 2.2, two sets were found to be most relevant to the current level of study. The values of k_{eff} are given as a function of percentages which must be converted into mass of boron and iron to be useful in the present model. These conversions are given in Attachment VIII of Reference 2. The results are presented in the tables below.

(1) Partial Basket

The carbon steel tubes and guides have completely oxidized. The basket structure has collapsed, however, the fuel assemblies are still separated by the borated stainless steel plates between them. The borated stainless steel has partially corroded, with most of the borides conservatively assumed to quickly oxidize and immediately dissolve due to the high solubility of boron oxide. However, a small amount of boron remains trapped within the corrosion products. Although MCNP calculations did not explicitly model the trapped boron fraction, f , it is assumed that the results will be relatively insensitive to whether this small amount of boron is at the position initially occupied by the borated stainless steel plates or uniformly distributed throughout the package void space, as is assumed in the MCNP calculations. Table 5-1 below lists the results of the MCNP k_{eff} calculations for variations of this degraded configuration. In this table, the iron mass is the sum of the iron in the remaining uncorroded stainless steel plus the undissolved oxide, and the only boron is that remaining in the uncorroded stainless steel.

Table 5-1. Progressive Degradation of Borated Stainless Steel Control Panels

% SS-B Plate Thickness Remaining	% of WP Void Space Filled With Fe_2O_3	kg Fe	kg B	10,000 yr k_{eff}
50	0	929	15.24	0.917
50	10	2978	15.24	0.851
25	20	4608	7.618	0.857
25	15	3572	7.618	0.880
10	25	5399	3.05	0.887
10	20	4392	3.05	0.908
10	10	2271	3.05	0.944

(2) Assemblies Touching

The borated stainless steel is fully corroded, with large amounts of iron oxide remaining from corrosion of the carbon steel tubes and guides, and the stainless steel plates. With complete degradation of the stainless steel plates separating them, the fuel assemblies are assumed to have settled through the oxides and are now touching. Only small amounts of boron remain trapped within the mass of oxides, and are only released into solution as the oxide itself dissolves. The MCNP calculations modeled this configuration set with both the Fe and B uniformly distributed throughout the package void space. It is assumed that the k_{eff} calculated is a conservative approximation to the values which would be obtained by a more explicit model with some specific fraction of the Fe and B remaining in solid form at the initial location of the basket. Table 5-2 provides the results of the k_{eff} calculations for variations of this degraded configuration.

Table 5-2. MCNP Calculation Data Points for Fully Degraded Basket

% of WP Void Filled With Fe ₂ O ₃	% of Original B-10 Remaining In WP	kg Fe	kg B	10,000 yr k_{eff}
30	0	6283	0.0	0.928
30	2	6283	0.6	0.913
30	5	6283	1.5	0.890
20	0	4188	0.0	0.979
20	5	4188	1.5	0.941
20	10	4188	3.05	0.902
20	15	4188	4.57	0.872
10	10	2094	3.05	0.947
10	15	2094	4.57	0.909
10	20	2094	6.1	0.879

Both of these sets also assumed that the carbon steel had already corroded by the time of the stated stainless steel corrosion, with the corrosion products contributing to the reservoir of iron oxide which is uniformly distributed throughout the water in the waste package.

5.2 Regression Analysis of the Data: Commercial SNF

The regression lines and goodness-of-fit for the two configurations are given by the following equations (where Fe is in metric tons and B is in kilograms):

Partial basket:

$$k_{\text{eff}} = 1.026 - 0.0242 \cdot \text{Fe} - 0.00645 \cdot \text{B}, \quad R^2=0.91$$

Assemblies touching:

$$k_{\text{eff}} = 1.068 - 0.0221 \cdot \text{Fe} - 0.0236 \cdot \text{B}, \quad R^2=0.99$$

Pooled data sets (17 data points):

$$k_{\text{eff}} = 0.989 - 0.0132 \cdot \text{Fe} - 0.00679 \cdot \text{B}, \quad R^2=0.54.$$

It should be noted that the partial basket regression implicitly incorporates the effect of decreasing basket thickness, which is generally proportional to the explicitly decreasing amounts of boron and iron.

The fact that the pooled data set has such a small R^2 indicates that the two sets represent somewhat different physical processes, which is consistent with the fact that the partial basket variation incorporates the effect of varying assembly spacing, while the assemblies touching case does not. This distinction will be reflected in the calculations of earliest time to criticality performed in Section 6.2, below. In those calculations the configuration generator code calculates the boron and iron concentration decrements at each time step to reflect the corrosion and removal process, and at each time step the k_{eff} is calculated as a function of the remaining boron and iron, using the partially basket regression while the stainless steel is still intact and the assemblies touching regression after the stainless steel has completely corroded.

6.0 Evaluation of Criticality: Sample Results

This section presents summaries of the results of the long-term criticality evaluations done through 1996 for commercial SNF. They present different pieces of the overall methodology described in Section 1. In Section 6.1, a complete set of scenarios for internal criticality is simplified so that the processes are reduced to events whose occurrence can be described by probability density functions in continuous time. The probability density functions for infiltration rate are developed from the environmental analysis described in Section 2.1.3, above. The probability density functions for basket corrosion/degradation are developed from the data analysis summarized in Section 3.2, above. The results are expressed in terms of the expected number of criticalities as a function of time.

In Section 6.2 the range of possible scenarios for degraded basket internal criticality is described by the range of concentrations of neutron absorbers (Fe and B) remaining in the waste package as a function of time. The results are expressed in terms of the earliest time to criticality for maximum and minimum values of a set of important parameters whose values are subject to considerable uncertainty. This analysis illustrates most of the methodology; the only missing component is the establishment of probabilities for the range of values of the principal uncertain parameters.

In section 6.3 an upper bound for the probability of accumulating a critical mass in the far field is estimated using the methodology described in Section 2.3.3, above. The resulting probability is found to be very low for all commercial SNF, but the particular value is sensitive to the specific fissile concentration.

6.1 Criticality Expectation as a Function of Time

This example is a summary of the results presented *Initial Waste Package Probabilistic Criticality Analysis: Uncanistered Fuel* in 1995 (Ref. 1). The analysis used probability density functions for infiltration rate which represented a conservative interpretation of the Yucca Mountain groundwater hydrology models at that time. These models have recently been revised to show higher infiltration rates (Section TDSS 026, Bounding Water Percolation of Ref. 40). The new, increased average infiltration rate still falls within the range of the distribution used in Reference 1, but the new hydrology model does predict the possibility of large infiltration rates which fall outside the range already considered. Although the original infiltration rate model used in Reference 1 can no longer be considered as conservative, it is still useful to present the results without expending considerable resources to re-do the calculations and the associated documentation for the following reasons: (1) the Yucca Mountain hydrology model is still in a state of flux and may be significantly modified by the results of tests presently underway in the Exploratory Studies Facility (ESF, the tunnel drilled through the repository horizon); (2) the lack of conservatism in the hydrology model is compensated (to some unknown extent) by the over-conservatism in the corrosion models for the waste package barriers and basket; and (3) this example is for illustration purposes only.

For this example, the sequence of processes most likely to produce a criticality is simplified to five events: (1) either a high or low infiltration rate incident on the waste package; (2) breach of the waste package barriers, given the infiltration rate; (3) dissolution of 60% of the borated stainless steel basket (which leads to removal of the released boron, all of which is presumed to be sufficiently soluble to remain in solution until it is removed by the water flushing), given the infiltration rate and the breach of the barriers; (4) waste package contains sufficient fissile material in the SNF; and (5) ponding of water in the waste package assuming that there is infiltrating water and waste package breach, but not conditioned, or depending, on the magnitude of time of occurrence. The first three of these events are characterized by probability density functions of the time of occurrence (or conditional occurrence for (2) and (3)). The last two events are simply characterized by the probability of their occurrence, without any time limits.

6.1.1 Probability Density Function for Infiltration Rate

The probability density function for infiltration rate is developed from three different probability density functions for three different projections of future climate.

6.1.1.1 PDF for Surface Water Infiltration of Repository Horizon at a Low Rate

This is the probability that a corrosively significant stream will pass through the waste

emplacement areas. Such a stream would have to accumulate sufficient volume to fill a waste package to a depth of at least 1 meter. Over a period of 10,000 years, this would require a flow rate of 0.1 mm/yr, which just was in the middle of the range of infiltration rates estimated for the repository area in 1995. However, in addition to ponding in the package, there must be enough flow to remove most of the boron neutron absorber from the waste package, in order to have a criticality. For this illustration it is assumed that at least a factor of 10 increase would be required for such a process, for a total infiltration rate of 1 mm/yr. [Note: This estimation of required flow rate is only to define this low infiltration category. The actual rate of basket corrosion/dissolution has already been estimated in Section 3.2 above.] For such an increased flow rate to be maintained over many years, there would have to be a significant climate change (one as significant as an ice age). It is conservatively assumed that such an event is certain to occur within 10,000 years (and that such an enhanced flow rate would be maintained thereafter). It should also be more likely at the end of this period than at the beginning, since such a changed climate would take thousands of years to develop. Nevertheless, a conservative probability model is chosen, the uniform distribution between 1,000 and 10,000 years, which can be expressed in units of per year as

$$f_1(t) = 1/9000 \quad 1000 < t < 10000 \quad (6-1)$$

This pdf is shown in Figure 6-1, together with the resulting cumulative distribution function (cdf).

6.1.1.2 PDF for Surface Water Infiltration of Repository Horizon at a High Rate

This would be an infiltration flow rate of greater than 10 mm/year, which is 10 times the low infiltration flow rate given above, and would be expected to give a correspondingly increased corrosion rate (on the waste package) and leach rate (for the boron). [It may be that 10 mm/yr is still so low as to not significantly disturb the corrosion passivating film, so that the conditional corrosion rate is not significantly higher than for low infiltration, but the boron leach rate would still be higher.] Such a high infiltration rate would require a very significant climate change, which we assume to be likely sometime between 2,000 years and 100,000 years (which would be likely to encompass several ice ages, and their aftermaths, which could result in increased atmospheric precipitation). As with the low infiltration case, we use the conservative uniform distribution, again expressed in units of per year

$$f_1(t) = 1/98000 \quad 2000 < t < 100000 \quad (6-2)$$

This pdf, together with the associated cdf, is shown in Figure 6-2.

6.1.1.3 PDF for Changing to a Very Wet Climate Which Raises the Water Table to Repository Horizon (flooding the repository)

The present tectonic trends are moving the climate in a dryer direction. For example, one major cause of the shift from a moist climate to a dry one over the past several million years has been the rise of the Sierra Nevada mountain range, which prevents the moist Pacific air from reaching Nevada. Flooding of the repository would require a substantial increase in rainfall, sustained

over a long time period, since the proposed repository horizon is approximately 300 meters above the current water table. The National Research Council has examined the possibility of water table rise to the level of the repository (Ref. 41). They reported that even a 100% increase in rainfall (and a corresponding 15-fold increase in recharge) would produce an insufficient rise (raising the level only 150 meters). Their report also indicated that the last ice age saw only a 40% increase in precipitation (Ref. 41, p. 6), and that as far back as 50,000 years ago the water table in the recharge area north of Yucca Mountain was no more than 100 meters above its present level (Ref. 41, p. 78).

Therefore, it is assumed that the probability of flooding due to climate change in the next 10,000 years to be zero. The probability of flooding thereafter is conservatively estimated from available geologic information. The National Research Council report cited above suggests that the return period for simple flooding to be greater than 10^6 years, and that the probability of flooding during the early part of this period is much less than later. Thus it is reasonable to assume an asymmetric triangular distribution with the upper limit at 10,000,000 years, which would be

$$f_1(t) = 2 \times 10^{-14} t \quad 10,000 < t < 10,000,000 \quad (6-3)$$

where t is expressed in years, and f_1 is expressed in units of per year. For simplicity, this density function has been normalized as if the lower limit were 0, instead of 10,000. This normalization approximation is valid to six significant figures, which is certainly adequate for this analysis.

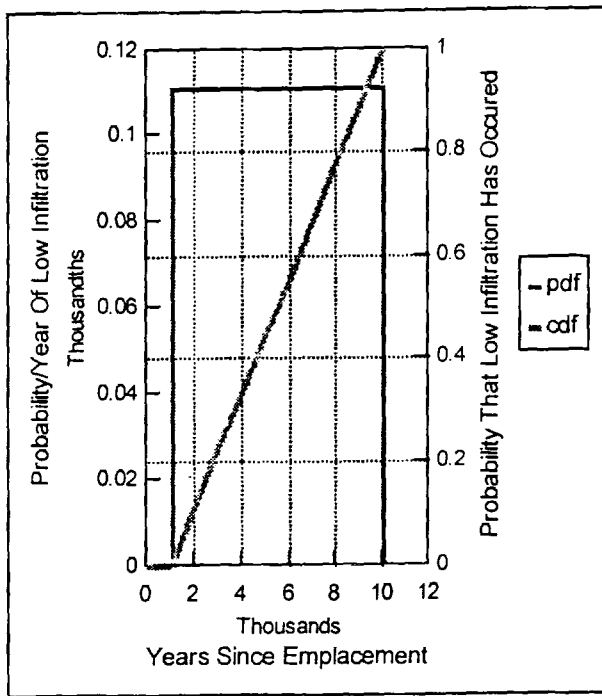


Figure 6-1. Distribution of time-to-occurrence of the low infiltration initiating event

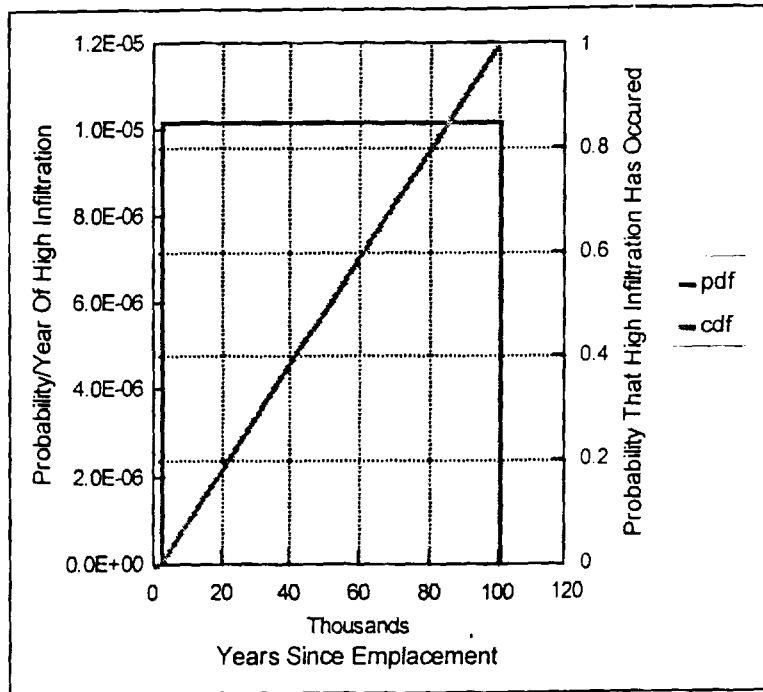


Figure 6-2. Distribution of time-to-occurrence of the high infiltration initiating event

6.1.2 Probability Density Function for Time to Breach Waste Package Barriers

The probability density function for time to breach waste package barriers is developed from two different probability density functions for two different projections of future climate. The development of these density functions is based on temperature distribution model discussed in Section 3.1 with numerical results summarized in Table 3-1. The penetration times for inner and outer barrier are totaled and used to fit a Weibull distribution to determine the pdf, f_2 . The Weibull parameter θ was manually selected to produce the best fit of the data. The details of this calculation are given in Reference 1.

It is assumed that high infiltration will cause the flow rate to be sufficient to ensure that the surface of the waste package below a dripping fracture is continuously covered with a film of water. Therefore, the continuous wetting barrier breach times in Table 3-1 were used to develop the pdf, f_2 , for high infiltration sequences. The details of this derivation are given in Reference 1. The resulting pdf, f_2 , is shown in Figure 6-3.

It is assumed that a fracture dripping at a low rate onto a waste package would be incapable of maintaining the surface of the package in a continuously wetted condition due to evaporation. Thus, the intermittent wetting barrier breach times in Table 3-1 were used to develop the pdf, f_2 , for low infiltration sequences. The details of this derivation are given in Reference 1. The resulting pdf, f_2 , is shown in Figure 6-4.

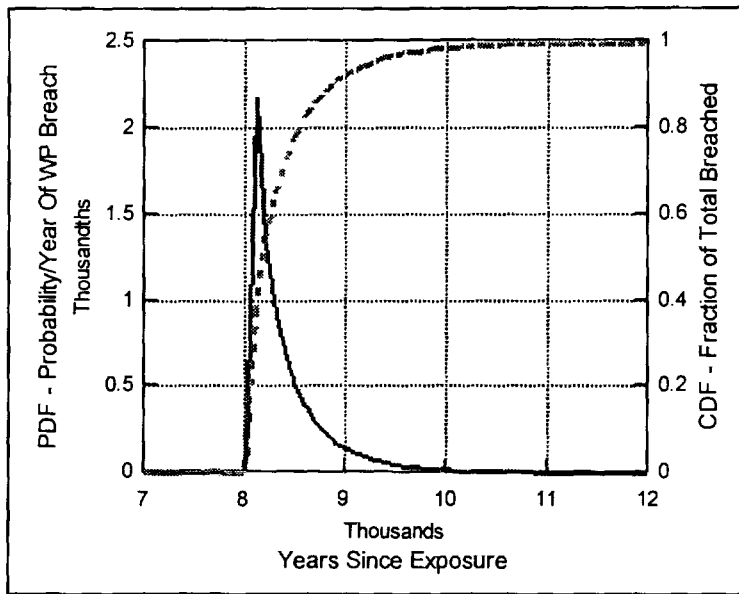


Figure 6-3. Distribution of WP breach failures from temperature distribution model given continuous wetting

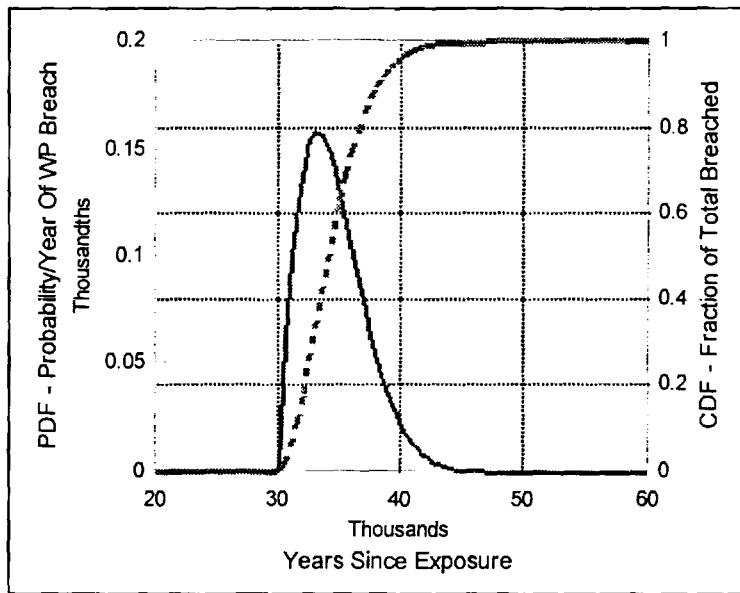


Figure 6-4. Distribution of WP breach failures from temperature distribution model given intermittent wetting

6.1.3 Probability Density Function for Time to Degrade Borated Stainless Steel Basket

The third event required for criticality is the removal of 60% of the boron from the waste package. The Weibull pdf's for basket degradation determined in Sections 3.2.2 and 3.2.3 for continuous wetting and intermittent wetting are shown in Figures 6-5 and 6-6, respectively. Their assignment to the three climatologic possibilities is as follows:

Sequences involving flooding of the emplacement drift would result in the flooding of the interior of a breached WP, thus continuously wetting the basket material. Therefore, the Weibull pdf for continuous wetting developed above will be used as the pdf for 60% borated stainless steel corrosion, f_3 , for the flooding sequences.

Sequences involving water dripping onto a breached WP, as a result of low or high infiltration rate, would not be expected to immediately fill the interior of the package. Many factors, including the rate of water flow into the WP and the interior temperature, will control the internal water level. Therefore, the Weibull pdf for intermittent wetting has been used as the pdf for 60% borated stainless steel corrosion, f_3 , for both the low and high infiltration sequences.

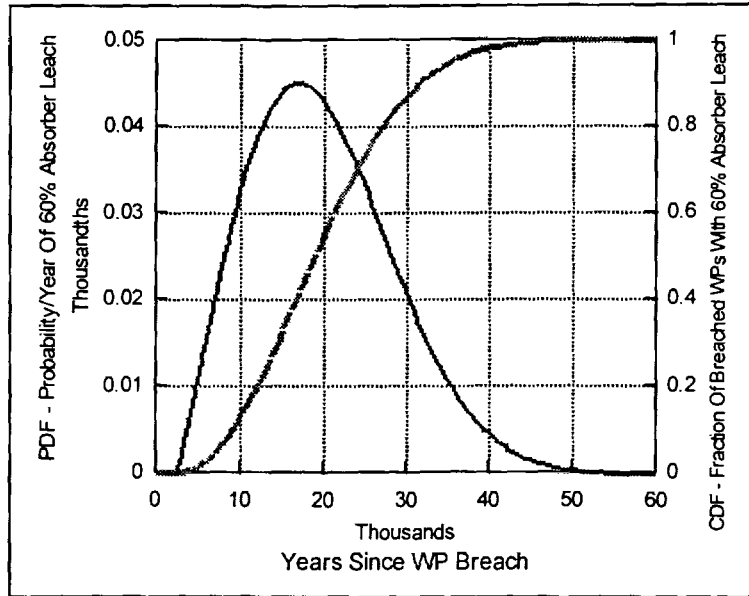


Figure 6-5. Distribution of time to leach 60% of neutron absorbing material from UCF-WP basket structure for continuously wetted conditions.

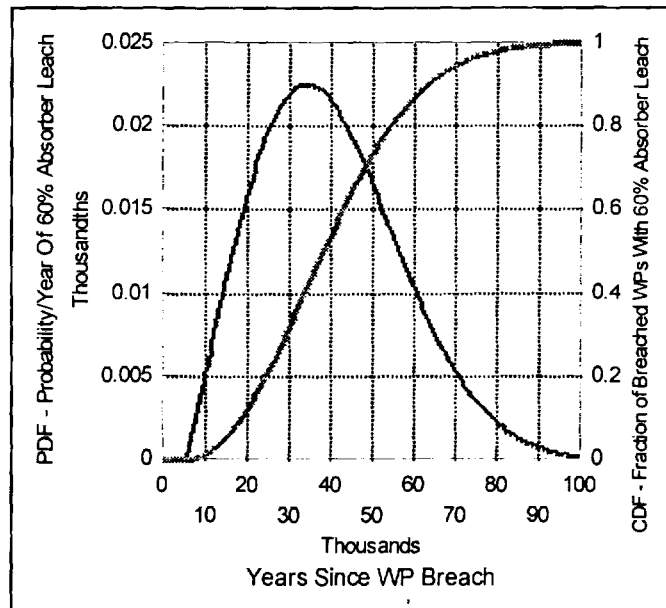


Figure 6-6. Distribution of time to leach 60% of neutron absorbing material from UCF-WP basket structure exposed to intermittent wetting conditions.

6.1.4 Probability of Sufficient Fissile Material in a Waste Package

After all the hazard events that are necessary for a criticality event (WP breach, absorber leach, and internal flooding) have occurred, there is still one fundamental requirement for each scenario: the SNF must be above a threshold combination of high enough fissile material and low enough burnup to become critical. For purposes of this study the threshold of criticality was taken to be $k_{\text{eff}} \geq 0.95$. This is the limit established by 10CFR60.131(h) (Ref. 49), in conformance with the margin usually required for nuclear power plant criticality evaluation. This threshold is usually lowered further below 1.0 by subtracting for bias and uncertainty, which will likely be determined as something between 0.0 and 0.03. In view of this uncertainty and the illustrative nature of this evaluation, the analysis did not apply this lowering of the criticality threshold. Deterministic neutronics calculations of k_{eff} for a range of values for age, for specific burnup and initial enrichment indicate that after emplacement, most assemblies will have a peak in criticality potential at approximately 10,000 years. In particular, 21 pressurized water reactor (PWR) assemblies having 3% initial enrichment and 20 GWd/MTU burnup (waste package criticality design basis fuel) in a waste package design with stainless steel basket, will have a peak $k_{\text{eff}}=0.965$ at 10,000 years which is followed by a slow decline to $k_{\text{eff}}=0.932$ at 200,000 years.

The determination of the fraction of the packages which will have $k_{\text{eff}} \geq 0.95$, when all of the boron is removed from the waste package consists of the following two steps. First, a geometry based difference between k_{∞} and k_{eff} was established based on the Design Basis Fuel Analysis (Ref. 42) which tabulated SNF statistics with respect to k_{∞} using a parameterization of k_{∞} as a function of age, burnup, and initial enrichment developed by ORNL (Ref. 43) for PWR fuel using 210 SCALE runs that covered a representative range of values of burnup and initial enrichment. In this tabulation an age of 5 yrs was used. The correspondence between k_{∞} and k_{eff} is then determined by calculating k_{∞} from the formula given by ORNL (Ref. 43) for the design basis fuel (age=5 yrs, burnup=20 GWd/MTU, initial enrichment=3%), with the result $k_{\infty}=1.138$. An MCNP calculation for the waste package filled with water and all the boron removed at 15,000 years after discharge showed this criticality design basis fuel to have a k_{eff} approximately equal to 0.980, so the difference between k_{∞} and k_{eff} is 0.158. This means that the k_{∞} corresponding to $k_{\text{eff}} = 0.95$ would be $1.138 - (0.98 - 0.95) = 1.108$. This procedure can be applied to other ages as follows: (1) determine the difference between 0.95 and k_{eff} , (2) add that difference to 1.138 to determine the k_{∞} which would correspond to a $k_{\text{eff}}=0.95$, and (3) consult the tabulation of k_{∞} percentiles in Reference 42 to determine the percentage of SNF which would have a higher k_{∞} . The results are given in Figure 6-7. For a discrete, and representative set of ages, the points on this curve are used as a multiplier as described in Section 6.1.6, below. This methodology is described in greater detail in Reference 1.

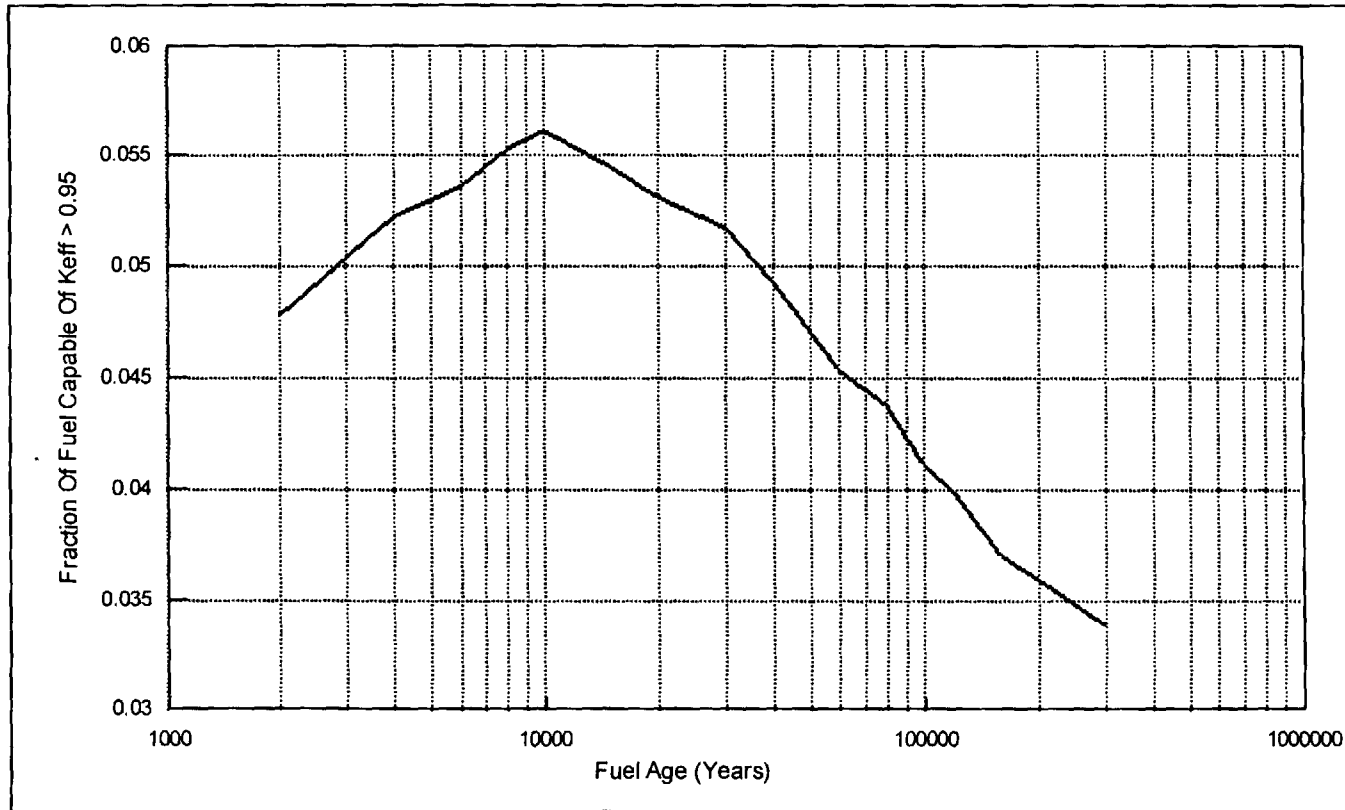


Figure 6-7. Fraction of design basis fuel (3% initial enrichment, 20 GWd/MTU Burnup) as a function of time capable of achieving $k_{eff} > 0.95$ in an UCF-WP geometry with no neutron absorber in the basket structure

6.1.5 Probability of Sufficient Moderator

For the overhead dripping scenarios, there must be holes around the middle of the package, but not the lower part. The most likely location is on the upper surface which is most exposed to dripping water. The conditional probability of such a hole configuration, given that there is sufficient corrosion to produce the holes in the first place, is assumed to be the product of the conditional probability of holes around the middle (0.1) and the conditional probability of no holes in the lower half, given that there are holes around the middle (0.1). This latter probability is actually quite conservative, since half of the weld around the lid will be in the lower, submerged half of the horizontal package, and this weld is more likely to corrode and leave a hole to prevent ponding. On the other hand, there is a possibility that the leached/corroded material could plug up such holes, so that subsequent ponding could be supported even if the initial hole configuration were not favorable to ponding. This analysis will be refined in the next few years; by the time of license application it will include:

- More precise modeling of corrosion from dripping, particularly in welds.
- Fluid dynamic modeling of leach and ponding processes, including the effects of alternative hole configurations.
- Deterministic evaluation of criticality for likely flooding and assembly geometry configurations.

6.1.6 Expectation of Criticality

The pdf for the occurrence of the first three of the above events will be convolved together to incorporate the fact that they must occur in the sequence indicated. In other words, the pdf for the occurrence of all three events, with the last event occurring at time t , requires that event 1 take place at some time, $0 < t_1 < t$, followed by event 2 at some time $t_1 + t_2$, such that $0 < t_1 + t_2 < t$, which is followed by event 3 occurring at time t . The pdf for t is then found from the two-fold convolution:

$$f(t) = \int_0^t f_1(t_1) dt_1 \int_0^{t-t_1} f_2(t_2) f_3(t-t_1-t_2) dt_2 \quad (6-4)$$

This pdf for the combined first three events is then multiplied by the probability of sufficient fissile material (which is a function of time) and by the probability of sufficient moderator, which are determined in Sections 6.1.4 and 6.1.5, respectively. The resulting pdf is then integrated to get the cumulative expectation of the number of criticalities occurring before a specified time. This result is shown in Figure 6-8. The result of excluding the time to WP barrier breach from the convolution (i.e., assuming the barriers are breached a time zero) is also shown in Figure 6-8.

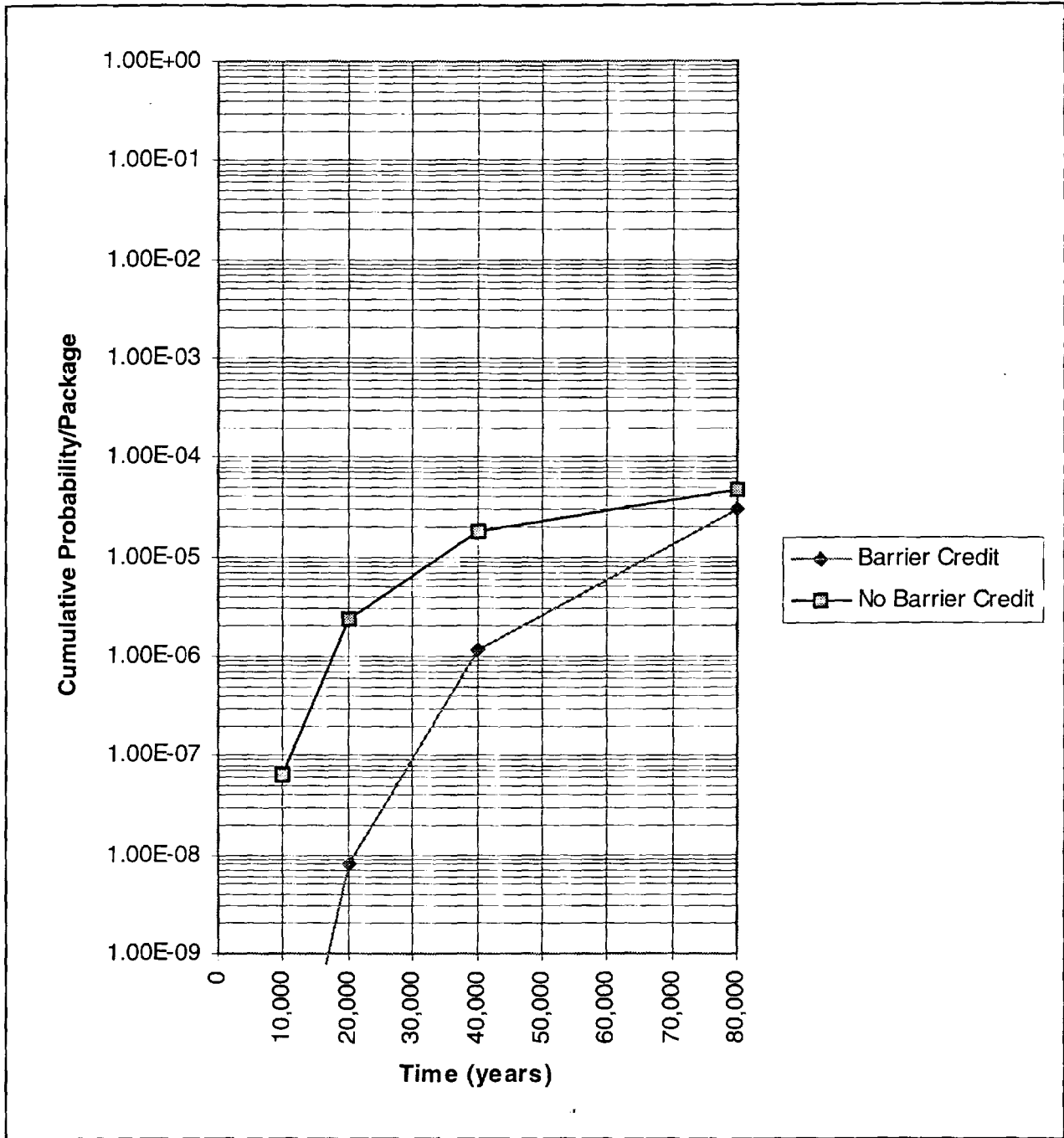


Figure 6-8. Cumulative per-package criticality probability for various times since emplacement with and without credit for the WP barriers

6.2 Earliest Times To Internal WP Criticality: Commercial SNF Example

The final step in the process is to integrate the configuration dependent k_{eff} regressions with the configuration bookkeeper to allow an estimate of the flooded and degrading WP k_{eff} as a function of time. In the configuration bookkeeper, the boron and iron concentrations are decreased at each time step to reflect the corrosion and removal process. In this simple deterministic example, the five basic parameters affecting the corrosion of basket materials and the removal of boron and iron from the WP are varied between the high and low values discussed in Section 3.2. The minimum amount of time required to remove sufficient boron and iron such that the flooded WP k_{eff} exceeds 0.91 (the regulatory threshold for criticality determined as the sum of the 10CFR60.131(h) required 5% margin of safety and the estimated bias and uncertainty of the MCNP calculation) is estimated for various combinations of the five parameters. Future versions of the configuration bookkeeper will have probability distributions assigned to these parameters so that the probability of exceeding the defined criticality limit as a function of time can be estimated.

6.2.1 Nominal Range of Trapped Boron Fraction

The calculations generally show the greatest sensitivity to the corrosion rate of borated stainless steel, so all calculations are presented for both high and low values of this parameter. The dependence on the other four parameters is demonstrated with two combination sets. For the first combination set, four configurations are generated by selecting one parameter at a time to have its high value with the other three parameters having their low values. The results are given in Table 6-1. For the second combination set, six configurations are generated by selecting two parameters at a time to have high values, with the other two parameters having low values. The results are given in Table 6-2. It should be noted that the trapped boron fraction, f , is the only parameter which is negatively correlated with criticality, so its lower numerical value is given the designation of high, as was indicated in Table 4-1.

The following observations on the results presented in Tables 6-1 and 6-2 are of interest:

- For all of the cases the remaining iron oxide is in excess of 5,300 kg, which is nearly all the iron in the intact basket. The boron remaining is less than 2 kg, which means that most of it has been removed. This is a consequence of the Fe solution limit, which keeps most of the iron in solid oxide, even at the high exchange rate.
- Under the worst case conditions: (1) waste package filling with water and remaining filled for tens of thousands of years, (2) a high value for the drip rate (7.19 mm/yr), and (3) a high value for the exchange rate, the smallest time to criticality can be 12,000 years following penetration of the waste package barriers. The simultaneous occurrence of these three conditions should be considered extremely unlikely.
- Although not directly apparent, some significant effect of lowering the Fe solubility limit

when the trapped boron fraction is large can be inferred by comparing the last 2 lines of Table 6-2 with the 2 lines immediately above. Comparing the times for the same stainless steel corrosion rates there is seen to be only a 50% decrease while increasing the drip rate by more than an order of magnitude. This limitation to a small decrease is due to the large decrease in the iron solubility limit (going from 1.33 kg to 0.021 kg) which keeps a significant amount of boron trapped in the oxide. This behavior is in contrast with the same change in parameters going from the first 2 lines of the table to the third and fourth lines. In this comparison the decrease is approximately an order of magnitude. The fundamental difference is that the trapped boron is very low, so lowering the Fe solubility limit to slow the removal of the oxide has little effect. The influence of Fe solubility limit is more strongly demonstrated in the sensitivity study in the next section.

It should be noted that the criticality calculations were made for the approximate time of peak post-closure k_{eff} ($\approx 10,000$ years). This is close to the least time to criticality for the most reactive configurations, so it is a reasonable approximation. Furthermore, the approximation is conservative; the longer times to criticality are underestimated because the MCNP calculated k_{eff} is too high because it has been calculated at nearly its peak. Future versions of these k_{eff} fits will also incorporate the effects of time, once sufficient MCNP runs have been performed to characterize this effect for each configuration.

Table 6-1. Times to Earliest Possible Criticality with One Parameter High

SS Corrosion rate (kg/yr)	Drip rate (mm/yr)	Exchange efficiency	f, Trapped boron fraction	Fe solubility limit (kg)	High parameter	Earliest time to criticality (yr)
0.0544	0.53	0.01	0.02	0.021	f	1.35x10 ⁵
0.163	0.53	0.01	0.02	0.021	f	1.22x10 ⁵
0.0544	0.53	0.01	0.05	1.33	Fe sol	2.06x10 ⁵
0.163	0.53	0.01	0.05	1.33	Fe sol	1.92x10 ⁵
0.0544	7.19	0.01	0.05	0.021	Drip rate	4.21x10 ⁴
0.163	7.19	0.01	0.05	0.021	Drip rate	2.16x10 ⁴
0.0544	0.53	0.1	0.05	0.021	Exchg	4.58x10 ⁴
0.163	0.53	0.1	0.05	0.021	Exchg	2.61x10 ⁴

Table 6-2. Times to Earliest Possible Criticality with Two Parameters High

SS Corrosion rate (kg/yr)	Drip rate (mm/yr)	Exchange efficiency	f, Trapped boron fraction	Fe solubility limit (kg)	High parameters	Earliest time to criticality (yr)
0.0544	0.53	0.01	0.02	1.33	f, Fe sol	1.35x10 ⁵
0.163	0.53	0.01	0.02	1.33	f, Fe sol	1.22x10 ⁵
0.0544	7.19	0.01	0.02	0.021	f, Drip rate	3.67x10 ⁴
0.163	7.19	0.01	0.02	0.021	f, Drip rate	1.62x10 ⁴
0.0544	0.53	0.1	0.02	0.021	f, Exchg	3.84x10 ⁴
0.163	0.53	0.1	0.02	0.021	f, Exchg	1.89x10 ⁴
0.0544	7.19	0.01	0.05	1.33	Fe, Drip rate	4.16x10 ⁴
0.163	7.19	0.01	0.05	1.33	Fe, Drip rate	2.14x10 ⁴
0.0544	0.53	0.1	0.05	1.33	Fe, Exchg	4.53x10 ⁴
0.163	0.53	0.1	0.05	1.33	Fe, Exchg	2.58x10 ⁴
0.0544	7.19	0.1	0.05	0.021	Dr, Exchg	2.85x10 ⁴
0.163	7.19	0.1	0.05	0.021	Dr, Exchg	1.20x10 ⁴

6.2.2 Sensitivity Analysis: Extending the Range of the Trapped Boron Fraction

Increasing the value of trapped boron fraction only slightly above 0.05 will markedly increase the earliest time to criticality. With the same configuration selection scheme as was used for Tables 6-1 and 6-2, above, the range of values is changed to 0 to 0.055. The results are presented in Tables 6-3 and 6-4, below.

The following observations on the sensitivity results presented in Tables 6-3 and 6-4 are of interest:

- The earliest times to criticality for the $f=0$ cases show only a small decrease compared with the corresponding $f=0.02$ cases in Tables 6-1 and 6-2, indicating that $f=0.02$ does not trap enough boron in the oxide to prevent criticality.
- The last 4 lines of Table 6-3 show the striking effect of lowering the Fe solubility limit when the trapped boron fraction exceeds a threshold. This is in contrast with the first 2 lines of the table which also have the lower value of Fe solubility, but the trapped boron fraction is zero so there is little effect.
- Comparison of the last 2 lines in Table 6-4 with the 2 lines immediately above shows that only a slight change from $f=0.050$ to $f=0.055$ has reversed the relative dominance of drip rate and Fe solubility limit. Instead of a 50% decrease in earliest time to criticality when going from high Fe solubility limit and low drip rate to low Fe solubility limit and high drip rate, Table 6-4 shows nearly a 100% increase.

Table 6-3. Sensitivity to Trapped Boron Fraction with One Parameter High

SS Corrosion rate (kg/yr)	Drip rate (mm/yr)	Exchange efficiency	f, Trapped boron fraction	Fe solubility limit (kg)	High parameter	Earliest time to criticality (yr)
0.0544	0.53	0.01	0	0.021	f	1.20x10 ⁵
0.163	0.53	0.01	0	0.021	f	1.07x10 ⁵
0.0544	0.53	0.01	0.055	1.33	Fe sol	6.61x10 ⁵
0.163	0.53	0.01	0.055	1.33	Fe sol	5.64x10 ⁵
0.0544	7.19	0.01	0.055	0.021	Drip rate	>10 ⁶
0.163	7.19	0.01	0.055	0.021	Drip rate	>10 ⁶
0.0544	0.53	0.1	0.055	0.021	Exchg	>10 ⁶
0.163	0.53	0.1	0.055	0.021	Exchg	>10 ⁶

Table 6-4. Sensitivity to Trapped Boron Fraction with Two Parameters High

SS Corrosion rate (kg/yr)	Drip rate (mm/yr)	Exchange efficiency	f, Trapped boron fraction	Fe solubility limit (kg)	High parameters	Earliest time to criticality (yr)
0.0544	0.53	0.01	0	1.33	f, Fe sol	1.19x10 ⁵
0.163	0.53	0.01	0	1.33	f, Fe sol	1.07x10 ⁵
0.0544	7.19	0.01	0	0.021	f, Drip rate	3.55x10 ⁴
0.163	7.19	0.01	0	0.021	f, Drip rate	1.51x10 ⁴
0.0544	0.53	0.1	0	0.021	f, Exchg	3.68x10 ⁴
0.163	0.53	0.1	0	0.021	f, Exchg	1.73x10 ⁴
0.0544	7.19	0.01	0.055	1.33	Fe, Drip rate	6.05x10 ⁴
0.163	7.19	0.01	0.055	1.33	Fe, Drip rate	4.97x10 ⁴
0.0544	0.53	0.1	0.055	1.33	Fe, Exchg	8.13x10 ⁴
0.163	0.53	0.1	0.055	1.33	Fe, Exchg	6.73x10 ⁴
0.0544	7.19	0.1	0.055	0.021	Dr, Exchg	3.18x10 ⁵
0.163	7.19	0.1	0.055	0.021	Dr, Exchg	2.68x10 ⁵

6.3 Far-Field Criticality Analysis: Commercial SNF

The neutronics calculations of Section 5 and the probability calculation methodology of Section 2.3.3 are combined to estimate the upper bound of the probability for accumulating a critical mass, in the far field, of fissile material from a single waste package.

6.3.1 Critical Mass of Commercial SNF Uranium

A set of 10 uranium/water concentrations in tuff was evaluated to determine the minimum critical mass/radius spheres. This set represented 3 SNF types, chosen to represent the 2%, 4%, and 13% most stressing fuel with respect to fissile content. For each of these fuel types, the analysis was a two step process. First the most critical volume % UO_2 (highest k_{∞}) was determined for a family of water concentrations by calculating k_{∞} , using MCNP, for a range of UO_2 volume %. The k_{∞} values for one fuel type (PWR, 3% initial enrichment, 20 GWd/MTU) are shown in Figure 6-9. [It should be noted that the water concentrations in this figure are expressed as a volume percent of the tuff water mixture without uranium (for convenience of analysis in Reference 24 from which the figure is taken), while the UO_2 concentrations are expressed as a volume percent of the total rock (including the UO_2).]

The second step is to calculate the k_{eff} , again using MCNP, for a range of radii, and interpolate to determine the critical radius, at which the value of k_{eff} is equal to the criticality threshold. The most appropriate value of criticality threshold k_{eff} was 1-(bias and uncertainty of the computational process) - (twice standard deviation of the specific Monte Carlo calculation). For these cases, the bias and uncertainty is lower than the usual value because it refers to the fissile content only. This is because we have made the conservative assumption that none of the neutron absorbers from the SNF are in the uranium-bearing groundwater from the repository, either having been removed from the SNF matrix much earlier than the fissile nuclides, or having remained in the matrix after removal of the fissile material. This process is illustrated in Figure 6-10, for the UO_2 concentration giving the highest peak k_{∞} for the family of water concentrations in Figure 6-9. Both figures are from Reference 24.

The details of the calculations are given in Reference 24. The results are summarized in Table 6-5.

Far-Field External Criticality Analysis 3.0% / 20 GWD/MT UO_2 in Tuff/Water

○ 30% H_2O △ 20% H_2O ◇ 47% H_2O ▽ 40% H_2O

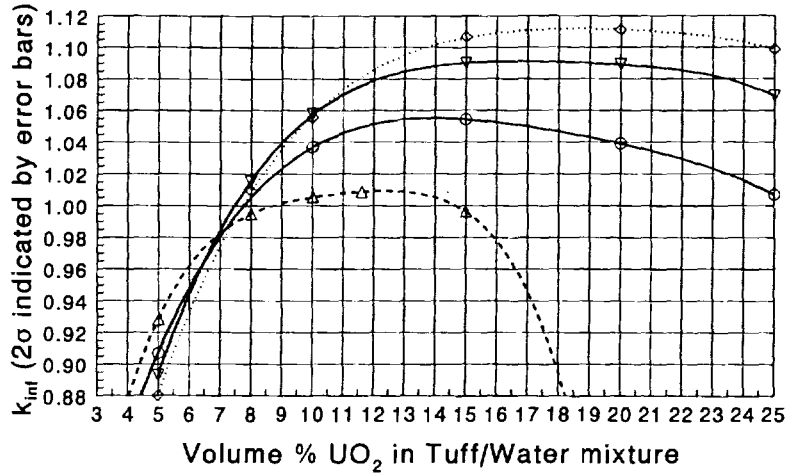


Figure 6-9. k_{eff} of various concentrations of UO_2 , tuff, and water for UO_2 from PWR SNF with 3% initial enrichment and 20 GWd/MTU burnup (error bars were not plotted if the 2σ value was smaller than the data point marker)

Far-Field External Criticality Analysis 3.0% Enriched, 20 GWD/MT, 18.5 vol% UO

+ 47% Water in Tuff

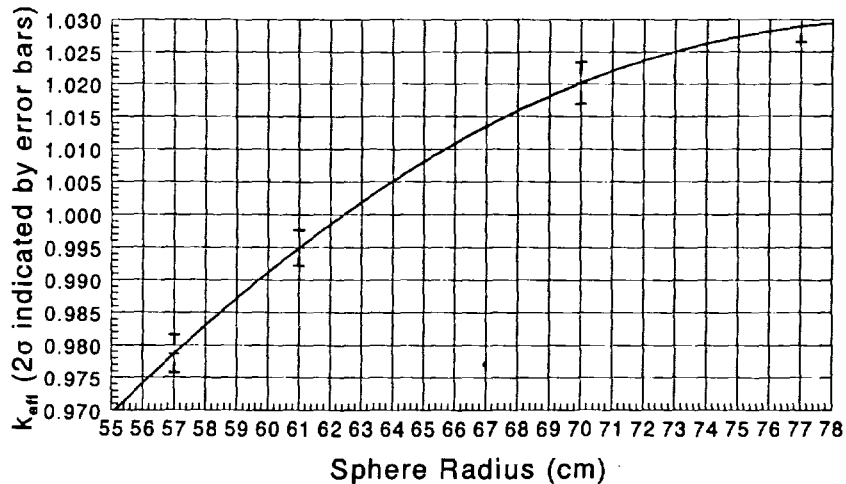


Figure 6-10. k_{eff} as a function of sphere radius for 18.5 vol% 3%/20 UO_2 in saturated tuff with 47% porosity

Table 6-5. Representative SNF/Environment Configurations and Resulting Spherical Critical Masses

SNF enrich & burnup (GWd/MTU)	Fissile % of SNF**	UO ₂ vol % in rock*	H ₂ O vol % in rock*	UO ₂ wt % in rock†	H ₂ O wt % in rock	Critical mass (MTU)*
3%, 20	1.94	18.5	38.3	58	11	1.6
3%, 20	1.94	8	43.2	35	17	10.1
3%, 20	1.94	17	33.2	54	9.6	2.50
3%, 20	1.94	8	36.8	33	14	10.1
3%, 20	1.94	15	25.5	48	7.5	6.5
3%, 20	1.94	10	27.0	37	9.1	7.4
3%, 20	1.94	8	27.6	32	10	18.0
3%, 20	1.94	11.6	17.7	39	5.5	55.2
3.5%, 30	1.87	14	25.8	46	7.8	11.1
4.0%, 40	1.82	15	25.5	48	7.5	30.9

* These values correspond to those given in Reference 24, Section 8.

** These values were derived under worst case reactor burn conditions, as contrasted with average reactor burn conditions used to develop the Characteristics Database (Ref. 3).

† The UO₂ wt % is computed from the volume percents by the formula $10.96U_{v\%}/(10.96U_{v\%}+W_{v\%}+2.52T_{v\%})$, and the water wt% in a similar manner, where U_{v%} is the volume percent of UO₂, W_{v%} is the volume percent of water and T_{v%} is the volume percent of tuff.

6.3.2 Probability That Randomly Selected Cluster Will Have Sufficient Reducing Material

The methodology described in Section 2.3.3 for calculating the conditional probability that a randomly selected log would have at least a specific mass of organic material can be applied to the critical masses given in Table 6-5. The result is the table of the probabilities that a critical mass could be accumulated, Pr{cluster/log}, given in Table 6-6. To go from a mass of organic material which could accumulate a critical mass to the actual accumulation of a critical mass requires the very conservative assumption that the mass of organic material will be just as efficient at accumulating uranium as were the logs on the Colorado plateau.

Table 6-6. Upper Bound of Probabilities of Log Clusters Which Could Be Capable Of Precipitating a Uranium Concentration Sufficient For Criticality

Fissile %	UO ₂ (g/cm ³)	H ₂ O (g/cm ³) *	Critical radius (m)†	Critical mass (metric ton)†	Pr{cluster/log} ‡
1.94	2.03	0.383	0.394	0.520	1.58x10 ⁻⁴
1.94	0.877	0.432	0.961	3.283	3.71x10 ⁻¹⁴
1.94	1.86	0.332	0.470	0.813	9.63x10 ⁻⁷
1.94	0.877	0.368	0.961	3.283	8.31x10 ⁻¹¹
1.94	1.64	0.255	0.673	2.112	1.52x10 ⁻¹¹
1.94	1.10	0.270	0.803	2.405	1.43x10 ⁻¹⁰
1.94	0.877	0.276	1.167	5.850	1.52x10 ⁻²¹
1.94	1.27	0.177	1.496	17.940	1.03x10 ⁻⁵⁷
1.87	1.53	0.258	0.824	3.608	4.7x10 ⁻¹⁸
1.82	1.64	.255	1.133	10.042	7.18x10 ⁻⁴⁶

* This column is simply the vol% water of Table 6-5 divided by 100.

† These columns computed in Attachment II, Reference 3 as adjustments from the values in Reference 24. The critical mass is, therefore, adjusted from the values given in Table 6-5.

‡ The arithmetic means from Attachment II, Reference 3 have been used for conservatism.

6.3.3 Calculation of Expected Number of Criticalities

The expected number of criticalities is the product of three factors:

- The number of waste packages with sufficient fissile content to provide a source for a reducing zone

- The probability of the stream from a single waste package encountering a reducing zone, $Pr\{\log\}$
- The probability of the reducing being of sufficient size to remove a critical mass, $Pr\{\text{cluster}/\log\}$

The number of waste packages for each criticality threshold is determined from the tabulation of percentiles of number of PWR assemblies having greater than a specified k_{∞} given in Reference 42, where the k_{∞} is calculated as a function of enrichment and burnup according to the procedure also given in that reference. The results are given in Table 6-7.

Table 6-7. Percentile of SNF Having Less Fissile % Than Stated Value

% enrichment, burnup (GWd/MTU)	% Fissile	k_{∞}	Fissile content percentile
3.0%, 20	1.94	1.13	98
3.5%, 30	1.87	1.08	96
4.0%, 40	1.82	1.04	87

Using the expected total of 12,000 waste packages of commercial SNF (Ref. 31), and making the conservative assumption that the packages are loaded homogeneously (so that all the high fissile fuel is grouped together), the number of packages having higher fissile content (or higher k_{∞}) than the indicated values can be estimated by multiplying the total number of waste packages by the complement of the percentile in the above table, and dividing by 100.

For $Pr\{\log\}$ the conservative alternative from Table 2-2, 4.1×10^{-4} is used. For $Pr\{\text{cluster}/\log\}$ the values from Table 6-6 are used, except that the cases which require a high volume % water should have the probabilities of Table 6-6 multiplied by the probability of finding such a high porosity in the saturated zone. From Table 6-5 it is seen that the first 4 cases all require more than 30 vol% water (which is equivalent to porosity in the saturated zone). From Table 6-5 it is seen that the first and third cases will be the only ones contributing significantly to total probability. These cases require 38.3 and 33.2 percent porosity, respectively. From Reference 3, Figure 4.1-1, it is seen that the probabilities of having such high porosities are 0.01 and 0.23, respectively. Multiplying by the corresponding probabilities in Table 6-5 and adding gives 1.8×10^{-6} for the porosity adjusted $Pr\{\text{cluster}/\log\}$.

Although only the first and third cases of Table 6-5 can contribute significantly to the overall expected number of criticalities, it is still useful to present the results for the last 2 cases which represent different fuel characteristics, and a lower fissile content. These cases do not need to be porosity adjusted because they have porosities of less than 26%, which can be found in over 90% of the rock. The results are summarized in Table 6-8

Table 6-8. Summary of Upper Bound for Probability of Criticality as a Function of Fissile Content

% fissile	Number packages with more fissile	Pr{cluster log}	Expected criticalities
1.94*	240	$1.8 \times 10^{-6**}$	1.8×10^{-7}
1.87*	480	$4.70 \times 10^{-18} *$	9.2×10^{-19}
1.82*	1560	$7.18 \times 10^{-46} *$	4.6×10^{-46}

* From Table 6-6

** Porosity adjusted as described above

6.3.4 Adjustment for Critical Masses Greater Than a Single Waste Package

For those cases with required critical mass significantly greater than 10 tons (the contents of 1 waste package) some focusing of the flow from 2 or more waste packages would be necessary. There are two mechanisms for such focusing: (1) random fractures which accidentally happen to channel the flow in a concentrating direction, and (2) highly permeable rock which acts as an attractor for groundwater streamlines. This section provides a simplified analysis of the first mechanism. It should be noted that this section stands alone, and is for illustrative purposes only.

Assuming that the outflows (if any) from the individual packages move mainly vertically, or at least in parallel, worst case spreading would decrease the probability by multiplying by a factor less than the ratio of the critical sphere cross section area divided by the repository area enclosing the required number of waste packages, which could be quite a small factor if the design basis waste packages are distributed throughout the repository. There are four cases in Table 7-1 which require significantly more than 10 tons of uranium, but this correction has not been applied because the initial calculation showed the probability to be incredibly small. It should be noted that groundwater focusing does occur naturally, but rarely, as demonstrated by artesian springs being at the focus of a large catchment area.

It is, nevertheless, useful to estimate the per-package multiplicative factor. At 80 MTU/acre, and approximately 10 MTU/pkg, the average repository area per waste package is 493 m²; a typical critical sphere radius from Table 6-6 is 1 meter, so the reduction factor would be $\pi/493 = 0.006$.

Some recent unpublished work suggests that narrow, individual waste package, plumes may persist even into the saturated zone. However the more conventional model is Gaussian plume spreading (resulting in dilution or reduction in concentration of contaminants) of flow from a single package of such magnitude that even the smallest critical mass requirements of Table 6-6 would require more than one waste package. The following simplified analysis indicates the magnitude of such a dispersion.

It is conservatively assumed that the groundwater which has passed through a waste package flows vertically downward through the unsaturated zone with no lateral dispersion. In the saturated zone, the flow follows the fluid potential gradient with a dispersion approximated by Eq. 7.6-5 of Reference 6, which gives the concentration as a function of vertical distance below the water table, z , distance from the plume centerline, y , and downstream distance, x :

$$C(x,y,z)=(2Q/u)\exp\{-y^2/[4D_y(x/u)]-z^2/[4D_z(x/u)]\}/[4\pi\phi(D_yD_z)^{.5}(x/u)]$$

where Q is the mass flux from a point source, u is the groundwater velocity, ϕ is the porosity, and D_y and D_z are the diffusion coefficients in the y and z directions and are modeled by:

$$D_y = \beta_y xu, \quad D_z = \beta_z xu$$

Conservatively assuming $y=0$, the concentration will peak at a downstream distance of $x=z*\text{sqrt}(1/\beta_z)/2$.

The remaining parameters are modeled as follows:

$$\phi=V_{\text{sat}}/u, \quad Q=C_{\text{uz}}V_{\text{uz}}A,$$

where A is the waste package footprint, and the subscripts indicate the zone to which the parameters apply, which reduces the concentration formula to:

$$C/C_{\text{uz}} = 4V_{\text{uz}}A\text{sqrt}(\beta_z/\beta_y)\exp(-1)/[V_{\text{sat}}z^2]$$

Generally, $V_{\text{uz}} < V_{\text{sat}}$, $\beta_z/\beta_y < 0.1$, and for any appreciable distance below the water table $A \ll z^2$, so the concentration of uranium from a waste package will be diluted by at least a few orders of magnitude by the time it has moved a few hundred meters below the water table (top of the saturated zone).

Since the smallest critical mass found in this study is 16% of a waste package (1.6 tons required for the smallest critical mass out of approximately 10 tons uranium in the whole waste package), this dilution implies that the streams from a number of waste packages would have to be combined to deposit a single critical mass. Since the probabilities calculated without this correction are already very small, the correction was not quantified further nor applied.

7.0 Criticality Consequences

The purpose of this section is to illustrate the estimation of the consequences of an internal criticality event, under the assumption that such an event does occur. For this illustration, it is assumed that such an internal criticality event occurs at 15,000 years following emplacement. This time is in the middle of the range of peak k_{eff} (10,000 to 30,000 years after emplacement, depending on the SNF burnup and initial enrichment). Furthermore, in order to support the maintenance of a criticality internal to the WP for a duration of 10,000 years, it is necessary to assume that the highest possible infiltration rate (10 mm/yr) does occur and that the high infiltration can have, at most, a 10,000 year duration. The basis for the first assumption is that it is the approximate time of the highest postclosure criticality potential for the PWR criticality design basis SNF (as has been demonstrated by many time-dependent k_{eff} calculations), and, as has been noted in Section 6.2.1, it corresponds, approximately to the earliest potential criticalities. The basis for the second assumption is that it is the expected upper bound for the conditions supporting criticality (high infiltration, integrity of the lower part of the barrier, sufficient fissile material remaining). The consequences of such a criticality event will be discussed in terms of the heat generated and the change in the radionuclide inventory of the waste package. These calculations presented here are described in more detail in Reference 4.

7.1 Estimated Power and Duration of an Internal Criticality

It is assumed that if a criticality is possible, it is gradually approaching a critical condition ($k_{\text{eff}}=1$) as a result of positive reactivity insertions caused by a slow loss of boron and iron from the package interior. Once a WP reaches a k_{eff} of 1, continued small positive reactivity insertions will cause the power output of the WP to begin to slowly rise (i.e., a long reactor period). If the power exceeds a certain limit, the rate at which water is consequentially removed from the WP will exceed the rate of input, and the resulting water level drop will provide a negative reactivity insertion driving the WP back towards a subcritical condition. Conversely, if insufficient power is produced, the water level will be maintained and the exchange process discussed previously will continue to remove dissolved boron, thus providing a continued source of positive reactivity insertions until the point of equilibrium is achieved. The maximum steady state power can then be estimated by determining the power required to maintain the bulk WP water temperature at the point where water is removed at the same rate that it drips into the WP. The WP must produce sufficient power to raise the temperature of the incoming water to this equilibrium value, as well as account for heat losses to the environment by radiation and/or conduction.

It is conservatively assumed that airflow is stagnant in a drift at the 15,000 year-plus time frame under consideration, and evaporation can be modeled as diffusion of water vapor into air. The first step is to obtain the diffusion coefficient for water into air. The following expression obtained from Reference 32 provides an approximation for the diffusion coefficient as a function of temperature:

$$D(T) = [435.7 \cdot T^{3/2} \cdot (M_1^{-1} + M_2^{-1})^{1/2}] / (P_{\text{atm}} \cdot (V_1^{1/3} + V_2^{1/3})) \quad (7-1)$$

where $D(T)$ is the diffusion coefficient in cm^2/s at temperature T ,
 T is the temperature in K,

P_{atm} is the atmospheric pressure (1.0132×10^5 Pa),
 V_1, V_2 are the molecular volumes of substances 1 and 2 (in this case water, 18.8 cm^3/mole , and air, 29.9 cm^3/mole , respectively), and
 M_1, M_2 are the molecular weights of substances 1 and 2 (water, 18.02 kg/kmol , and air, 28.97 kg/kmol).

An additional factor of 0.056 cm^2/s has been added to values calculated by Eq. 7-1 to correspond with empirical measurements of the diffusion coefficient of water vapor into air at 8°C and 25°C .

With the diffusion coefficient determined, the volumetric flow rate of water out of the package due to evaporation is determined using the integrated form of Stefan's law (Ref. 32):

$$V_{\text{evap}}(T) = [(D(T) \cdot P_{\text{atm}} \cdot M_1 \cdot A \cdot v(T)) / (R_0 \cdot T \cdot z)] \cdot \ln[(P_{\text{atm}} - p(T) \cdot \text{RH}) / (P_{\text{atm}} - p(T))] \quad (7-2)$$

where, $V_{\text{evap}}(T)$ is the volumetric evaporation rate,
 $D(T)$ is the diffusion coefficient at temperature T ,
 T is the temperature,
 P_{atm} is the atmospheric pressure,
 $p(T)$ is the saturation pressure of water at temperature T ,
 R_0 is the Universal Gas Constant (8.315 $\text{kJ}/\text{kmol} \cdot \text{K}$),
 z is the distance from the water surface to the bulk environment,
 $v(T)$ is the specific volume of the water at temperature T ,
 A is the surface area of the water in the WP,
 RH is the drift relative humidity (taken to be 96%), and
 M_1 is the molecular weight of water.

The maximum rate of water dripping on a WP in TSPA-95 (Ref. 6) was assumed to be approximately 1.9×10^5 cm^3/yr , and was assumed (in TSPA-95) to occur 50,000 years after emplacement. [It should be noted that recent studies have suggested that the peak infiltration rate might be as large as 50 mm/yr , which would increase the power level by nearly a factor of 5.] More refined calculations of inventory increment will utilize the more recent, higher estimate of infiltration rate.

Using Eq. 7-2, the WP would have to produce sufficient power to maintain the water in the WP at a temperature of 57.4°C , as well as compensate for other mechanisms of heat loss, to match this drip rate. This indicates that evaporation alone will be sufficient to remove the incoming water, and bulk boiling will not occur.

It is assumed for this analysis that the WP configuration has a slightly negative moderator temperature coefficient, which also contributes to slowing the rate of power increase so that a stable power level is gradually reached. This assumption is based on previous analyses of the ACD 21 PWR Uncanistered Fuel WP (Ref. 39) which indicated that the first 5% reduction in moderator density from that used in the calculation (sat. liq. at 27°C) will result in a negative reactivity insertion of approximately 10^{-2} ($\Delta k/k$) for the criticality design basis fuel (Section 5, Ref. 33). For comparison purposes, a 30°C increase results in only a 1% density reduction.

These particular values are mentioned only to show that steady state is achieved; they have no direct impact on what that steady state actually is. The actual values of the parameters of the steady state are determined by the methodology described in the following paragraphs.

The amount of reactor heat dissipated by heating the incoming water, which is assumed to be at a temperature of 30°C, to a temperature of 57.4°C is given by the following expression:

$$q_{\text{water}} = [C_p(30^\circ\text{C}) \cdot V_{\text{drip}} \cdot \Delta T] / v(30^\circ\text{C}) \quad (7-3)$$

where, q_{water} is the heat input required to raise the water temperature 27.4°C,
 V_{drip} is the rate of water dripping into the WP,
 $C_p(30^\circ\text{C})$ is the specific heat of water at 30°C,
 $v(30^\circ\text{C})$ is the specific gravity of water at 30°C, and
 ΔT is the temperature increase (27.4°C).

Using Eq. 7-3, only 0.677 W are required to raise the temperature of the water to the point where the evaporation rate equals the rate of influx.

Once at 57.4°C, the amount of power required to vaporize water at a rate of $1.9 \times 10^5 \text{ cm}^3/\text{yr}$ of water must also be accounted for. This is equal to the product of the heat of vaporization at 57.4°C, 2,364.8 kJ/kg (linear interpolation from Reference 34, Table A-3), the volume of water to be evaporated, $1.9 \times 10^5 \text{ cm}^3/\text{yr}$, and the density of water at 57.4°C, 984.4 kg/m³. Multiplying the above three values and performing the appropriate unit conversions yields an additional 14 W.

As stated above, additional heat losses will also occur due to radiation and/or conduction heat transfer to the local environment. The actual configuration of the drift thousands of years after emplacement cannot be defined sufficiently to allow a detailed heat transfer estimate. It is highly likely that a portion of the WP may be covered with rubble, possibly as a result of the gradual collapse of the drift, and both radiation and conduction mechanisms will be active. However, examination of ideal radiation-only and conduction-only systems should respectively provide an upper and lower bound on the heat loss from a WP with a bulk water temperature of 57.4°C. Heat losses due to radiation alone can be estimated by treating the WP and drift as a system of concentric cylinders, with the WP surface at 57.4°C, and the drift wall assumed to maintain a constant 30°C. The radiation heat transfer rate is then given by:

$$q_{\text{rad}} = [\sigma \cdot A_1 \cdot (T_1^4 - T_2^4)] / [\epsilon_1^{-1} + (A_1/A_2)(\epsilon_2^{-1} - 1)] \quad (\text{Ref. 32}) \quad (7-4)$$

where, q_{rad} is the radiation heat transfer rate,
 T_1 is the WP surface temperature,
 T_2 is the drift wall temperature,
 A_1 is the WP surface area,
 A_2 is the drift surface area,
 ϵ_1 is the emissivity of oxidized carbon steel, 0.80,
 ϵ_2 is the emissivity of tuff rock, 0.85, and

σ is the Stephan-Boltzman constant ($5.669 \times 10^{-8} \text{ W/m}^2\text{K}^4$).

Using the above equation, radiation heat loss from a 57.4°C WP is estimated to be 3,859 W. Again assuming the system of concentric cylinders and a drift wall temperature of 30°C , a WP entirely covered by crushed tuff would lose heat by conduction according to:

$$q_{\text{cond}} = [2\pi \cdot k \cdot L \cdot (T_1 - T_2)] / [\ln(d_2/d_1)] \quad (\text{Ref. 32}) \quad (7-5)$$

where,

q_{cond}	is the conduction heat transfer rate,
k	is the average thermal conductivity of crushed tuff,
L	is the WP outer length less that of the skirts,
T_1	is the WP surface temperature,
T_2	is the drift wall temperature,
d_1	is the WP outer diameter, and
d_2	is the drift diameter.

Solving the above equation for a WP surface temperature of 57.4°C indicates that 504 W will be lost if all heat transfer occurs by conduction through crushed tuff. Assuming the more likely configuration of a WP covered half-way with rubble, the heat loss is approximated by taking the mean of the radiation and conduction heat transfers, 2.182 kW. This is not quite equivalent to assuming that half the package area is devoted to radiative heat transfer and the other half to conductive transfer; the difference is that the conductive transfer is not quite proportional to surface area, as can be seen from Eq. 7-5. Since the power dissipated in heating the water dripping in to 57.4°C and vaporizing it at that temperature has been shown to total less than 15 W, it is not added in this approximation.

The above power represents a conservative estimate of output power because, in reality, there will be a number of negative feedback mechanisms which will severely limit the actual Δk and the criticality duration. Some of these mechanisms include the decreases in the infiltration rate resulting from climatic cycles, the production of neutron absorbing fission products, the depletion of fissile nuclides, changes in moderator density, corrosion of the cladding or spacer grids (leading to consolidation of the fuel rods), and corrosion of the remainder of the WP barriers (leading to the formation of drainage holes). The combined effect of these mechanisms will likely limit any single WP criticality event to a relatively short duration, with criticality events reoccurring in the same WP in a cyclic pattern as long as the necessary conditions continue to recur. Therefore, use of a steady state power of 2.182 kW to estimate total burnup resulting from a long-term postclosure internal WP criticality should be a reasonable approximation to the cumulative effect of multiple pulses.

The overall duration of such a cyclic criticality is also dependent on some of the above-mentioned feedback mechanisms, primarily the continued availability of water, the ability of the WP to hold water, and the depletion of fissile nuclides. While the climate cycle period over the past 2 million years has been approximately 100,000 years, infiltration rates near the peak (which are required to maintain the steady state power level and water exchange rates discussed previously) may occur for only several thousand years (Ref. 6). Based on this information, a

range of 1,000 year to 10,000 year durations has been evaluated, for the purposes of estimating the effects of criticality on radionuclide inventory. A 10,000 year criticality at a steady state power level of 2.182 kW yields an additional burnup of 7,965 MWd for the SNF in the WP (817 MWd/MTU). Such long periods of steady state power production are expected to be conservative because of the cyclic nature of the criticality itself, the duration of the peak infiltration rates, and the expectation that the WP will have a much lower probability of being able to hold water by the time the next peak in infiltration returns.

7.2 Effects of an Internal Criticality on the Radionuclide Inventory of the WP

7.2.1 ORIGEN-S Calculations

To evaluate the effects of a criticality on the radionuclide inventory of a WP, the computer code ORIGEN-S was run using the criticality design basis fuel, and the steady state power of 2.182 kW discussed in Section 7.1 above. The criticality was assumed to occur after the fuel had aged/decayed for 15,000 years and was maintained at the above mentioned power for three durations: 1,000, 5,000, and 10,000 years. The output of these runs was the radionuclide inventory, in curies, at the times corresponding to the end of each criticality, and at fuel ages (time since reactor discharge) of 45,000 and 65,000 years. A fourth, decay-only case was run to determine the radionuclide inventories at the above times for fuel which did not experience a criticality event. The details of the ORIGEN-S calculations performed to obtain the radionuclide inventories for both decay-only and fission-plus-decay cases are reported in Reference 35.

To provide a comparison between a WP which experienced a criticality, and one only decayed, 36 of the 39 isotopes in the TSPA-95 radionuclide inventory list (Ref. 6) were extracted from the ORIGEN-S output (Ref. 35). Comparisons of the activities of ^{36}Cl , ^{59}Ni , and ^{63}Ni were not made because the present ORIGEN-S analysis has not yet been extended to activation products. Differences were reported in terms of the percentage change in the activity of each radionuclide at each time, and the percentage change

The calculations to determine the difference in radionuclide activities between the decay-only and criticality cases were performed using Excel v5.0. The radionuclide increment and comparison results are summarized in Tables 7-1, 7-2, and 7-3 for the 1,000 year, 5,000 year, and 10,000 year duration criticalities, respectively.

7.2.2 Neutron Activation Estimates

Neutron activation of stable isotopes in the WP materials and water represents another potential source of radionuclides which may be produced during such a criticality. The ORIGEN-S output (Ref. 35) indicated that the total average neutron flux in the 2.182 kW WP was $\approx 2.9 \times 10^8$ neutrons/cm²s, and that 10.9% of this flux was in the thermal part of the spectrum. ^{14}C and ^{36}Cl are two radionuclides in the TSPA-95 radionuclide inventory which may be produced from activation of trace elements in the water. ^{14}C is primarily produced by the $^{14}\text{N}(n,p)$ reaction and the $^{17}\text{O}(n,\alpha)$ reaction, although much smaller quantities may also be produced by multiple neutron captures in ^{16}O ($^{16}\text{O}(n,\gamma)-^{17}\text{O}(n,\alpha)-^{14}\text{C}$). The number density for ^{14}N in 57.4°C water in

equilibrium with air at atmospheric pressure is given by the following expression:

$$N_{N14} = (A_{N14} \cdot \rho_w \cdot v_N \cdot P_{atm} \cdot N_a \cdot 2) / (M_w \cdot H_N) \quad (7-6)$$

where,

- N_{N14} is the number density of ^{14}N ,
- A_{N14} is the abundance of ^{14}N (99.63%),
- ρ_w is the density of water at 57.4°C,
- v_N is the volume fraction of N_2 in air (78.08%),
- M_w is the molecular weight of water,
- P_{atm} is the air pressure,
- N_a is Avogadro's Number (6.022×10^{23} atoms/mole), and
- H_N is Henry's Law solubility of N_2 in water at 57.4°C in atm. N_2 /(mole N_2 /mole water).

This yields 4.35×10^{17} atoms of ^{14}N per cm^3 of water. The number density of ^{17}O in water is simply computed by:

$$N_{O17} = (A_{O17} \cdot \rho_w \cdot N_a) / M_w \quad (7-7)$$

where,

- N_{O17} is the number density of ^{17}O ,
- A_{O17} is the abundance of ^{17}O ,
- ρ_w is the density of water at 57.4°C,
- M_w is the molecular weight of water, and
- N_a is Avogadro's Number.

This yields 1.32×10^{19} ^{17}O atoms/ cm^3 . The amount of oxygen dissolved in the water is insignificant compared to that in the water itself, and has been neglected for this calculation.

Given the above flux and thermal fraction, and assuming that the number density of ^{14}N and ^{17}O remains constant, the production rate of ^{14}C can be calculated as follows:

$$^{14}\text{C} = \lambda_{C14} \cdot (N_{N14} \cdot \sigma_{pN14} + N_{O17} \cdot \sigma_{\alpha O17}) \cdot \phi \cdot f \cdot V_{WP} \quad (7-8)$$

where,

- ^{14}C is the production rate of ^{14}C ,
- λ_{C14} is the ^{14}C decay constant ($\ln 2$ /half-life),
- N_{N14} is the number density of ^{14}N ,
- N_{O17} is the number density of ^{17}O ,
- $\sigma_{\alpha O17}$ is the microscopic thermal cross section for the $^{17}\text{O}(n,\alpha)$ reaction (0.24 barns),
- σ_{pN14} is the microscopic thermal cross section for the $^{14}\text{N}(n,p)$ reaction (1.81 barns),
- ϕ is the average total neutron flux,
- f is the fraction of the flux in the thermal part of the spectrum, and
- V_{WP} is the volume of water in the fully flooded WP.

Using the parameters given in Reference 2 (Section 4.1.7), this yields 1.98 μCi of $^{14}\text{C}/\text{yr}$ of WP criticality, which is not contained by the cladding and may be available for immediate release from the WP. However, this production rate is almost six orders of magnitude below the Nuclear Regulatory Commission (NRC) release limits for the site of 0.796 Ci of $^{14}\text{C}/\text{yr}$ (Ref. 6) and thus should have no impact on site performance.

Similarly, ^{36}Cl may be produced during the criticality by neutron activation of ^{35}Cl in the water. Chemical analyses of J-13 (Ref. 38) well water have found it to nominally contain 7.5 $\mu\text{g Cl}/\text{mL}$. However, evaporation of water from the WP would be expected to increase this concentration. Corrosion tests involving boiling J-13 well water, tuff rock, and stainless steel specimens found that the stable concentration of Cl^- had increased to 161 $\mu\text{g}/\text{mL}$ after 1 year (Ref. 38). These values can be used to determine nominal and high ^{35}Cl number densities as follows:

$$N_{\text{Cl}35} = (C_{\text{Cl}} \cdot A_{\text{Cl}35} \cdot N_a) / M_{\text{Cl}} \quad (7-9)$$

where,

$N_{\text{Cl}35}$	is the number density of ^{35}Cl ,
$A_{\text{Cl}35}$	is the abundance of ^{35}Cl ,
C_{Cl}	is the concentration of Cl^- in the water,
M_{Cl}	is the molecular weight of Cl , and
N_a	is Avogadro's Number.

This yields a nominal value of 9.65×10^{16} atoms of $^{35}\text{Cl}/\text{cm}^3$ or a high value of 2.07×10^{18} ^{36}Cl atoms/ cm^3 if the high concentration is used. The production rate of ^{36}Cl can then be calculated by:

$$^{36}\text{C} = \lambda_{\text{Cl}36} \cdot (N_{\text{Cl}35} \cdot \sigma_{\gamma\text{Cl}35}) \cdot \phi \cdot f \cdot V_{\text{WP}} \quad (7-10)$$

where,

^{36}C	is the production rate of ^{36}Cl ,
$\lambda_{\text{Cl}36}$	is the ^{36}Cl decay constant ($\ln 2/\text{half-life}$),
$N_{\text{Cl}35}$	is the number density of ^{35}Cl ,
$\sigma_{\gamma\text{Cl}35}$	is the microscopic thermal cross section for the $^{35}\text{Cl}(n,\gamma)$ reaction,
ϕ	is the average total neutron flux,
f	is the fraction of the flux in the thermal part of the spectrum, and
V_{WP}	is the volume of water in the fully flooded WP.

This yields a nominal production rate of 0.04 $\mu\text{Ci}/\text{yr}$ of ^{36}Cl and a high rate of 0.86 $\mu\text{Ci}/\text{yr}$. Both of these values are also several orders of magnitude below the NRC site release limits of 7.13 mCi/yr and should not impact site performance.

The overall effect of the criticality can be summarized by the percentage increase in the total curies for the 36 isotopes utilized in TSPA-95 immediately after the criticality ends and at later times. Table 7-4 shows this comparison. The explicitly stated times are measured from emplacement. The duration of criticality times are relative to the start of criticality at 15,000 years, so the absolute (measured from emplacement) times at the end of criticality are determined by adding the duration of criticality to 15,000 years.

Table 7-1. Effects of 1,000 Year Criticality on the Radionuclide Inventory of a PWR Fuel Assembly

	16,000 yr				45,000 yr				65,000 yr			
	Act. (Ci)	Act. (Ci)	% Diff.	% Diff.	Act. (Ci)	Act. (Ci)	% Diff.	% Diff.	Act. (Ci)	Act. (Ci)	% Diff.	% Diff.
	Critical	Decay Only	Isotope	Total	Critical	Decay Only	Isotope	Total	Critical	Decay Only	Isotope	Total
ac227	4.9e-003	4.3e-003	1.6e+001	4.9e-004	1.0e-002	1.0e-002	3.0e+000	5.6e-004	1.3e-002	1.3e-002	2.3e+000	9.3e-004
am241	2.6e+000	2.2e-003	1.2e+005	1.9e+000	2.0e-004	2.0e-004	-1.5e+000	-5.6e-006	3.9e-005	3.9e-005	-1.5e+000	-1.9e-006
am242m	2.0e-003	0.0e+000	N/A	1.4e-003	0.0e+000	0.0e+000	0.0e+000	0.0e+000	0.0e+000	0.0e+000	0.0e+000	0.0e+000
am243	4.8e-001	4.5e-001	7.2e+000	2.3e-002	3.1e-002	2.9e-002	7.2e+000	3.9e-003	4.8e-003	4.5e-003	7.2e+000	9.9e-004
c 14	4.9e-006	4.8e-006	2.5e+000	8.7e-008	1.5e-007	1.4e-007	2.8e+000	7.5e-009	1.3e-008	1.3e-008	2.3e+000	9.3e-010
cm244	1.7e-002	0.0e+000	N/A	1.2e-002	0.0e+000	0.0e+000	0.0e+000	0.0e+000	0.0e+000	0.0e+000	0.0e+000	0.0e+000
cm245	2.1e-003	2.1e-003	-1.4e+000	-2.2e-005	2.0e-004	2.0e-004	-1.5e+000	-5.6e-006	3.9e-005	3.9e-005	-1.5e+000	-1.9e-006
cm246	9.6e-005	8.8e-005	9.2e+000	5.8e-006	1.4e-006	1.3e-006	9.5e+000	2.3e-007	7.3e-008	6.7e-008	9.2e+000	1.9e-008
cs135	2.0e-001	2.0e-001	9.9e-001	1.4e-003	2.0e-001	2.0e-001	1.0e+000	3.8e-003	2.0e-001	2.0e-001	1.0e+000	6.2e-003
i129	8.8e-003	8.8e-003	4.5e-001	2.9e-005	8.8e-003	8.8e-003	4.5e-001	7.5e-005	8.8e-003	8.8e-003	3.4e-001	9.3e-005
nb 93m	3.5e-001	3.5e-001	5.8e-001	1.4e-003	3.4e-001	3.4e-001	2.9e-001	1.9e-003	3.4e-001	3.4e-001	2.9e-001	3.1e-003
nb 94	1.9e-005	1.4e-005	4.0e+001	4.0e-006	7.1e-006	5.0e-006	4.1e+001	3.9e-006	3.6e-006	2.5e-006	4.1e+001	3.2e-006
np237	3.8e-001	3.8e-001	2.6e-001	7.2e-004	3.8e-001	3.8e-001	2.6e-001	1.9e-003	3.8e-001	3.8e-001	2.7e-001	3.1e-003
pa231	4.9e-003	4.3e-003	1.6e+001	4.9e-004	1.0e-002	1.0e-002	3.0e+000	5.6e-004	1.3e-002	1.3e-002	1.6e+000	6.2e-004
pb210	8.0e-002	8.0e-002	0.0e+000	0.0e+000	2.1e-001	2.1e-001	4.7e-001	1.9e-003	2.8e-001	2.8e-001	7.1e-001	6.2e-003
pd107	2.6e-002	2.6e-002	3.8e-001	7.2e-005	2.6e-002	2.6e-002	3.8e-001	1.9e-004	2.6e-002	2.6e-002	7.7e-001	6.2e-004
pu238	2.9e+000	0.0e+000	N/A	2.1e+000	0.0e+000	0.0e+000	0.0e+000	0.0e+000	0.0e+000	0.0e+000	0.0e+000	0.0e+000
pu239	1.0e+002	1.0e+002	9.7e-001	7.2e-001	4.5e+001	4.5e+001	6.7e-001	5.6e-001	2.6e+001	2.5e+001	7.9e-001	6.2e-001
pu240	2.9e+001	2.8e+001	4.3e+000	8.7e-001	1.4e+000	1.3e+000	3.8e+000	9.4e-002	1.7e-001	1.6e-001	4.4e+000	2.2e-002
pu241	3.2e+000	2.1e-003	1.5e+005	2.3e+000	2.0e-004	2.0e-004	-1.5e+000	-5.6e-006	3.9e-005	3.9e-005	-1.5e+000	-1.9e-006
pu242	2.7e-001	2.7e-001	-3.7e-001	-7.2e-004	2.6e-001	2.6e-001	-3.9e-001	-1.9e-003	2.5e-001	2.5e-001	-4.0e-001	-3.1e-003
ra226	8.0e-002	8.0e-002	-1.3e-001	-7.2e-005	2.1e-001	2.1e-001	4.7e-001	1.9e-003	2.8e-001	2.8e-001	7.1e-001	6.2e-003
ra228	9.0e-008	9.0e-008	0.0e+000	0.0e+000	2.8e-007	2.8e-007	3.6e-001	1.9e-009	4.1e-007	4.1e-007	4.9e-001	6.2e-009
se 79	1.4e-001	1.4e-001	7.3e-001	7.2e-004	7.5e-002	7.5e-002	6.7e-001	9.4e-004	4.9e-002	4.9e-002	6.1e-001	9.3e-004
sm151	7.9e-001	0.0e+000	N/A	5.7e-001	0.0e+000	0.0e+000	0.0e+000	0.0e+000	0.0e+000	0.0e+000	0.0e+000	0.0e+000
sn126	1.3e-001	1.2e-001	8.1e-001	7.2e-004	1.0e-001	1.0e-001	0.0e+000	0.0e+000	8.9e-002	8.8e-002	4.5e-001	1.2e-003
tc 99	3.8e+000	3.7e+000	5.3e-001	1.4e-002	3.4e+000	3.4e+000	5.9e-001	3.8e-002	3.2e+000	3.2e+000	3.1e-001	3.1e-002
th229	1.1e-002	1.2e-002	-8.7e-001	-7.2e-005	5.1e-002	5.1e-002	0.0e+000	0.0e+000	7.8e-002	7.8e-002	0.0e+000	0.0e+000
th230	9.2e-002	9.2e-002	-2.2e-001	-1.4e-004	2.2e-001	2.2e-001	4.5e-001	1.9e-003	2.9e-001	2.9e-001	7.0e-001	6.2e-003
th232	9.0e-008	9.0e-008	0.0e+000	0.0e+000	2.8e-007	2.8e-007	3.6e-001	1.9e-009	4.1e-007	4.1e-007	4.9e-001	6.2e-009
u233	2.5e-002	2.5e-002	-8.0e-001	-1.4e-004	6.7e-002	6.7e-002	0.0e+000	0.0e+000	9.3e-002	9.3e-002	1.1e-001	3.1e-004
u234	6.7e-001	6.7e-001	9.0e-001	4.3e-003	6.3e-001	6.3e-001	9.6e-001	1.1e-002	6.1e-001	6.0e-001	1.0e+000	1.9e-002
u235	1.6e-002	1.6e-002	-6.4e-001	-7.2e-005	1.8e-002	1.8e-002	-5.6e-001	-1.9e-004	1.8e-002	1.8e-002	-5.4e-001	-3.1e-004
u236	1.3e-001	1.3e-001	7.9e-001	7.2e-004	1.3e-001	1.3e-001	0.0e+000	0.0e+000	1.4e-001	1.3e-001	7.5e-001	3.1e-003
u238	1.5e-001	1.5e-001	0.0e+000	0.0e+000	1.5e-001	1.5e-001	0.0e+000	0.0e+000	1.5e-001	1.5e-001	0.0e+000	0.0e+000
zr 93	3.5e-001	3.5e-001	5.8e-001	1.4e-003	3.4e-001	3.4e-001	2.9e-001	1.9e-003	3.4e-001	3.4e-001	2.9e-001	3.1e-003
36 Iso.												
Totals	1.5e+002	1.4e+002	8.5e+000	0.0e+000	5.4e+001	5.3e+001	7.3e-001	0.0e+000	3.3e+001	3.2e+001	7.3e-001	0.0e+000

Table 7-2. Effects of 5,000 Year Criticality on the Radionuclide Inventory of a PWR Fuel Assembly

	20,000 yr				45,000 yr				65,000 yr			
	Act. (Ci) Critical	Act. (Ci) Decay Only	% Diff. Isotope	% Diff. Total	Act. (Ci) Critical	Act. (Ci) Decay Only	% Diff. Isotope	% Diff. Total	Act. (Ci) Critical	Act. (Ci) Decay Only	% Diff. Isotope	% Diff. Total
Ac227	8.8e-003	5.2e-003	7.0e+001	3.1e-003	1.2e-002	1.0e-002	2.0e+001	3.8e-003	1.4e-002	1.3e-002	1.0e+001	4.0e-003
Am241	2.7e+000	1.6e-003	1.7e+005	2.3e+000	1.9e-004	2.0e-004	-7.5e+000	-2.8e-005	3.6e-005	3.9e-005	-7.4e+000	-9.0e-006
Am242m	2.4e-003	0.0e+000	N/A	2.0e-003	0.0e+000	0.0e+000	0.0e+000	0.0e+000	0.0e+000	0.0e+000	0.0e+000	0.0e+000
Am243	4.4e-001	3.1e-001	4.4e+001	1.1e-001	4.2e-002	2.9e-002	4.4e+001	2.4e-002	6.4e-003	4.5e-003	4.3e+001	6.0e-003
C 14	3.5e-006	3.0e-006	1.7e+001	4.3e-007	1.7e-007	1.4e-007	1.7e+001	4.5e-008	1.5e-008	1.3e-008	1.7e+001	6.8e-009
Cm244	1.6e-002	0.0e+000	N/A	1.3e-002	0.0e+000	0.0e+000	0.0e+000	0.0e+000	0.0e+000	0.0e+000	0.0e+000	0.0e+000
Cm245	1.4e-003	1.5e-003	-7.1e+000	-9.3e-005	1.9e-004	2.0e-004	-7.0e+000	-2.6e-005	3.6e-005	3.9e-005	-7.4e+000	-9.0e-006
Cm246	7.4e-005	4.9e-005	5.1e+001	2.1e-005	1.9e-006	1.3e-006	5.2e+001	1.2e-006	1.0e-007	6.7e-008	5.2e+001	1.1e-007
Cs135	2.1e-001	2.0e-001	4.4e+000	7.6e-003	2.1e-001	2.0e-001	4.5e+000	1.7e-002	2.1e-001	2.0e-001	4.5e+000	2.8e-002
I129	9.0e-003	8.8e-003	2.0e+000	1.5e-004	9.0e-003	8.8e-003	2.0e+000	3.4e-004	9.0e-003	8.8e-003	2.0e+000	5.6e-004
Nb 93m	3.5e-001	3.5e-001	2.0e+000	5.9e-003	3.5e-001	3.4e-001	2.0e+000	1.3e-002	3.5e-001	3.4e-001	2.1e+000	2.2e-002
Nb 94	4.1e-005	1.2e-005	2.5e+002	2.5e-005	1.8e-005	5.0e-006	2.5e+002	2.4e-005	8.9e-006	2.5e-006	2.5e+002	2.0e-005
Np237	3.8e-001	3.8e-001	1.0e+000	3.4e-003	3.8e-001	3.8e-001	1.1e+000	7.5e-003	3.8e-001	3.8e-001	1.3e+000	1.5e-002
Pa231	8.8e-003	5.2e-003	7.0e+001	3.1e-003	1.2e-002	1.0e-002	2.0e+001	3.8e-003	1.4e-002	1.3e-002	1.0e+001	4.0e-003
Pb210	1.0e-001	1.0e-001	-9.9e-001	-8.5e-004	2.2e-001	2.1e-001	2.3e+000	9.4e-003	2.9e-001	2.8e-001	3.6e+000	3.1e-002
Pd107	2.7e-002	2.6e-002	1.9e+000	4.2e-004	2.7e-002	2.6e-002	1.9e+000	9.4e-004	2.7e-002	2.6e-002	2.3e+000	1.9e-003
Pu238	3.0e+000	0.0e+000	N/A	2.5e+000	0.0e+000	0.0e+000	0.0e+000	0.0e+000	0.0e+000	0.0e+000	0.0e+000	0.0e+000
Pu239	9.6e+001	9.2e+001	3.6e+000	2.8e+000	4.7e+001	4.5e+001	3.8e+000	3.2e+000	2.6e+001	2.5e+001	4.0e+000	3.1e+000
Pu240	2.3e+001	1.9e+001	2.6e+001	4.1e+000	1.7e+000	1.3e+000	2.6e+001	6.4e-001	2.0e-001	1.6e-001	2.6e+001	1.3e-001
Pu241	2.6e+000	1.5e-003	1.7e+005	2.2e+000	1.9e-004	2.0e-004	-7.5e+000	-2.8e-005	3.6e-005	3.9e-005	-7.4e+000	-9.0e-006
Pu242	2.7e-001	2.7e-001	-1.1e+000	-2.5e-003	2.5e-001	2.6e-001	-1.2e+000	-5.6e-003	2.5e-001	2.5e-001	-1.6e+000	-1.2e-002
Ra226	1.0e-001	1.0e-001	-9.9e-001	-8.5e-004	2.2e-001	2.1e-001	2.8e+000	1.1e-002	2.9e-001	2.8e-001	3.9e+000	3.4e-002
Ra228	1.1e-007	1.1e-007	0.0e+000	0.0e+000	2.8e-007	2.8e-007	1.4e+000	7.5e-009	4.2e-007	4.1e-007	1.7e+000	2.2e-008
Se 79	1.3e-001	1.3e-001	3.2e+000	3.4e-003	7.7e-002	7.5e-002	3.1e+000	4.3e-003	5.1e-002	4.9e-002	3.1e+000	4.6e-003
Sm151	8.0e-001	0.0e+000	N/A	6.8e-001	0.0e+000	0.0e+000	0.0e+000	0.0e+000	0.0e+000	0.0e+000	0.0e+000	0.0e+000
Sn126	1.2e-001	1.2e-001	2.5e+000	2.5e-003	1.0e-001	1.0e-001	2.0e+000	3.8e-003	9.1e-002	8.8e-002	2.5e+000	6.8e-003
Tc 99	3.8e+000	3.7e+000	2.2e+000	6.8e-002	3.5e+000	3.4e+000	2.1e+000	1.3e-001	3.3e+000	3.2e+000	1.9e+000	1.9e-001
Th229	1.6e-002	1.6e-002	-6.1e-001	-8.5e-005	5.1e-002	5.1e-002	-3.9e-001	-3.8e-004	7.8e-002	7.8e-002	1.3e-001	3.1e-004
Th230	1.1e-001	1.1e-001	-8.8e-001	-8.5e-004	2.3e-001	2.2e-001	2.7e+000	1.1e-002	3.0e-001	2.9e-001	3.8e+000	3.4e-002
Th232	1.1e-007	1.1e-007	0.0e+000	0.0e+000	2.8e-007	2.8e-007	1.4e+000	7.5e-009	4.2e-007	4.1e-007	1.7e+000	2.2e-008
U233	3.1e-002	3.1e-002	-1.9e+000	-5.1e-004	6.7e-002	6.7e-002	-1.5e-001	-1.9e-004	9.3e-002	9.3e-002	3.2e-001	9.3e-004
U234	6.9e-001	6.6e-001	5.3e+000	3.0e-002	6.6e-001	6.3e-001	5.3e+000	6.2e-002	6.3e-001	6.0e-001	5.2e+000	9.6e-002
U235	1.6e-002	1.6e-002	-1.9e+000	-2.5e-004	1.8e-002	1.8e-002	-1.1e+000	-3.8e-004	1.8e-002	1.8e-002	-1.6e+000	-9.3e-004
U236	1.3e-001	1.3e-001	1.6e+000	1.7e-003	1.4e-001	1.3e-001	2.2e+000	5.6e-003	1.4e-001	1.3e-001	2.2e+000	9.3e-003
U238	1.5e-001	1.5e-001	0.0e+000	0.0e+000	1.5e-001	1.5e-001	0.0e+000	0.0e+000	1.5e-001	1.5e-001	0.0e+000	0.0e+000
Zr 93	3.5e-001	3.5e-001	2.0e+000	5.9e-003	3.5e-001	3.4e-001	2.0e+000	1.3e-002	3.5e-001	3.4e-001	2.1e+000	2.2e-002
36 Iso.												
Totals	1.4e+002	1.2e+002	1.5e+001	0.0e+000	5.5e+001	5.3e+001	4.2e+000	0.0e+000	3.3e+001	3.2e+001	3.7e+000	0.0e+000

Table 7-3. Effects of 10,000 Year Criticality on the Radionuclide Inventory of a PWR Fuel Assembly

	25,000 yr				45,000 yr				65,000 yr			
	Act. (Ci)	Act. (Ci)	% Diff.	% Diff.	Act. (Ci)	Act. (Ci)	% Diff.	% Diff.	Act. (Ci)	Act. (Ci)	% Diff.	% Diff.
	Critical	Decay Only	Isotope	Total	Critical	Decay Only	Isotope	Total	Critical	Decay Only	Isotope	Total
Ac227	1.4e-002	6.3e-003	1.2e+002	8.0e-003	1.5e-002	1.0e-002	4.9e+001	9.2e-003	1.6e-002	1.3e-002	2.4e+001	9.6e-003
Am241	2.1e+000	1.1e-003	2.0e+005	2.2e+000	1.7e-004	2.0e-004	-1.4e+001	-5.5e-005	3.4e-005	3.9e-005	-1.5e+001	-1.8e-005
Am242m	1.9e-003	0.0e+000	N/A	2.0e-003	0.0e+000	0.0e+000	0.0e+000	0.0e+000	0.0e+000	0.0e+000	0.0e+000	0.0e+000
Am243	4.1e-001	1.9e-001	1.1e+002	2.2e-001	6.3e-002	2.9e-002	1.1e+002	6.3e-002	9.5e-003	4.5e-003	1.1e+002	1.6e-002
C14	2.4e-006	1.6e-006	4.8e+001	8.0e-007	2.1e-007	1.4e-007	4.9e+001	1.3e-007	1.9e-008	1.3e-008	4.8e+001	1.9e-008
Cm244	1.5e-002	0.0e+000	N/A	1.6e-002	0.0e+000	0.0e+000	0.0e+000	0.0e+000	0.0e+000	0.0e+000	0.0e+000	0.0e+000
Cm245	8.8e-004	1.0e-003	-1.4e+001	-1.5e-004	1.7e-004	2.0e-004	-1.4e+001	-5.5e-005	3.4e-005	3.9e-005	-1.5e+001	-1.8e-005
Cm246	5.2e-005	2.4e-005	1.2e+002	2.9e-005	2.8e-006	1.3e-006	1.2e+002	2.8e-006	1.5e-007	6.7e-008	1.2e+002	2.5e-007
Cs135	2.2e-001	2.0e-001	8.4e+000	1.7e-002	2.2e-001	2.0e-001	9.0e+000	3.4e-002	2.2e-001	2.0e-001	8.5e+000	5.3e-002
I129	9.2e-003	8.8e-003	4.1e+000	3.7e-004	9.2e-003	8.8e-003	4.1e+000	6.8e-004	9.2e-003	8.8e-003	4.0e+000	1.1e-003
Nb 93m	3.6e-001	3.4e-001	4.1e+000	1.4e-002	3.6e-001	3.4e-001	4.1e+000	2.6e-002	3.5e-001	3.4e-001	3.8e+000	4.0e-002
Nb 94	7.4e-005	1.0e-005	6.4e+002	6.5e-005	3.7e-005	5.0e-006	6.4e+002	6.1e-005	1.9e-005	2.5e-006	6.4e+002	5.0e-005
Np237	3.9e-001	3.8e-001	2.1e+000	8.2e-003	3.9e-001	3.8e-001	2.1e+000	1.5e-002	3.8e-001	3.8e-001	2.4e+000	2.8e-002
Pa231	1.4e-002	6.3e-003	1.2e+002	8.0e-003	1.5e-002	1.0e-002	4.9e+001	9.2e-003	1.6e-002	1.3e-002	2.4e+001	9.6e-003
Pb210	1.3e-001	1.3e-001	-7.9e-001	-1.0e-003	2.2e-001	2.1e-001	4.7e+000	1.9e-002	3.1e-001	2.8e-001	1.1e+001	9.9e-002
Pd107	2.7e-002	2.6e-002	3.8e+000	1.0e-003	2.7e-002	2.6e-002	3.8e+000	1.9e-003	2.7e-002	2.6e-002	4.2e+000	3.4e-003
Pu238	3.1e+000	0.0e+000	N/A	3.1e+000	0.0e+000	0.0e+000	0.0e+000	0.0e+000	0.0e+000	0.0e+000	0.0e+000	0.0e+000
Pu239	8.7e+001	8.0e+001	8.6e+000	7.0e+000	4.9e+001	4.5e+001	8.9e+000	7.5e+000	2.8e+001	2.5e+001	9.1e+000	7.1e+000
Pu240	1.8e+001	1.1e+001	6.9e+001	7.7e+000	2.2e+000	1.3e+000	6.8e+001	1.7e+000	2.7e-001	1.6e-001	6.9e+001	3.4e-001
Pu241	2.1e+000	1.0e-003	2.1e+005	2.2e+000	1.7e-004	2.0e-004	-1.4e+001	-5.5e-005	3.4e-005	3.9e-005	-1.5e+001	-1.8e-005
Pu242	2.6e-001	2.7e-001	-2.6e+000	-7.1e-003	2.5e-001	2.6e-001	-2.7e+000	-1.3e-002	2.4e-001	2.5e-001	-2.8e+000	-2.2e-002
Ra226	1.3e-001	1.3e-001	-7.9e-001	-1.0e-003	2.2e-001	2.1e-001	4.7e+000	1.9e-002	3.1e-001	2.8e-001	1.1e+001	9.9e-002
Ra228	1.5e-007	1.5e-007	6.8e-001	1.0e-009	2.8e-007	2.8e-007	2.2e+000	1.1e-008	4.2e-007	4.1e-007	2.9e+000	3.7e-008
Se 79	1.2e-001	1.1e-001	6.1e+000	7.1e-003	7.9e-002	7.5e-002	6.3e+000	8.8e-003	5.2e-002	4.9e-002	6.3e+000	9.6e-003
Sm151	8.1e-001	0.0e+000	N/A	8.2e-001	0.0e+000	0.0e+000	0.0e+000	0.0e+000	0.0e+000	0.0e+000	0.0e+000	0.0e+000
Sn126	1.2e-001	1.2e-001	5.1e+000	6.1e-003	1.1e-001	1.0e-001	4.9e+000	9.4e-003	9.3e-002	8.8e-002	5.0e+000	1.4e-002
Tc 99	3.8e+000	3.6e+000	4.1e+000	1.5e-001	3.5e+000	3.4e+000	4.1e+000	2.6e-001	3.3e+000	3.2e+000	3.8e+000	3.7e-001
Th229	2.3e-002	2.3e-002	-1.7e+000	-4.1e-004	5.1e-002	5.1e-002	-1.2e+000	-1.1e-003	7.8e-002	7.8e-002	-1.3e-001	-3.1e-004
Th230	1.4e-001	1.4e-001	0.0e+000	0.0e+000	2.3e-001	2.2e-001	5.0e+000	2.1e-002	3.1e-001	2.9e-001	7.3e+000	6.5e-002
Th232	1.5e-007	1.5e-007	6.8e-001	1.0e-009	2.8e-007	2.8e-007	2.2e+000	1.1e-008	4.2e-007	4.1e-007	2.9e+000	3.7e-008
U233	3.7e-002	3.9e-002	-3.1e+000	-1.2e-003	6.7e-002	6.7e-002	-6.0e-001	-7.5e-004	9.3e-002	9.3e-002	3.2e-001	9.3e-004
U234	7.2e-001	6.5e-001	1.1e+001	7.4e-002	6.9e-001	6.3e-001	1.1e+001	1.3e-001	6.6e-001	6.0e-001	1.1e+001	2.0e-001
U235	1.6e-002	1.6e-002	-3.6e+000	-6.1e-004	1.7e-002	1.8e-002	-2.8e+000	-9.4e-004	1.8e-002	1.8e-002	-2.7e+000	-1.5e-003
U236	1.4e-001	1.3e-001	3.1e+000	4.1e-003	1.4e-001	1.3e-001	4.5e+000	1.1e-002	1.4e-001	1.3e-001	4.5e+000	1.9e-002
U238	1.5e-001	1.5e-001	0.0e+000	0.0e+000	1.5e-001	1.5e-001	0.0e+000	0.0e+000	1.5e-001	1.5e-001	0.0e+000	0.0e+000
Zr 93	3.6e-001	3.4e-001	4.1e+000	1.4e-002	3.6e-001	3.4e-001	4.1e+000	2.6e-002	3.5e-001	3.4e-001	3.8e+000	4.0e-002
36 Iso.												
Total	1.2e+002	9.8e+001	2.4e+001	0.0e+000	5.8e+001	5.3e+001	9.9e+000	0.0e+000	3.5e+001	3.2e+001	8.5e+000	0.0e+000

Table 7-4. Percentage Increase in Total Curies of the 36 TSPA-95 Isotopes

Duration of Criticality	Percent Increase at End of Criticality	Percent Increase at 45,000 years	Percent Increase at 65,000 years
1,000 years	8.5% (16k years)	0.73%	0.73%
5,000 years	15% (20k years)	4.2%	3.7%
10,000 years	24% (25k years)	9.9%	8.5%

Figure 7-1 gives the total activity in Ci/Assembly for the design basis SNF which has had the 10,000 year criticality starting at year 15,000 compared with the same fuel without the criticality. Figure 7-2 magnifies the time range from 10,000 years to 60,000 years, which emphasizes the increase in radioactivity immediately following the criticality. It is seen that while the increase in radioactivity is 24% of the simple decayed activity at the time of ending of the criticality, the increase is only a very small percent of the total activity at times near the time of emplacement (below 1,000 years). Furthermore, the percent difference becomes very small for times long after the ending of the criticality.

**Inventory of 36 TSPA 95 Nuclides as a Function of Time for a
PWR SNF Assembly After a 10,000 Year Internal Criticality
Starting at 15,000 Years**

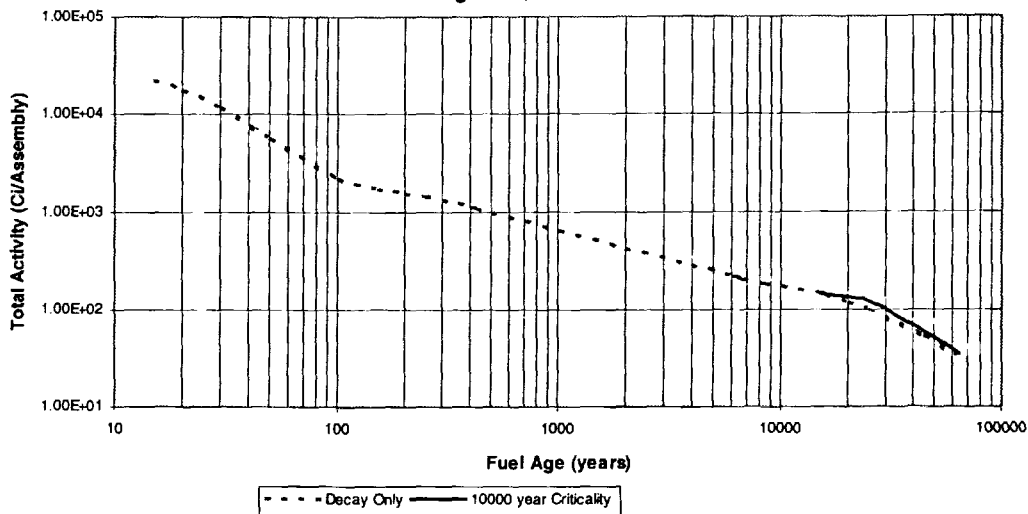


Figure 7-1. Inventory of 36 TSPA-95 Nuclides in 3% 20 GWd/MTU PWR SNF as a Function of Time, with the Increase From a 10,000 year Steady State Internal Criticality Indicated

**Inventory of 36 TSPA 95 Nuclides as a Function of Time for a PWR SNF
Assembly After A 10,000 Year Criticality
Starting at 15,000 Years**

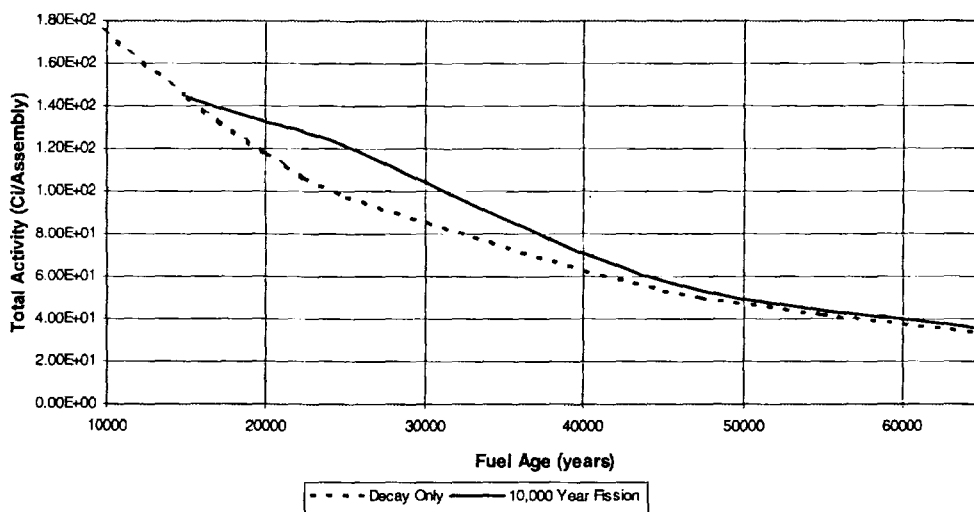


Figure 7-2. Inventory of 36 TSPA-95 Nuclides in 3% 20 GWd/MTU PWR SNF as a Function of Time from 10,000 to 60,000 Years, with the Increase From a 10,000 year Steady State Internal Criticality Indicated

8.0 Conclusions

It should also be noted that the topics covered by these conclusions are of sufficient importance that they will be addressed again in the 1997 summary report. Based on the analysis to date using values of environmental parameters currently sanctioned by the project, it is not expected that any subsequent conclusions will be inconsistent with those given herein. If any inconsistencies between these conclusions and those to be given in the 1997 summary report are identified, they will be noted and explained therein.

The analyses performed during this time period had two general purposes: (1) to evaluate the criticality potential of the range of possible degraded mode configurations internal to the waste package and of the possible accumulations of fissile material external to the waste package, and (2) to estimate the consequences of a criticality if it were to occur. The following summarizes the most significant of the conclusions reported in References 1 through 4.

Degraded internal criticality

- The earliest time to criticality is strongly dependent on a number of parameters which are presently the subject of significant uncertainty: (1) the ability of the WP to hold sufficient quantities of moderator for long periods of time (which may be affected by several factors, including corrosion of the WP bottom, the balance between evaporation and drip rates, and the buildup of moderator excluding oxides and mineral deposits), (2) the fraction of boron trapped in the solid iron oxide, (3) the stainless steel corrosion rate, (4) the upper limit for dissolved iron in the waste package water, (5) the efficiency of exchanging water between a filled waste package and the external environment, and (6) the drip rate. (Section 6.2)
- For very small values of the trapped boron fraction (which is the most conservative assumption, and the one for which there appears to be the most experimental evidence), the dominant parameters are generally the stainless steel corrosion rate, the drip rate, and the exchange rate. The exception is for low values of the drip rate and exchange rate; the earliest time to criticality will be insensitive to the borated stainless steel corrosion rate because the time is much longer than the time to corrode the borated stainless steel even at the lower corrosion rate. (Section 6.2)

External criticality

- The only feasible mechanism for concentrating a critical mass of commercial SNF uranium is for uranium-bearing groundwater to contact a reducing zone of significant size; the strongest reducing zones for the concentration of uranium have been the accumulation of organic material; the only place in the tuff beneath Yucca Mountain where such an accumulation of organic material might occur is at the base of the tuff. (Section 2.3.3.1)

- The probability of collecting a local concentration of organic material large enough to precipitate a critical mass of low enriched uranium (from commercial SNF) is incredibly small. (Table 6-8)
- While there is significant potential for adsorption of uranium from groundwater by zeolites of the type found in abundance at Yucca Mountain, the maximum concentration achievable from such adsorption would be far below that necessary for criticality in commercial SNF. Furthermore, it can be concluded that the extensive zeolite layers will remove a major fraction of the uranium from any groundwater stream from the repository, thereby reducing the amount of uranium reaching any organic reducing zones and providing an additional measure of conservatism for the evaluation of those postulated reducing zones discussed in this document. (Section 2.3.3.2)
- A screening of known uranium ore deposits was unable to identify any other mechanisms for uranium concentration which could possibly produce a high enough concentration to produce criticality in commercial SNF. (Sections 2.3.3.1,2,3)

Consequences

- For a WP which achieves criticality, the consequences measured in curies of increased inventory of radionuclides will increase with increasing criticality duration. For the longest likely duration, the increase in curies of the 36 nuclides of greatest interest to Performance Assessment will be approximately 24% (with respect to the same SNF decayed to the same time) immediately after the ending of criticality and less than 10% 40,000 years later. Even these small percentages are stated overly-conservative because they are with respect to the criticality design basis fuel which has a burnup of only 20,000 MWd/MTU. Typical PWR fuel will have more than twice this burnup from its reactor history, and therefore will have twice as large decay radiation at any time of comparison. For such fuel, the percentage increases in curies would be less than half the values calculated here.

9.0 References

1. *Initial Waste Package Probabilistic Criticality Analysis: Uncanistered Fuel*, Document Identifier Number (DI#): B00000000-01717-2200-00079 REV 01, Civilian Radioactive Waste Management System (CRWMS) Management and Operating Contractor (M&O).
2. *Second Waste Package Probabilistic Criticality Analysis: Generation and Evaluation of Internal Criticality Configurations*, DI#: BBA000000-01717-2200-00005 REV 00, CRWMS M&O.
3. *Probabilistic External Criticality Evaluation*, DI#: BB0000000-01717-2200-00037 REV 00, CRWMS M&O.
4. *Probabilistic Criticality Consequence Evaluation*, DI#: BBA000000-01717-0200-00021 REV 00, CRWMS M&O.
5. *Disposal Criticality Analysis Methodology Technical Report*, DI#: B00000000-01717-5705-00020 REV 00, CRWMS M&O.
6. *Total System Performance Assessment 1995: An Evaluation of the Potential Yucca Mountain Repository*, DI#: B00000000-01717-2200-00136 REV 01, CRWMS M&O.
7. Garside, L.J., *Radioactive mineral occurrences in Nevada*, Nevada Bureau of Mines and Geology, Bulletin 81, 1973.
8. French, D.E., *Origin of Oil in Railroad Valley, Nye County, Nevada*, The Wyoming Geological Association Earth Science Bulletin, 16, 1983 (pp. 9-21).
9. Grow, J.A., Barker, C.E., Harris, A.G., *Oil and Gas Exploration Near Yucca Mountain, Southern Nevada, High Level Radioactive Waste Management, Fifth Annual International Conference, ASCE & ANS, 1994*, pp. 1298-1315.
10. Katayama, N., Kubo, K., Hirono, S., *Genesis of Uranium Deposits of the Tono Mine, Japan, in Formation of Uranium Ore Deposits, IAEA-SM-183/19*, International Atomic Energy Agency, 1974, pp. 437-452.
11. Basinski, P. *The Mineralogy and Uranium Potential of Bedded Zeolites in the Northern Reese River Valley, Lander County, Nevada*, Master's degree thesis, University of Nevada Reno, December 1978.
12. Brinck, J.W., *The Geologic Distribution of Uranium as a Primary Criterion for the Formation of Ore Deposits, in Formation of Uranium Ore Deposits, IAEA-SM-183/19*, International Atomic Energy Agency, 1974.

13. Finch, W.I., Butler, A.P.Jr., Armstrong, F.C., Weissenborn, A.E., Staatz, M.H., Olson, J.C., *Nuclear Fuels, from United States Mineral Resources*, Ed. Brobst, D.A., Pratt, W.P., United States Geologic Survey Prof. Paper 820, 1973.
14. Smellie, J., *The Fossil Nuclear Reactors of Oklo, Gabon*, Radwaste Magazine, March 1995, pp. 18-27.
15. Goodell, P.C., *Geology of the Pena Blanca Uranium Deposits, Chihuahua, Mexico*, from *Uranium in Volcanic and Volcaniclastic Rocks*, AAPG Studies in Geology No. 13, 1981.
16. George-Aniel, B., Leroy, J.L., Poty, B., *Volcanogenic Uranium Mineralizations in the Sierra Pena Blanca District, Chihuahua, Mexico: Three Genetic Models*, *Economic Geology*, 86, March-April 1991, pp. 233-248.
17. Castor, S.B., Berry, M.R., *Geology of the Lakeview Uranium District, Oregon, from Uranium in Volcanic and Volcanoclastic Rocks*, AAPG Studies in Geology No. 13, 1982, pp. 55-62.
18. Schrader, E., *Relationships between Uranium and trace metal concentrations in volcanic rocks from Nevada*, *Economic Geology*, 72, pp. 104-107, 1977.
19. Breger, I.A., *The Role of Organic Matter in the Accumulation of Uranium, in Formation of Uranium Ore Deposits*, IAEA-SM-183/19, International Atomic Energy Agency, 1974.
20. Hess, F.L., *Uranium, Vanadium, Radium, Gold, Silver, and Molybdenum Sedimentary Deposits, in Ore Deposits of the Western States*, Lindgren Volume of The American Institute of Mining and Metallurgical Engineers, New York, 1933.
21. Chenoweth, W.L., *The Uranium-Vanadium Deposits of the Uravan Mineral Belt and Adjacent Areas, Colorado and Utah*, New Mexico Geological Society Guidebook, 32nd Field Conference, Western Slope Colorado, 1981, pp. 165-170.
22. Gascoyne, M., *Geochemistry of the Actinides and Their Daughters, in Uranium Series Disequilibrium: Applications to Environmental Problems*, Ed. Ivanovich, M. and Harmon, R.S., Clarendon Press - Oxford, 1982.
23. Thamm, J.K., Kovschak, A.A., Adams, S.S., *Geology and Recognition Criteria for Sandstone Uranium Deposits of the Salt Wash Type, Colorado Plateau Province*, Prepared for the U.S. Department of Energy, Grand Junction Office, CO, GJBX-6(81), January 1981.
24. *Preliminary Criticality Analysis of Degraded SNF Accumulations External to a Waste Package*, DI#: BBA000000-01717-0200-00016 REV 00, CRWMS M&O.

25. Fischer, R.P., *Vanadium Deposits of Colorado and Utah*, Geological Survey Bulletin 936-P, 1942.
26. *Progress Report on the Results of Testing Advanced Conceptual Design Metal Barrier Materials Under Relevant Environmental Conditions For A Tuff Repository*, Lawrence Livermore National Laboratory (LLNL), UCID-21044, December 1987.
27. Van Konynenburg, R.A., Curtis, P.G., *Scoping Corrosion Tests on Candidate Waste Package Basket Materials for The Yucca Mountain Project*, LLNL, Summary Acct. OL252 AJD, August 31, 1995.
28. *Emplaced Waste Package Structural Capability Through Time Report*, DI#: BBAA00000-01717-5705-00001 REV 00, CRWMS M&O.
29. *Corrosion Rates for Carbon Steel*, Interoffice Correspondence LV.WP.JKM.03/96.060, J.K. McCoy, March 15, 1996, CRWMS M&O.
30. *Electrochemical Determination of The Corrosion Behavior of Candidate Alloys Proposed for Containment Of High Level Nuclear Waste in Tuff*, LLNL, UCID-20174, June 1984.
31. *FY95 CDA Update OFF Waste Stream Data*, Interoffice Correspondence SA.VA.JK.04/95.045, Davis, J., Fleming, M., King, J., April 3, 1995, CRWMS M&O.
32. Holman, J.P., *Heat Transfer*, 7th Edition, McGraw-Hill Publishing Company, 1990.
33. *Mined Geologic Disposal System Advanced Conceptual Design Report, Volume III of IV, Engineered Barrier Segment/Waste Package*, DI#: B00000000-01717-5705-000027 REV 00, CRWMS M&O.
34. Moran, M.J., Shapiro, H.N., *Fundamentals of Engineering Thermodynamics*, John Wiley & Sons, 1988.
35. *AUCF Waste Package Criticality and SAS2H Evaluations*, Interoffice Correspondence LV.WP.DAT.03/96.070, Dan Thomas, March 26, 1996, CRWMS M&O.
36. *Material Compositions and Number Densities for Neutronics Calculations*, DI#: BBA000000-01717-0200-00002 REV 00, CRWMS M&O.
37. *Technical Document Preparation Plan for the Supporting Analysis Results Summary Reports for the Disposal Criticality Analysis Methodology Reports*, DI#: B00000000-01717-4600-00087 REV00, CRWMS M&O.
38. *Pitting, Galvanic, and Long-Term Corrosion Studies on Candidate Container Alloys for the Tuff Repository*, U.S. Nuclear Regulatory Commission, NUREG/CR-5709, January

- 1992.
39. *UCF Waste Package Criticality Analysis*, DI#: BBA000000-01717-0200-00005 REV 00, CRWMS M&O.
 40. *Controlled Design Assumptions Document*, DI#: B00000000-01717-4600-00032 REV 04, ICN1, CRWMS M&O.
 41. *Ground Water at Yucca Mountain, How High Can it Rise*, National Research Council, National Academy Press, Washington, D.C., 1992.
 42. *Waste Package Design Basis Fuel Analysis*, DI#: BBA0000000-01717-0200-00121 REV 00, CRWMS M&O.
 43. Cerne, S.P., Hermann, O.W., and Westfall, R.M., *Reactivity and Isotopic Composition of Spent PWR Fuel as a Function of Initial Enrichment, Burnup, and Cooling Time*, Oak Ridge National Laboratory, ORNL/CSD/TM-244, 1987.
 44. *Rock Size Required to Cause a Through Crack in Containment Barriers*, DI#: BBAA00000-01717-0200-00015 REV 00, CRWMS M&O.
 45. *Q-List*, YMP/90-55Q, REV 4, Yucca Mountain Site Characterization Project.
 46. *Perform Probabilistic Waste Package Design Analyses*, QAP 2-0 Activity Evaluation WP-25, 8/03/97, CRWMS M&O.
 47. *Quality Assurance Requirements and Description*, DOE/RW-0333P, REV 7, Department of Energy (DOE) Office of Civilian Radioactive Waste Management.
 48. *Estimate of mineralized areas*, Interoffice Correspondence, LV.WP.PG.05/96-120, Gottlieb, P., May 30, 1996, CRWMS M&O.
 49. *10CFR Part 60; Disposal of High-Level Radioactive Wastes in Geologic Repositories; Design Basis Events; Final Rule*, U.S. Nuclear Regulatory Commission, Federal Register, Volume 61, Number 234, pp. 64257-64270, December 4, 1996.